The Effect of Temperature and Variation of Salinity during One Dimensional Compression

A thesis submitted by

Amanda Renee Parry

in partial fulfillment of the requirements for the degree of

Master of Science

in

Civil and Environmental Engineering

TUFTS UNIVERSITY

August 2018

Adviser: John T. Germaine, Research Professor

The Effect of Temperature and Variation of Salinity during One Dimensional Compression

by

Amanda Renee Parry

Submitted to the Department of Civil and Environmental Engineering on June 14, 2018
in Partial Fulfillment of the Requirements for the Degree of Master of Science
in Civil and Environmental Engineering

ABSTRACT

Understanding the uniaxial compression behavior of soil is important to engineers in the offshore oil and gas industry. Laboratory compression test data is a key parameter to characterizing overpressure zones underground. This research investigates two parameters related to one-dimensional compression behavior through a rigorous laboratory experimental program.

First, the effect of temperature on compression behavior is examined using data from ten constant rate of strain tests. Five elevated temperature tests are compared to five room temperature tests in the stress range of 0.1 to 40 MPa to conclude that temperature does not have an effect on compression behavior.

Additionally, there is an investigation of how the pore fluid salinity of a specimen changes with compression. The results of twenty-one salinity tests indicate that salinity decreases with compression. Following the experimental program a model is developed to predict the salinity at a given stress level and compared to the collected data.

Thesis Supervisor: John T. Germaine

Title: Research Professor, Department of Civil and Environmental Engineering

ACKNOWLEDGEMENTS

Without a doubt, the person I want to thank first and foremost is my advisor and mentor Dr. Jack Germaine (Dr. G). Since meeting Dr. G as a junior at MIT, he has mentored and encouraged me to immerse myself in the world of soil mechanics research and to appreciate the unique challenges of working with soil and laboratory equipment. My first class with him exposed me to the field of geotechnical engineering, a field in which I discovered a passion and am excited to make a career. I am inspired by the dedication and immense knowledge he has for this field, but also his sense of humor and patience while working with students. I am grateful to have learned from one of the best.

I would like to thank my other teachers in geotechnical engineering: Dr. Lucy Jen, Prof. Laurie Baise, Dr. Dick Plumb, Damian Siebert, Prof. Andrew Whittle, and Prof. Herbert Einstein. Each of these people taught me with their personalized expertise and excitement, and their passion for learning and solving problems was contagious.

Additionally, I am grateful to all of the people in the UT GeoFluids Consortium, especially Prof. Peter Flemings and Dr. Maria Nikolinakou. UT GeoFluids gave me the opportunity to work with some of the smartest people I have met and helped me develop my communication and presentation skills.

I'm also thankful to the Tufts University School of Engineering for selecting me as the inaugural recipient of the Linda M. Abriola Graduate Fellowship. I am honored to receive an award in Professor Abriola's name, and the fellowship helped reduce the financial burden of graduate school and allow me to focus solely on my studies and research during my time at Tufts.

Finally, to my family and friends, thank you. You provided the support, the ears to listen, laughs to relax, and the best company over the past two years. My family supported me every step of the way as I decided to pursue a graduate degree and provided many home cooked meals and cookies along the way. Liz, Mark, Deniz, Lichen, Chunwei, Nick, Tony, Parker, Marshall, Stephen, and James, I'm so thankful Tufts brought us together and your friendship made graduate school all the more worth it. I will always appreciate the extended lunch breaks and the conversation (or debates) that came with them.

Table of Contents

List of Tables

List of Figures

List of Symbols

°C	Degrees Celsius
µm	Micrometer
Å	Angstrom
CH	High Plasticity Clay
cm	Centimeteres
CR	Compression Ratio
CRS	Constant Rate of Strain
e	Void Ratio
g/L	Grams per Liter
GeoFluids	UT GeoFluids Consortium
GoM-EI	Gulf of Mexico - Eugene Island
IODP	International Ocean Drilling Program
kg	kilograms
km	Kilometer
LIR	Load Increment Ratio
LVDT	linear voltage displacement transducer
MIT	Massachusetts Institute of Technology
mol	molarity
MPa	Megapascals
mv	Volume compressibility
n	Porosity
nm	Nanometer
PCB	Printed Circuit Board
psi	Pounds per Square Inch
PVA	Pressure Volume Actuator
RGoM-EI	Resedimented Gulf of Mexico - Eugene Island
S	Percent Saturation

SSD	Surface saturated dry
TAG Lab	Tufts Advanced Geomaterial Laboratory
USCS	Unified Soil Classification System
UT	University of Texas, Austin
V	volt
VCL	Virgin Compression Line
XRD	X-ray Diffraction

1 Introduction

1.1 Problem Statement

Soil behavior is a complex but intriguing field to study. Every soil deposit has its own unique properties and nuances, so there are always new questions to answer and ideas to investigate. Traditional geotechnical engineering does not typically encounter material at depths of hundreds of meters to kilometers underground and under tens to hundreds of megapascals (MPa) of pressure. Petroleum engineers, however, are very interested in understanding the sediments and mudrocks that exist at these great depths and extreme conditions for applications in resource extraction. It requires unique experimental programs and advanced laboratory equipment to perform laboratory tests on representative materials to learn about the soil from deep under the ocean floor. The Tufts Advanced Geomaterial Laboratory (TAG Lab) works on exactly these types of research questions.

One of the many unique aspects of drilling as deep as the oil industry does is the temperature gradient that exists beneath the earth's crust becomes relevant. The mudrocks deep down exist at in-situ temperatures higher than the temperatures experienced in laboratory settings. Prior research in the TAG Lab on the compression properties of mudrocks does not account for the temperature gradient. When these existing laboratory results are compared to in situ porosity versus depth curves there is a difference between the two sets of data. The first goal of this research is to evaluate if temperature has an effect on the compression properties of mudrocks and therefore, could explain the difference between experimental data and in-situ measurements.

Compression of fine grained materials is interesting because it is controlled by what happens at the molecular scale. Part two of this research investigates one of the

microscopic physical processes of clay behavior. Part two investigates how the salinity of the pore fluid of a specimen changes with increased stress levels, a component of the clay-water-electrolyte system behavior. Previous researchers have investigated how the clay-water-electrolyte system affects the compression behavior, however, no detail was given as to how the system changed with the applied compression. Understanding how the salinity changes with compression will provide insight into what happens to clay particles at the microscopic level when compressed.

1.2 Thesis Scope and Objectives

There are two main objectives of this research – one temperature related and one salinity related. The first is to understand how the compression properties of soil are affected by elevated temperatures. This research includes an extensive testing program to investigate the effect. Constant rate of strain (CRS) tests are run at elevated temperatures to collect data related to the one dimensional compression properties of the material. Results from elevated temperature tests are compared to room temperature tests to determine if the increased temperature has an effect on the compression properties. Other researchers have examined this topic before and found that the typical compression curve shifts down (lower porosity or void ratio for a given stress value) when tested at higher temperatures.

Following the temperature research, the second goal is to understand how the salinity of a soil specimen changes with compression and develop a model that is able to predict the change. This research measures the salinity of a suite of CRS test specimen that were each compressed to a different stress level to evaluate how the salinity changes from a known initial salinity. Following the experimental program, details of clay mineralogy are used to propose a model that takes seven inputs and calculates the expected Interpreted Specimen Salinity.

All of this research contributes to the greater research goals of the UT GeoFluids Consortium (GeoFluids). GeoFluids is a joint venture between Dr. Jack Germaine's experimental geotechnical engineering group at Tufts University and Dr. Peter Fleming's geomechanical modeling group at the University of Texas, Austin that is sponsored by many oil and gas industry companies. The overall goal of the UT GeoFluids Consortium is to "study the state and evolution of pressure, stress, deformation and fluid flow through experiments, models, and field studies."

1.3 Organization of this Thesis

This thesis is organized into eight chapters. The chapters include Introduction, Background Information, Materials, Equipment, Procedures, Influence of Temperature on CRS Compressibility Results, Salinity Results and Model Development, and Summary, Conclusions, and Recommendations.

Chapter 2 describes the relevant background information to the problem statements. It begins by defining mudrocks then transitions to information related to the temperature research. The final two sections are related to the salinity research. For both components there is a discussion of why the investigation is relevant to field applications.

Chapter 3 provides the details on the specific mudrock tested in this research. It also briefly describes the resedimentation procedure and why it is used in the TAG Lab.

Chapter 4 provides all the details of the equipment used in the experimental programs for this research. A significant amount of time went into outfitting CRS equipment to be able to be heated to a controlled temperature and redesigning computer control boxes that are used across the TAG Lab. These two components are described in detail.

Chapter 5 provides step-by-step instructions for all the experimental procedures used in this research. After the physical test instructions, all the equations used to analyze test

data are provided and explained. Pictures are included to aid researchers in following the provided instructions.

Chapter 6 is the first of two results sections. All of the results related to the temperature research are included in this chapter. The results include compression curves, regression lines for data sets, and permeability information. The chapter concludes with a discussion of the results and how they compare to what exists in the literature.

Chapter 7 discusses the results of the salinity testing program. Additionally, it describes the model developed to predict specimen salinity and compares the model to collected data to assess its relevance and appropriateness.

Chapter 8 gives a summary of the work included in this research and the conclusions drawn based on the experimental results. It also recommends topics for future related work.

2 Background Information

2.1 Introduction

This chapter provides the relevant background information related to this research. Section 2.2 defines and describes the composition of mudrocks down to the mineralogical scale. Section 2.3 discusses the relevance of temperature research to practical applications and Section 2.4 summarizes some of the studies by other researchers on the same topic. Then there is a transition to pore fluid salinity research. Section 2.5 discusses the importance of pore fluid salinity to field measurements and drilling operations, and Section 2.6 provides a summary of the limited amount of existing literature related to pore fluid salinity and compression behavior.

2.2 Mudrock Composition

The word mudrock is defined differently depending on what paper or textbook is referenced. In general it is used to describe some type of fine-grained rocks, and in UT GeoFluids the word is specifically for fine-grained, siliciclastic sedimentary rocks: rocks that are made up primarily of silt and clay-size particles (Boggs, 2006). This research is performed exclusively on a mudrock from over two kilometers below the seafloor in the Gulf of Mexico, identified as Gulf of Mexico – Eugene Island (GoM-EI) material. GoM-EI is used extensively for laboratory experimentation in the TAG Lab and more specific information about GoM-EI and its soil properties is included in Section 3.2.

Before continuing the definition of clay needs to be clarified because in soil mechanics it can be ambiguous. “Clay” can refer to a material particle size. If used as a particle size term it is referring to the smallest constituent of soil, typically defined as the particles that are smaller than 2 μm (Mitchell, 1976). On the other hand, clay can also refer to specific minerals deemed “clay minerals” (Mitchell 1976). The clay minerals are

crystalline particles comprised of a combination of minerals that come from a particular group and are mainly made up of combinations of silica tetrahedral sheets and hydrous oxide octahedral sheets (Mitchell, 1976). The ambiguity comes from the fact that the clay minerals do not need to be smaller than 2 µm and all particles in a soil that are smaller than 2 µm do not need to be composed of clay minerals. Therefore, it is important to make it clear if "clay" is being used to refer to a particle size or mineral composition.

Mudrocks have a high percentage of clay minerals, so it is imperative to understand the basics of clay mineralogy and the chemo-mechanical processes that happen at the microscopic scale. Mitchell (1976) provides a detailed overview of the concepts related to clay mineralogy and the interactions that occur between the clay-water-electrolyte system. Silica tetrahedral sheets and hydrous oxide octahedral sheets are combined to form clay layers and a combination of layers makes a clay particle (Figure 2-1). Clays can be organized into groups based on the number of sheets in a layer. Clays in certain groups are known to have some similar behaviors based on the chemical composition, although there is still significant variation even within one group.

GoM-EI is primarily made of the clay mineral smectite. Smectite is a "2:1" clay, meaning that there are two silica tetrahedral sheets sandwiching an octahedral sheet that make up the basic mineral (Figure 2-1) (Mitchell, 1976). The thickness of one smectite layer is assumed to be 9.6 Å (Fitts & Brown, 1999; Mitchell, 1976) (Figure 2-1). When clays are exposed to water, single clay layers hydrate and are attracted to each other and bonded together by van der Waals forces to create single clay particles (Figure 2-1) (Mitchell, 1976). The water that is between the two smectite layers is the interlayer (innerlayer in some sources) water composed of water molecules and dissolved cations. When clay minerals are hydrated there is no upper bound to the clay particle size, according to Mitchell (1976) hydrated particles can range from 9.6 Å thick (zero hydration, just a single clay layer) to infinity. In this research the total thickness of a hydrated clay particle is

assumed to be about 18 Å, based on research by Fitts and Brown (1999) on a similar smectite material. Previously, researchers in the TAG Lab used X-ray diffraction (XRD) to determine the GoM-EI particle size is approximately 5 nm. If the total particle thickness is 5 nm and a single hydrated sheet thickness is about 18 Å, then GoM-EI clay particles are composed of about three smectite layers (Ge, 2016).

Transitioning to a slightly larger scale, we look at how clay particles interact with the water (and possible ions) that surround them. This is referred to as the clay-water-electrolyte system (Mitchell, 1976). In any soil system there are typically three phases: air, water, and solid, and the water phase almost always has some dissolved ions. The void space of a soil specimen is comprised of the space occupied by the water and air phases. The solids space is occupied by the clay particles (and sand if present). One metric that is used to describe a soil specimen is the percent saturation, S (%), defined as the percentage of the void space filled with water. In the TAG Lab, test specimen are always about 100% saturated so the void space is completely filled with water and thus there is no air component. Two parameters that are used to evaluate the ratio of solids to voids are defined below. The void ratio, e, is calculated using Equation 2-1. Porosity, n, is calculated using Equation 2-2 below.

$$e = \frac{V_{voids}}{V_{solids}} \qquad (2-1)$$

$$n = \frac{V_{voids}}{V_{total}} \qquad (2-2)$$

During compression the void space decreases, squeezing pore fluid out of the specimen. One challenge in this research, and soil mechanics in general, is understanding how the clay particles, ions, and fluid are all interacting to determine the composition of the fluid expelled from the void space.

Part of the water that surrounds the clay particles in the void space is "trapped" in what is known as the diffuse double layer (Mitchell, 1976). Clay particles inherently have a negative surface charge. The negative surface charge attracts cations to the surface of the clay particle to balance the charge. The attraction of cations to the clay particle results in a higher concentration of cations adjacent to the clay surface (Figure 2-2). The negative surface charge combined with the distributed ion charges in the adjacent fluid is defined as the diffuse double layer (Mitchell, 1976). The thickness of the double layer affects clay behavior because it controls how nearby clay particles interact with each other. The characteristic thickness of the double layer is calculated using Equation 2-3:

$$\frac{1}{K} = \left(\frac{DkT}{8\pi n_0 e^2 v^2}\right)^{\frac{1}{2}} \qquad (2-3)$$

Where:

1/K = Thickness of double layer (cm)
D = Dielectric constant of medium
k = Boltzmann constant (ergs/K)
T = Temperature (Kelvin)
n_0 = Electrolyte concentration (ions/cm^3)
e = Electron charge (esu)
v = Cation valence

The variables that control the double layer thickness are the electrolyte concentration, cation valence, dielectric constant, and temperature. The most interesting and relevant parameter to this research is the electrolyte concentration. Figure 2-3 shows how the double layer thickness changes with different values of electrolyte concentration. For most of this research the concentration is about 80 g/L. Equation 1-3 uses the mol unit so converting g/L to mol, n_o in Equation 1-3 is 1.37 mol (≈80 g/L). For a salinity of 80 g/L the calculated characteristic double layer thickness (1/K) is small, only about 3 Å.

Clay mineralogy and the clay-water-electrolyte system are important concepts used in developing the salinity prediction model discussed in Chapter 7.

2.3 Porosity versus Depth Curves in the Gulf of Mexico

One TAG Lab and GeoFluids goal is to understand how laboratory scale experimental results are applicable to understanding in-situ soil conditions. One puzzling observation seen in the oil and gas industry is the discrepancy between lab derived porosity versus depth curves and field measurements. Based on existing data it is generally observed that the laboratory data yields a higher porosity than the field measurements at a given effective stress. There are two routes to follow to investigate this issue, first is to examine the laboratory data and interpretation. The other is to question the collection and interpretation of the field measurements.

Nooraiepour et al. (2017) published a study that directly compares field and lab measurements for material from the Southwest Barents Sea, off the northern coast of Norway. In this study, researchers collected mudstone drill cuttings from two wells and reconstituted them to specimen for laboratory CRS tests (Nooraiepour, Mondol, & Hellevang, 2016). Compression tests were run to stress levels of about 50 MPa to create laboratory compression curves that were compared to calculated in-situ values (Nooraiepour et al., 2016). The in-situ formation porosity was calculated using bulk density logs, and the bulk density logs and the drill cuttings used in the compression tests come from the same wells (Nooraiepour et al., 2016). Figure 2-5 shows the comparison between in-situ and laboratory data. It is evident from the two graphs of porosity versus depth that the field data (the discrete points) are consistently lower than the porosity values from experimental data. The different colors are for different depth ranges, but the trend of lower in-situ data exists for all depth ranges. Nooraiepour et al. proposes the difference between the log measurements and experimental data is due to chemical compaction that is experienced in-situ (Nooraiepour et al., 2016).

A second example of the difference between laboratory measurements and in-situ values is summarized in a thesis by Betts, a previous GeoFluids member (2014). His research also relies on GoM-EI material. Betts estimated the in-situ porosity and

effective stresses near the GoM-EI site using geophysical logs from a well in Eugene Island Block 331 (Betts & Flemings, 2014). Porosity values, n, were calculated based on an empirical relationship using sonic velocity logs of the well, and the total vertical stress at depth was estimated by integrating values from the bulk density log (Betts & Flemings, 2014). The predicted in-situ values are compared to a constant rate of strain test that was done on the same material, CRS1511, in Figure 2-5. Comparing the field derived data (pink and blue dot data sets) to the laboratory CRS curve (green data points), it is clear that one data set, the density log, is an overestimation and the other data set, sonic log, is an underestimation. In both cases, there is a difference between the field derived data and laboratory curve. The sonic log porosities (as opposed to the density log) are the values that better match the limited direct measurements of the in-situ core porosities (Figure 2-6), and those are the values that are shifted to a lower void ratio compared to the laboratory curve (Betts & Flemings, 2014).

Researchers in the TAG Lab propose four possible mechanisms that could explain the difference between laboratory and in-situ compression curves:

1. Salinity of the pore fluid
2. Smectite to illite mineralogical transformation
3. Secondary compression (creep)
4. Temperature

The salinity of the pore fluid hypothesis was debunked by Horan (2012) and Fahy (2014). They showed that generally for salinities greater than about 16 g/L the compression curves converge at high stress levels (more on this in Section 2.5). Currently another TAG Lab member, Chunwei Ge, is investigating the smectite to illite transformation question, the secondary compression component is yet to be investigated, and the effect of temperature is the topic of this thesis.

The motivation to consider the effect that temperature could play in compression tests is the temperature gradient that exists below the mudline. Figure 2-7 is an example of

the positive temperature gradient with depth that exists at one of the International Ocean Drilling Program (IODP) sites (Long, Flemings, Dugan, Germaine, & Ferrell, 2005). Approximately 700 meters below seafloor the temperature is about 14°C and increasing at a rate of 16.7°C/km (Long et al., 2005). The GoM-EI material in the TAG Lab comes from at least 2 km below the mudline so, using the IODP site as a guide, there is an in-situ temperature of at least 35°C. Therefore, it is reasonable to question if testing the GoM-EI material at elevated temperatures, closer to in-situ conditions, could cause laboratory results to be closer to in-situ measurements.

2.4 Previous Studies of Temperature and Compression

There are a handful of previous studies that evaluate the effect of temperature on compression behavior. The literature, however, is based on materials very different from GoM-EI. Additionally, the compression tests do not go to the high stress range that is of interest to the oil and gas industry and UT GeoFluids.

Plum and Esrig (1969) measured the compression behavior of a glacial lake clay from Newfield, New York and a commercially available illite material at two different temperatures, 24°C and 50°C. They batched their material to a high water content and poured the slurry into a consolidometer to be compressed to about 200 psi. The results from Plum and Esrig suggest that for a given stress range the porosity during a heated test is lower than the cool test, as seen in Figure 2-8. For both materials the compression curve is shifted lower for the heated tests. Additionally, Plum and Esrig conclude that the compressibility, the change in void ratio divided by the change in stress, is greater for the 50°C tests until about 300 psi where the compressibility is approximately equal for 50°C and 24°C tests (Plum & Esrig, 1969). This is apparent from the slope of the lines in Figure 2-8.

Campanella and Mitchell also studied how temperature effects the behavior of a remolded illite material (1968). They explored the effect of temperature on a variety of

soil behaviors including: volume changes, the coefficient of thermal expansion, and pore pressure behavior during compression. Their research on compression behavior was completed by triaxial consolidation tests at 25°C, 38°C, and 51°C. The results are included in Figure 2-9. All three specimen were consolidated to an effective stress of about 0.2 MPa at the testing temperature and then loaded incrementally with a load increment ratio of approximately 0.20 (Campanella & Mitchell, 1968). Based on the curves in Figure 2-9, Campanella and Mitchell draw similar conclusions to Plum and Esrig. The slope of all the virgin compression lines is parallel indicating that the compressibility of the material doesn't change with temperature (contrary to Plum and Esrig). On the other hand, Campanella and Mitchell's results agree that at a given effective stress value the porosity of the specimen in the heated test is lower than the cooler test. Campanella & Mitchell (1968) suggest that this trend makes sense because at higher temperatures there is a weaker soil structure, however, they do not provide an explanation for why the soil structure is assumed to be weaker.

A third study by researchers at the Massachusetts Institute of Technology (MIT) in the 1980s supports the results of Campanella and Mitchell and Plum and Esrig. In the 1980s, there was interest in potential petroleum reservoirs in the Beaufort Sea north of Alaska which motivated a laboratory testing program to understand the behavior of Arctic silt (Ladd, Weaver, Germaine, & Sauls, 1985). Typical room temperature oedometer tests were run on intact material as well as one temperature controlled test. The MIT researchers were interested in testing the Arctic silt material at temperatures closer to the in-situ conditions, so colder than room temperature, close to 0°C (Ladd et al., 1985; Young, 1986). To perform the compression test at controlled temperatures the oedometer cell was submerged in a constant temperature bath for the load-unload cycles (Young, 1986). The single compression test of interest has three load-unload cycles: first the specimen was loaded and unloaded at 1.4°C, then it was brought up to 20°C to be loaded and unloaded, and finally it was cooled back down to 1.4°C for the last load-unload cycle (Ladd et al., 1985; Young, 1986). Figure 2-10 shows the results from

this compression test. The shift between the virgin compression lines (VCL) of the 20°C cycle and the 0°C cycle is highlighted by the two dashed lines. The shift corresponds to an increase in effective stress of about 10% for the same value of strain (Young, 1986). This research again shows that the compression curve shifts to lower porosity values when specimen are compressed at increased temperatures.

The above observations set the stage for the current research which is to investigate if the trend of the shift in compression curves continues at higher stress levels that are of more relevance to the oil and gas industry and deep well boring situations. Based on existing literature it seems that when testing GoM-EI material at elevated temperatures the compression curve will shift down at low stresses.

2.5 Importance of In Situ Pore Fluid Salinity

The importance of in situ pore fluid salinity is twofold. First, salinity affects resistivity measurements that are relied on for porosity and pore pressure estimation during exploration, and second, salts in drilling mud affect borehole stability.

Overpressured formations have pore pressures higher than hydrostatic conditions. Knowing where overpressure zones exist and the associated pressure distribution is crucial for companies developing hydrocarbon reserves (Hottman & Johnson, 1966). One way that logging specialists identify overpressure zones is using resistivity measurements from a well bore. The resistivity is measured down a borehole and compared to a "normal compaction trend" plot. The deviations between the field data and normal compaction trend typically indicate something abnormal underground; usually engineers assume that if the field data trends towards low resistivity values then the formation at that depth is overpressured (Hottman & Johnson, 1966). However, salinity of the pore fluid and the mineralogy of the mudrock down the well also effect resistivity, an increase in salinity results in a drop in resistivity measurements. Unfortunately, there currently is no good way to differentiate which physical condition is responsible for changing a

resistivity measurement deep underground. Therefore, understanding the in-situ pore fluid salinity of a formation and how it might change with depth, and temperature, is crucial to better interpretation of resistivity measurements. For example, if it is understood that the salinity increases with depth then it indicates that a drop in the resistivity measurement does not necessarily mean that there is an overpressured zone in that area.

In situ salinity also has an effect on well-bore stability. When wells are drilled, mud is pumped down the hole to put a pressure on the walls of the hole. The applied pressure from the mud prevents the well from collapsing into itself (van Oort, 2003). Currently, oil based or synthetic based muds are used because they have the best performance record, but they don't have great environmental consequences (van Oort, 2003). Water-based muds would be an attractive alternative for environmental reasons, but the drilling performance needs to be improved first. Water-based muds are problematic because of the complicated way water and solutes interact with the mudrocks and the resulting transport processes and physico-chemical changes that can occur (van Oort, 2003). In-situ salinity is important in these scenarios because the water-based mud creates an interface of two different fluids, which causes osmosis and transport processes to occur. van Oort (2003) describes the swelling pressure that develops in the mudrock when it contacts the drilling fluid. Using muds that have a higher salinity than the in-situ pore fluid will result in ions diffusing from the mud into the mudrock, but it will also cause osmotic backflow of the mudrock pore water into the borehole (van Oort, 2003). These transport processes will affect the pore pressure in the mudrock and the swelling pressure and thus affect the effective stresses of the mudrock around the borehole which governs failure (van Oort, 2003). Therefore, when evaluating what drill mud to use and how it is going to interact with the mudrock interface, drilling engineers must consider the in-situ pore fluid salinity.

2.6 Previous Studies of Salinity Evolution and Compression Behavior

Previously UT GeoFluids researchers studied how different pore fluid salinities affect both compression and mechanical behaviors of soils. The previous research assumes the salinity of a test specimen is constant throughout the compression test. Horan performed CRS tests on Resedimented Boston Blue Clay (RBBC) batched with different pore fluid salinities. He concluded that changing the pore fluid salinity does not affect the compressional behavior (Figure 2-11) (Horan, 2012). Fahy (2014) continued this research and tested RGoM-EI material instead of RBBC. RBBC is a low plasticity illitic clay while RGoM-EI is primarily a high plasticity smectitic material. The conclusion of Fahy's research is that at low stress levels the pore fluid salinity does have an effect on the compressional behavior (Fahy, 2014). In Figure 2-12 it is clear at a given low stress level a material with a lower pore fluid salinity has the highest void ratio. As the stress increases, however, all of the compression curves converge to a narrower band of void ratios. Fahy (2012) also examined the permeability of RGoM-EI during CRS tests and reports that increasing the salinity also increases the permeability, which is seen in Figure 2-13. These two studies provide information about how salinity affects clay behavior but does not help us understand how the salinity changes (or does not) during compression testing. The research by Fahy and Horan is relevant, however, because it indicates that if the salinity is changing during compression it should not be affecting the compressional behavior especially at high stress levels.

One early study in the literature related to the salinity changing is by Engelhardt and Gaida (1963). This study examined how the pore fluid salinity of pure montmorillonite and kaolinite clays changes during incremental compression tests. Their experimental set up allowed them to analyze how the compaction rate of clay minerals with different pore fluid salinities changes (Figure 2-14). Engelhardt and Gaida define the compaction rate as the time it takes for a specimen to be compressed to a particular void ratio under a constant stress. There is a visible trend that the higher the pore fluid salinity the faster

the compaction rate. However, the density and viscosity of water both change with salt concentration, so the observed trend of a change in compaction rate with different pore fluid salinity concentrations is likely related to the change in the fluid properties. More importantly, they analyzed the expelled water (the water squeezed out during compression) to observe how its salinity changed through the course of a compression test in the stress range of 3 to 80 MPa. In the experimental set up the expelled pore fluid passes through a sieve plate and the salt concentration is calculated based on the salinity of that filtrate (Engelhardt & Gaida, 1963). Unfortunately, they do not include the method used to determine the salinity based on the filtrate. It is important to emphasize here that Engelhardt and Gaida are measuring the salinity of the expelled fluid from the compression tests (1963). The conclusion is that for kaolinite clays there is no chemical change in the pore fluid salinity, but for the montmorillonite clay there was a definite trend of decreasing salinity with decreasing porosity (increasing stress) (Figure 2-15) (Engelhardt & Gaida, 1963). Finally, they propose that the chemo mechanics that cause this phenomenon is the cation exchange capacity of montmorillonite clay particles (Engelhardt & Gaida, 1963).

A second study that examines how the salinity of a clay specimen evolves when being compression is by Fitts and Brown (1999). The goal of their research is to understand why there is an anomalous freshening of pore fluids in the N. Barbados accretionary wedge. Before Fitts and Brown, researchers attributed the anomalous freshening to fluid migration and lateral flow (Fitts & Brown, 1999). Fitts and Brown instead propose that the freshening is caused by a partial in situ dehydration of smectite (1999). Fitts and Brown evaluate this hypothesis using two methods: first, they rapidly load remolded specimen in a device that is similar to the Ocean Drilling Program pore water squeezer described in Manheim and Sayles (1974). Second, they slowly load pure montmorillonite samples in a “basic piston cylinder apparatus”. During both experiments, just like in Engelhardt and Gaida (1963), the pore water fluid that is expelled from the specimen being compressed is collected and analyzed to determine the salinity of the released

fluid. The conclusion is overall the pore fluid is freshening based on chlorine measurements of the effluent (Fitts & Brown, 1999). Perhaps the more interesting part of the research by Fitts and Brown is their argument for why the pore fluid is freshening. For all of their experiments, XRD is used on the test specimen before and after loading to determine the hydration state and *d*-spacing of the smectite particles. In all their analyses, there is a decrease in the *d*-spacing suggesting some dehydration. Fitts and Brown argue that the dehydration means the interlayer water (between two clay layers as in Figure 2-1) is beginning to collapse which releases fresh water (but no ions) into the pore fluid. The ions within the innerlayer are not released because they are so tightly attracted to the negative charge on the clay layer. Releasing freshwater into the free pore fluid from the inner layer dilutes the free pore fluid concentration and thus, when the free pore fluid is expelled during compression there is the trend of decreasing salinity (Figure 2-16).

One important caveat to this research is that both Fitts and Brown (1999) and Engelhardt and Gaida (1963) measure the salinity of the expelled pore fluid. Neither study evaluates the salinity of the material that is left behind. The goal of this research is to evaluate the salinity of specimen that are compressed to different stress levels and evaluate how it changes from the initial salinity. Furthermore, this research aims to develop a better understanding of why the salinity changes and be able to predict the salinity at a given stress level.

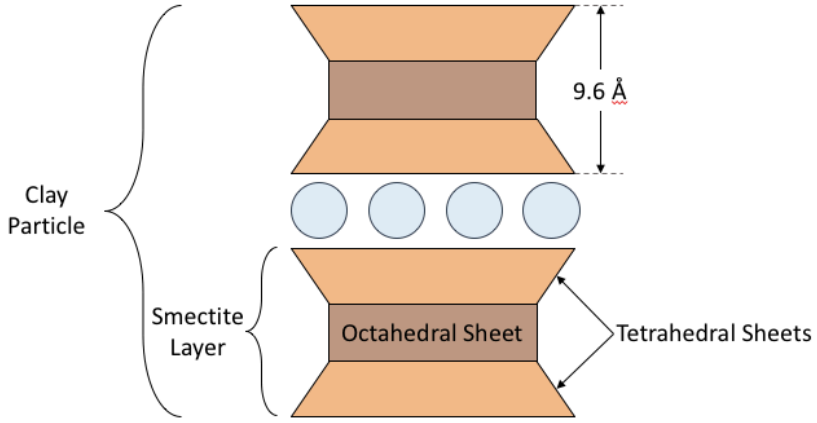

Figure 2-1: Schematic identifying the difference between a clay sheet, layer, and particle. A particle of smectite is used as the example.

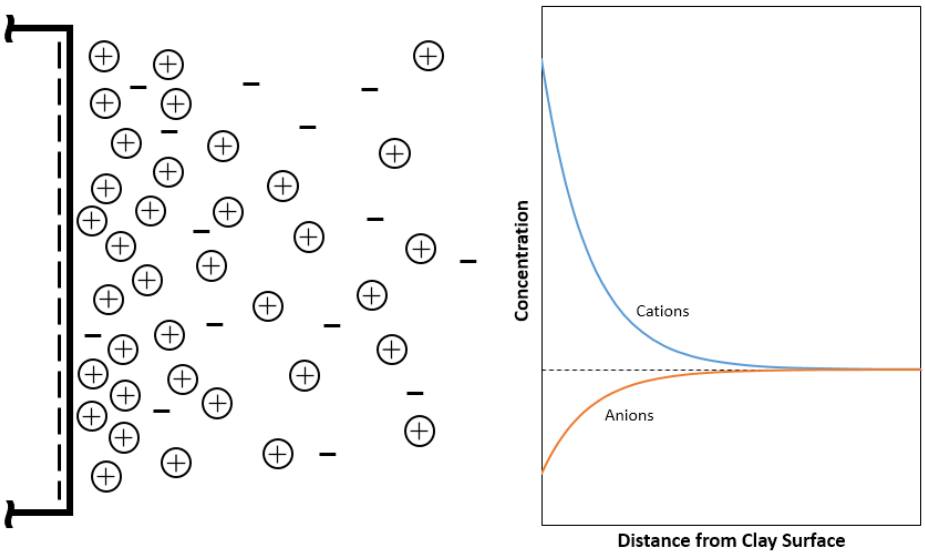

Figure 2-2: Distribution of cations and anions adjacent to clay particle surface (after Mitchell, 1976).

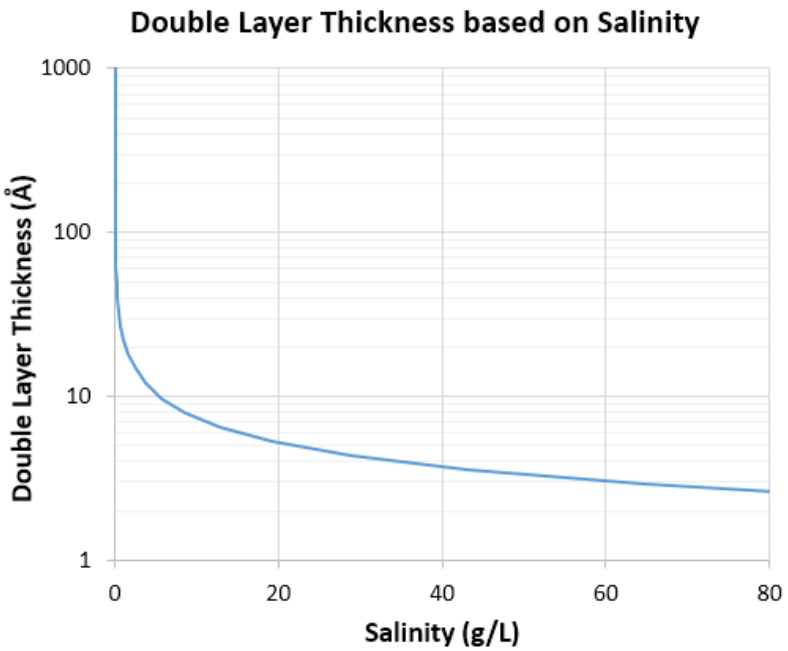

Figure 2-3: The effect of pore fluid salinity on thickness of the double layer (after Mitchell, 1976).

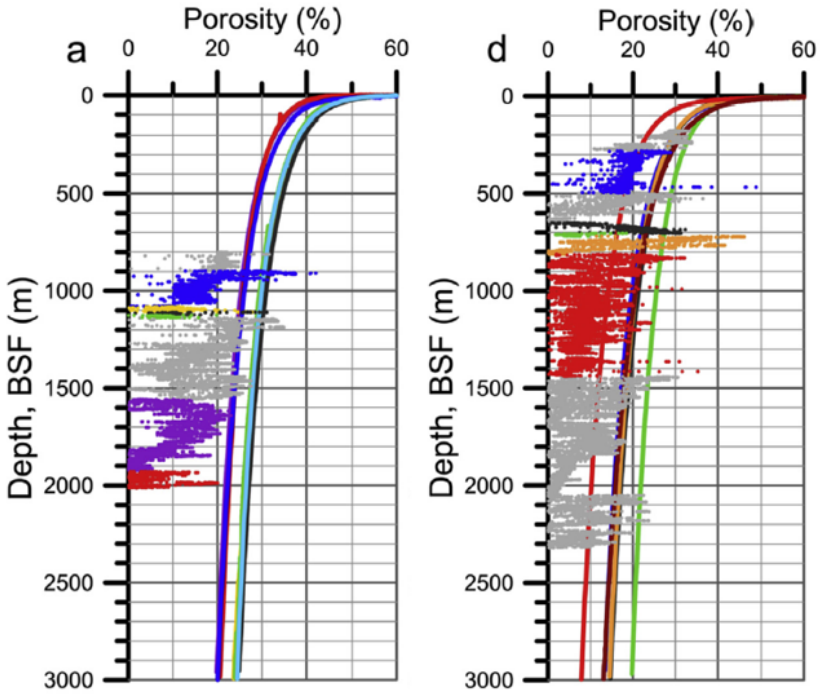

Figure 2-4: Porosity versus depth comparison between field and laboratory measurements for two wells. The different colors correspond to certain depth ranges. The dots are field measurements and the curves are laboratory data (from Nooraiepour et al., 2016).

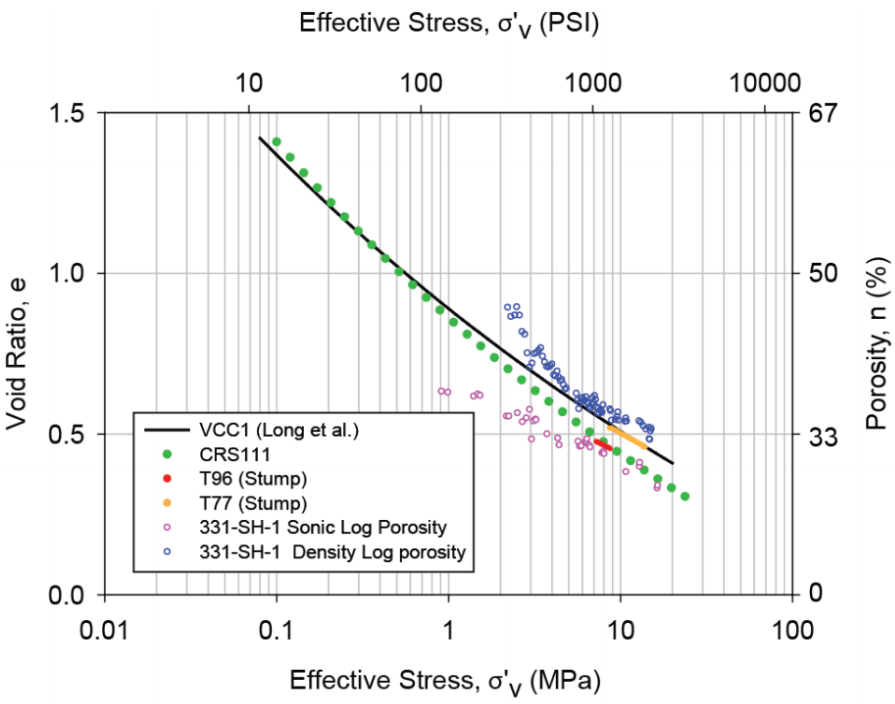

Figure 2-5: Comparison between CRS laboratory test and field measurements (from Betts & Flemings, 2014).

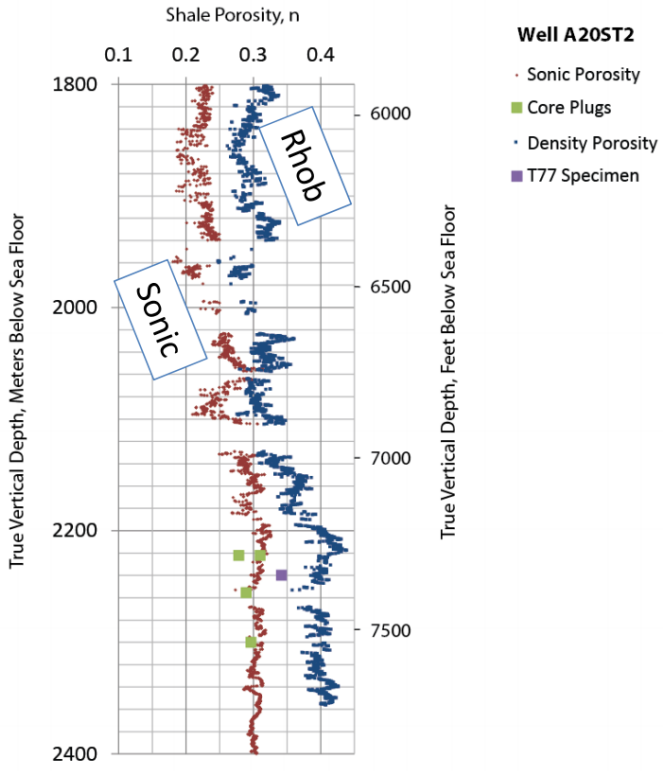

Figure 2-6: Comparison of calculated porosity values to in-situ porosity measurements (Betts & Flemings, 2014).

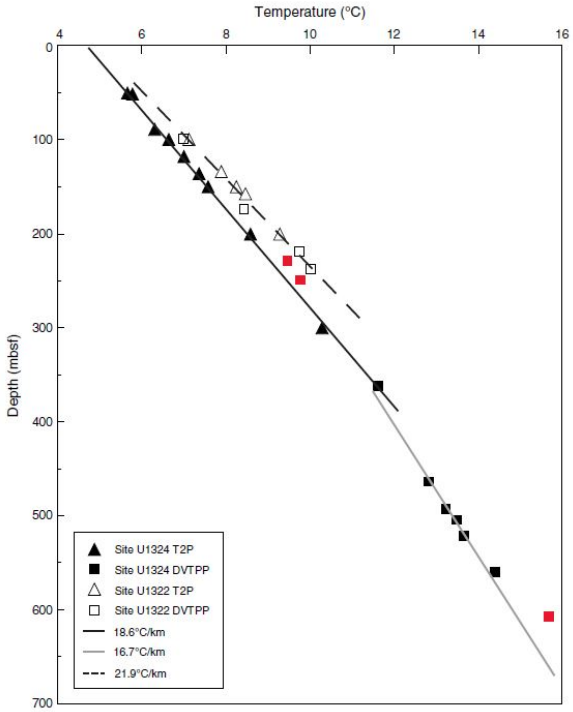

Figure 2-7: Example of the positive temperature gradient below the mudline at one of the IODP drilling sites (from Long et al. 2005).

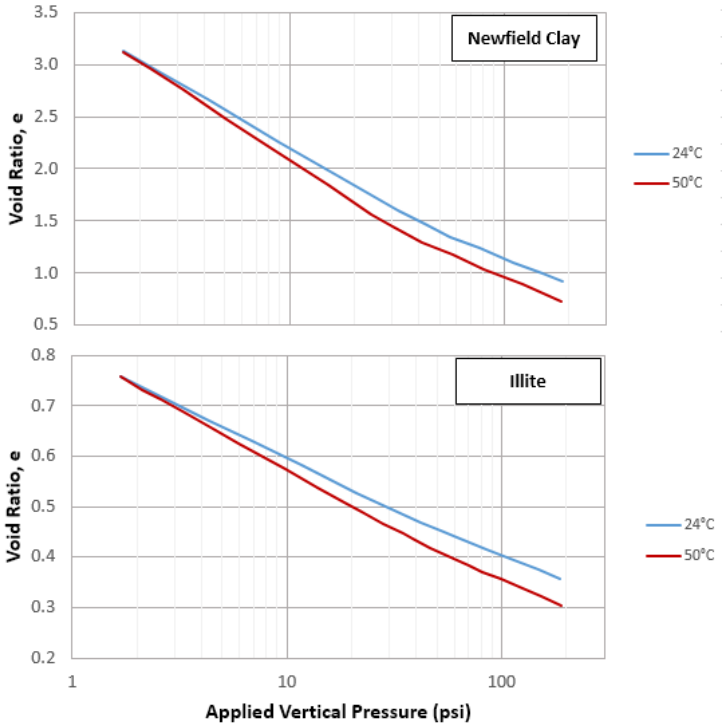

Figure 2-8: Temperature controlled compression test results for two different materials (after Plum and Esrig, 1969).

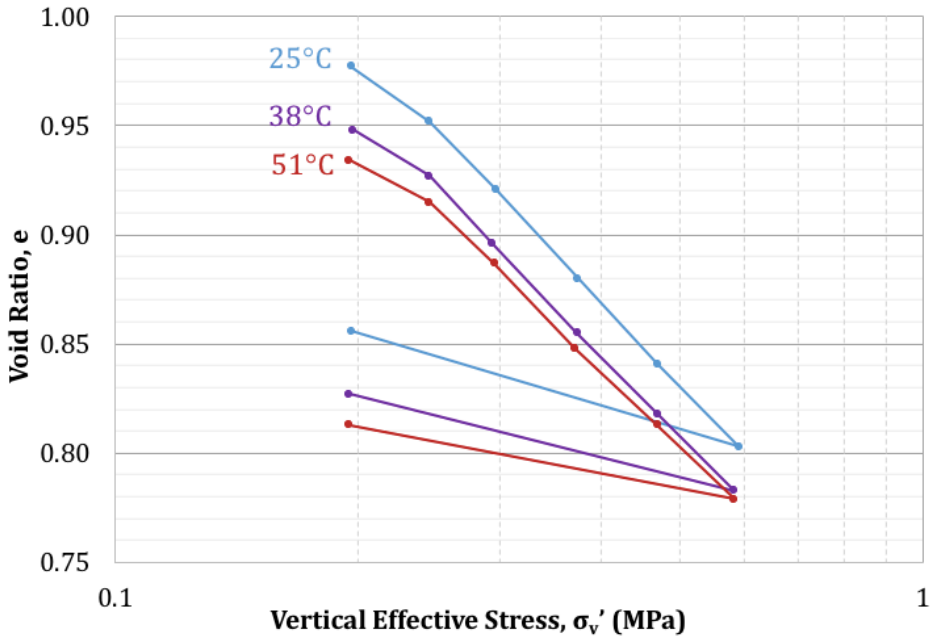

Figure 2-9: Temperature controlled oedometer test compression curves (after Campanella and Mitchell, 1968).

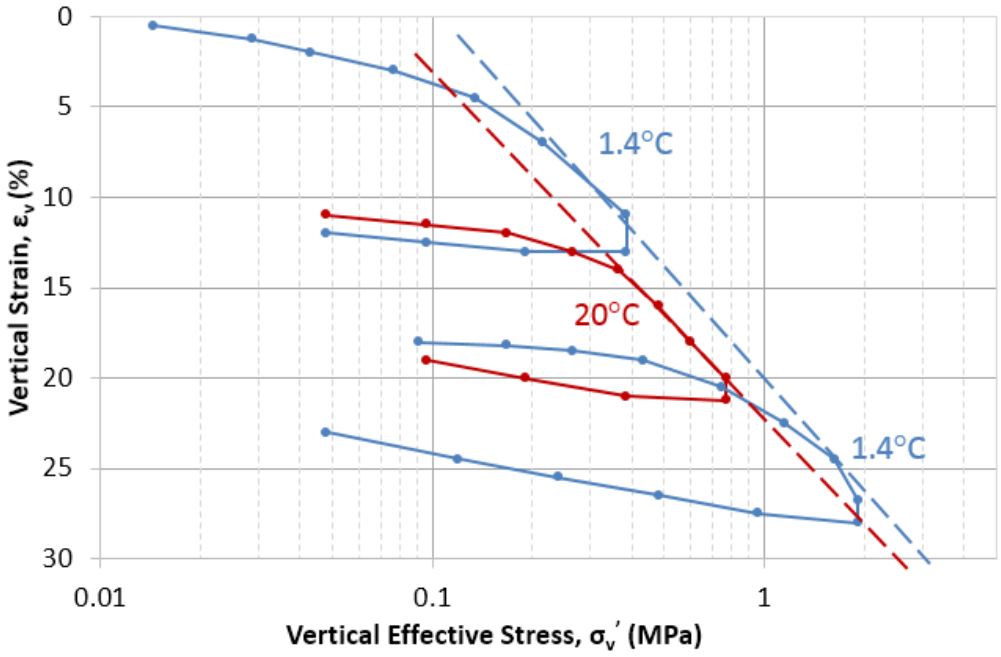

Figure 2-10: Temperature controlled compression test on Arctic Silt. Specimen was cooled instead of heated (after Ladd et al., 1985).

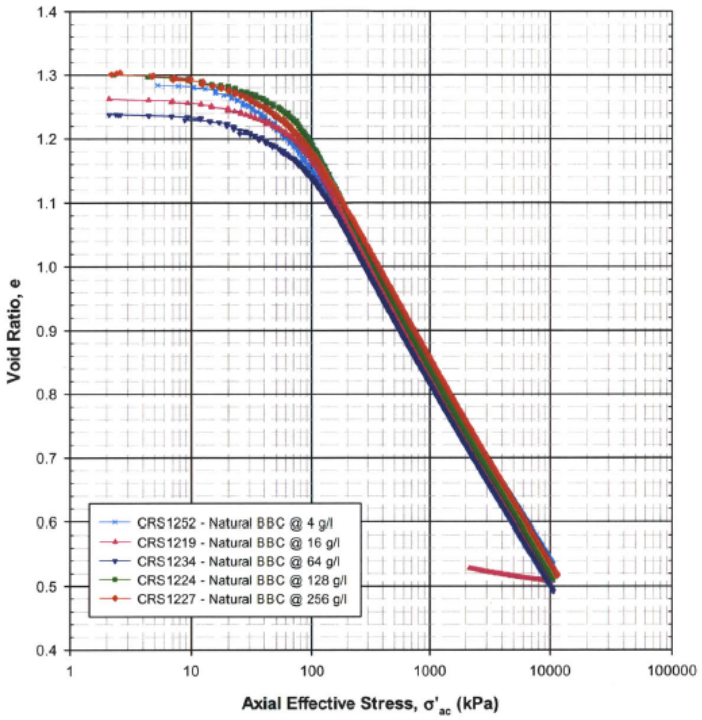

Figure 2-11: Compression test results on RBBC batched with different pore fluid salinity values (Horan, 2012).

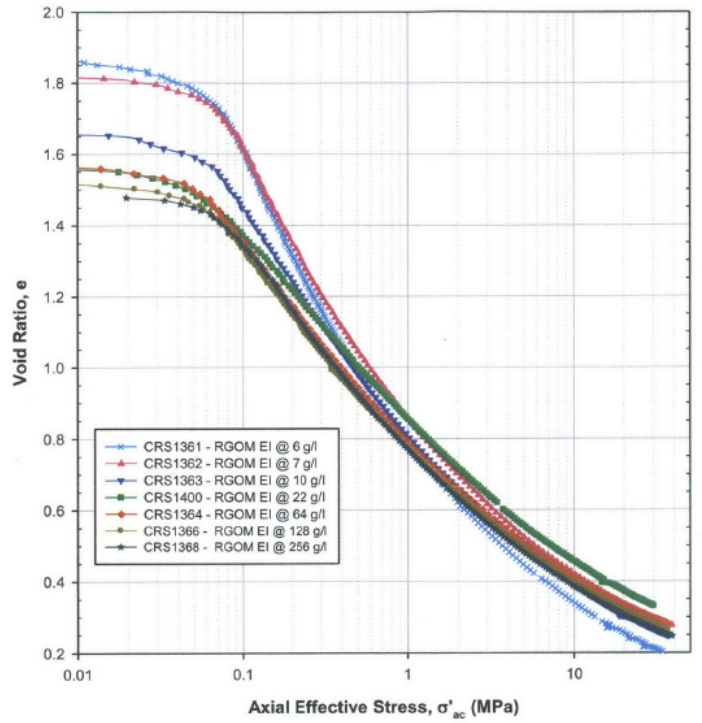

Figure 2-12: Compression test results on RGoM-EI batched with different pore fluid salinity values (Horan, 2012).

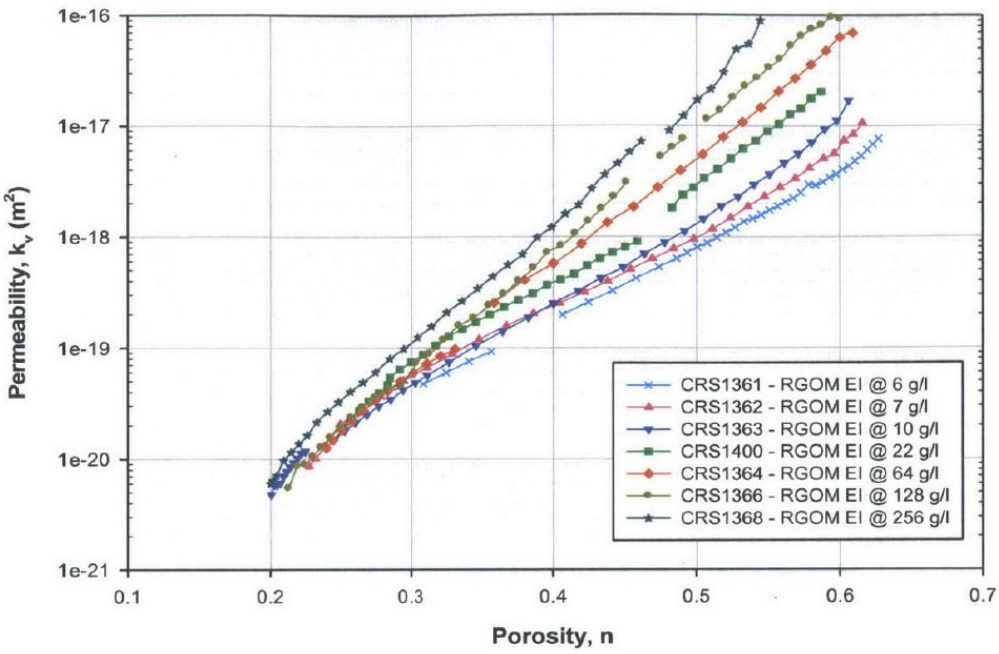

Figure 2-13: Permeability of RGoM-EI batched to different pore fluid salinities (Fahy, 2014).

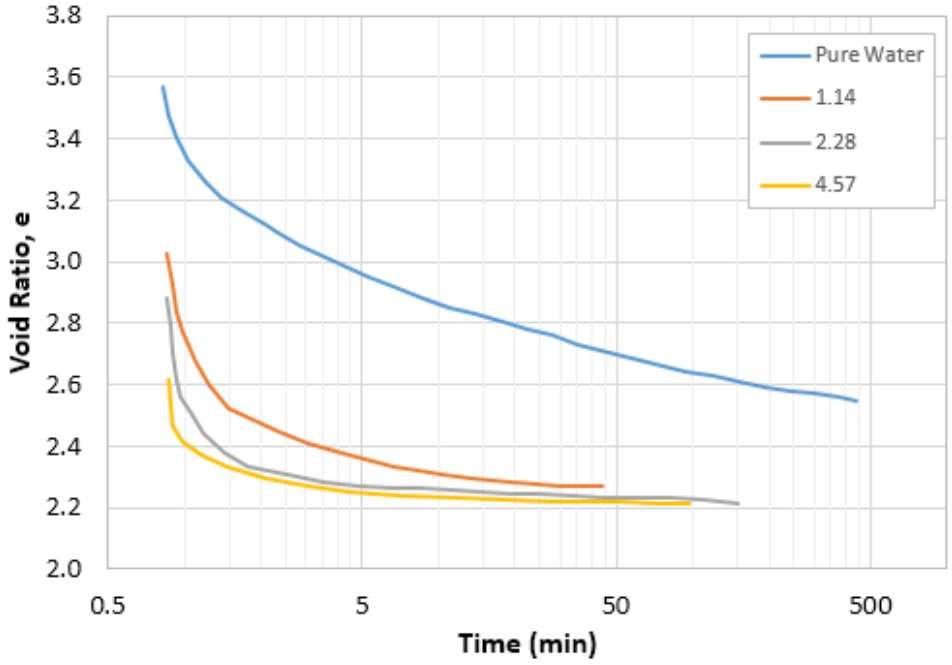

Figure 2-14: The effect of pore fluid salinity on compaction rate (after Engelhardt & Gaida, 1963).

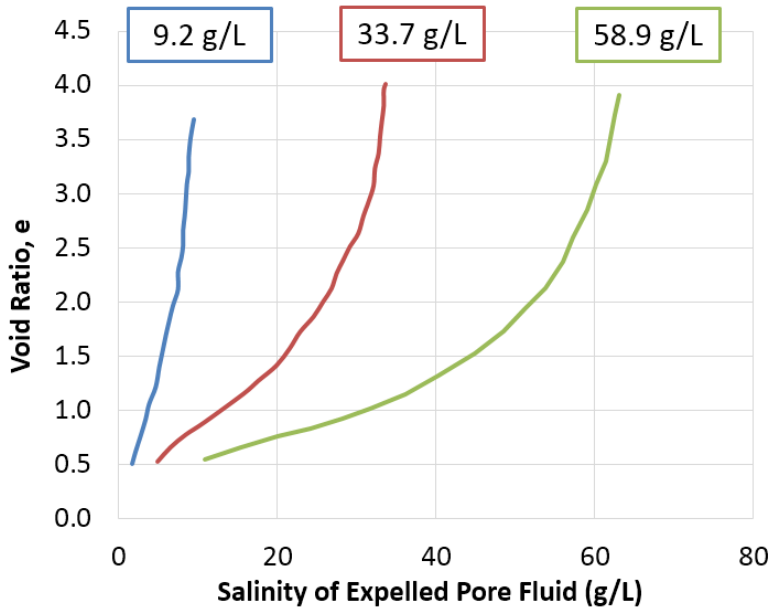

Figure 2-15: Salinity of expelled pore fluid during compression with different starting salinities (after Engelhardt & Gaida, 1963).

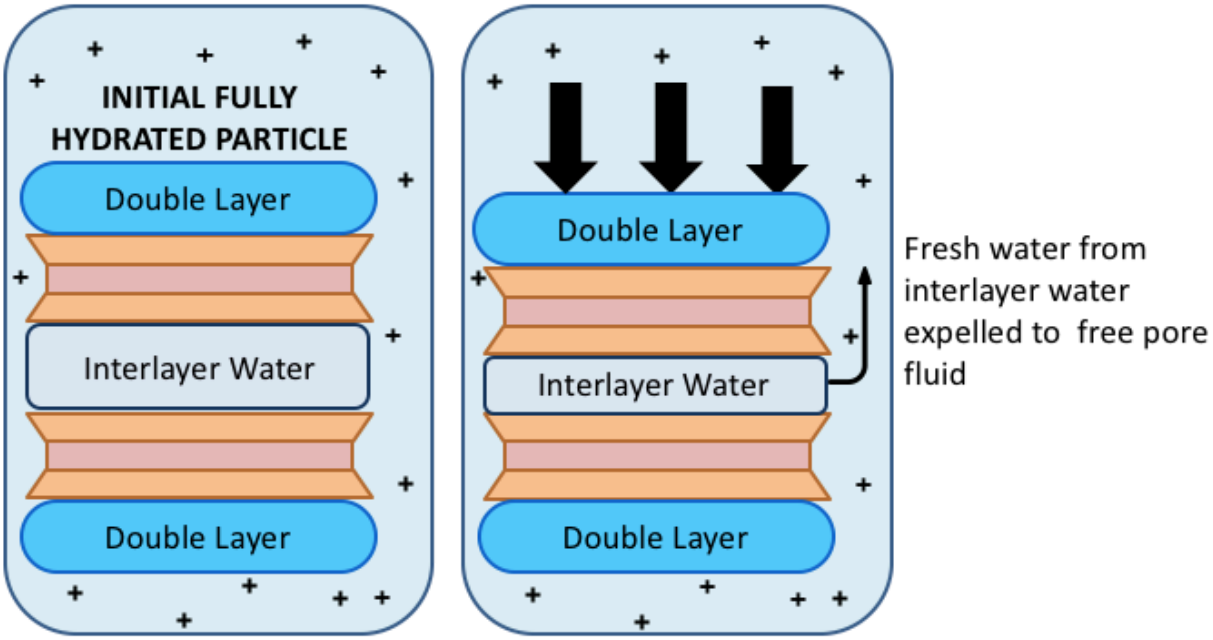

Figure 2-16: Proposed mechanism that causes free pore fluid to decrease in salinity with compression (after Fitts & Brown, 1999).

3 Materials

3.1 Introduction

The TAG Lab primarily uses resedimented material for laboratory testing programs. The resedimentation process eliminates the natural variability that exists between intact samples of the same material, as well as the problem of sample disturbance that occurs when taking samples from the ground. Section 3.2 identifies important properties of the mudrock used for this research, Resedimented Gulf of Mexico – Eugene Island (RGoM-EI). Section 3.3 outlines the resedimentation process.

3.2 Gulf of Mexico – Eugene Island

The primary source material relied on for this research is Gulf of Mexico – Eugene Island (GoM-EI) mudrocks. The material was collected from two cores drilled in Eugene Island Blocks 316 and 330 (Figure 3-1) (Betts, 2014). The material collected from the two cores comes from depths of approximately 2200 to 2500 meters below sea floor (Betts, 2014). Researchers at the University of Texas, Austin (UT) removed the mudrock material from the core tubing and left it out to air dry for 18 days (Betts, 2014). Once dry, the material was sent to an external processing facility where it was crushed so 99% passed a #100 sieve and then homogenized (Betts, 2014). The Tufts TAG Lab now has multiple 5 gallon buckets of this material for use in the laboratory. For this research, approximately half of one 5 gallon bucket was filled with a subsample of the material and once again homogenized (Figure 3-2).

Previous studies by UT GeoFluids researchers provide information to classify the GoM-EI material and the information is published in the UT GeoFluids Database. In the Unified Soil Classification System (USCS) RGoM-EI is a CH, high plasticity clay. RGoM-EI has a plasticity index of 63% and liquid limit of 87% (Figure 3-3). The material has a 44% clay

fraction (<2µm) which is primarily smectite and illite (Figure 3-4). The in-situ salinity and chemical composition of the pore fluid of GoM-EI is evaluated in detail in Losh et. al (2002). Although, as discussed in Section 2.6, research by previous UT GeoFluids members proves that the pore fluid salinity does not have much of an effect on mudrock mechanical behavior. Across UT GeoFluids research RGoM-EI is typically batched to a pore fluid salinity of 80 g/L (Hanley, 2017; Nordquist, 2015).

3.3 Resedimentation

The resedimentation process was developed at MIT and has been relied on heavily in research since its development in the 1960s. The method has been refined over the years and more detailed instructions can be found in Abdulhadi (2009) and Nordquist (2015) or Hanley (2017) for the first description of the method being used in the TAG Lab. To summarize, it is the process of K0 consolidating a homogeneous soil slurry in laboratory consolidometers to a desired stress level. The process is performed to create uniform specimen with a controlled stress history, which provides control when investigating soil behavior trends. It eliminates the problem of soil heterogeneity and in-situ sample disturbance.

3.3.1 Resedimentation Procedure

The resedimentation process requires mixing a measured amount of clay powder, water, and salt to produce a specimen that meets a target pore fluid salinity, final height, and stress level. Researchers in the TAG Lab use an Excel spreadsheet tool to calculate the appropriate amount of each ingredient based on a set of six inputs: batching water content, type of salt, temperature of initial specimen, salt concentration, mass of solids, and the natural salt content of clay powder. For all resedimentation included in this research, sea salt is used to replicate the natural conditions since the clay comes from below the ocean seafloor and the initial batch temperature is 24°C. Additionally, the natural salt content of GoM-EI clay powder is 8 g/kg, which is accounted for in the

calculation to determine the required mass to achieve the target batch salinity. The rest of the inputs for all resedimentation batches in this research are summarized in

Table 3-1. The rest of this section summarizes the steps to producing a resedimentation sample.

First, measure the correct amount of clay power, distilled water, and sea salt and mix them in a Kitchen Aid mixer. Add the distilled water and sea salt to the mixing bowl first so the sea salt dissolves into the water. Then slowly add the clay powder and mix for a couple minutes until the three components are blended well, resulting in a uniform slurry of cake batter consistency (Figure 3-5).

After mixing, cover the slurry in the stainless steel Kitchen Aid mixing bowl and set aside to equilibrate for 24 hours. Leave the slurry to equilibrate overnight so all of the clay has a chance to hydrate and absorb the amount of water required for the double and interlayers. After 24 hours remix the slurry in the Kitchen Aid bowl. When the slurry is mixed well again place it in the vacuum chamber under a vacuum of about 20 inches of Hg. The vacuum should be left on for approximately 20 minutes to deair the slurry mixture. After vacuuming, the slurry is ready to be tremied into the consolidometer.

While the slurry is under a vacuum, a consolidometer is set up for the incremental one-dimensional consolidation process. The consolidometer is an acrylic or PVC tube about 3.8 centimeters inner diameter. A small amount of silicon oil is used to lightly coat the consolidometer walls to help reduce side wall friction that can build up with compression of the slurry. A porous stone covered with a layer of nylon filter fabric is put in the base of the consolidometer. The porous stone and filter fabric must fit snugly into the consolidometer, if it is not snug enough to the inner diameter of the tube then use an additional layer of filter paper. Once the porous stone and filter fabric are in the base of the consolidometer, place the set up on top of a larger porous stone in a bath of water at the same salinity as the slurry (Figure 3-6). Once the consolidometer is set-up transfer the slurry into the consolidometer using the syringe apparatus shown in Figure 3-7, developed by Anthony Hanley (Hanley, 2017). Filling the syringe and subsequently

squirting the slurry into the consolidometer must be done slowly and with care to prevent air bubbles from entering the slurry. Fill the water bath so the water level is up to the bottom porous stone.

Leave the consolidometer filled with slurry in the water bath to sit overnight, approximately 24 hours. Then, place a filter paper and porous stone on top of the slurry as the first load increment. From here load the slurry incrementally with a load increment ratio (LIR), $\Delta\sigma/\sigma_v$, of 1. The first couple of load increments are applied using dead weights on top of the specimen. One of the deadweights is a PVC spacer that protrudes from the end of the consolidometer. When the weight is approximately 1 kg or greater add a PVC spacer to the bottom of the consolidometer tube as well. Adding the bottom spacer helps make the stress distribution from top to bottom of the specimen more uniform. Then, when the added weight reaches about 1.75 kg, place the hanger on top of the specimen and add the subsequent loads to the hanger below (Figure 3-8). During consolidation, the vertical deformation can be measured by an LVDT to see when the end of primary consolidation occurs. Each load increment is held until the end of primary consolidation (usually 24-48 hours). Throughout the resedimentation process keep the water bath level at the same level as the small porous stone inside of the consolidometer. This will ensure the sample remains completely saturated. If evaporation is occurring then add distilled water to the bath (since only water evaporates do not add salt water back as it will make the bath more saline).

The maximum stress for the CRS test specimen is about 1 ksc. Once this maximum stress is achieved the specimen is unloaded to an OCR of 4. It is unloaded to an OCR of 4 because then the soil is near hydrostatic effective stress conditions and the shear strains that inevitably develop during extrusion are minimal (Abdulhadi, 2009).

A resedimentation tube takes close to three weeks to prepare properly. Once at the correct stress level and OCR, leave the specimen in the tube until it is needed for a test.

For the CRS tests, extrude approximately 2.5 centimeters from the tube per test (since only a small chunk of the resedimentation tube is used, multiple tests can be run from the same tube). After extruding the sample for a CRS test, gently push the remaining material in the consolidometer back up into the tube. Then place the consolidometer (with the remaining material) on the PVC spacer in the water bath and put the final load back on top. Confirm the water bath is at the level of the porous stone, and leave the material in this set up until needed for the next CRS test.

Table 3-1: Record of all resedimentation tubes batched for research included in this thesis.

Resedimentation ID	Batch Water Content (%)	Salt Conc. (g/L)	Mass of Solids (g)	Mass of Salt (g)	Mass of Water (g)
RS547	120	80	450.00	49.13	598.95
RS550	110	80	800.00	79.34	967.27
RS551	110	80	800.00	79.34	967.27
RS480	110	80	219.78	21.80	265.73
RS485	122	80	250.00	25.58	336.20
RS486	122	80	250.00	25.58	336.20
RS488	120	80	250.00	25.07	330.09
RS570	120	80	100.00	10.03	132.04
RS571	136	5.9	250.00	0.01	340.02

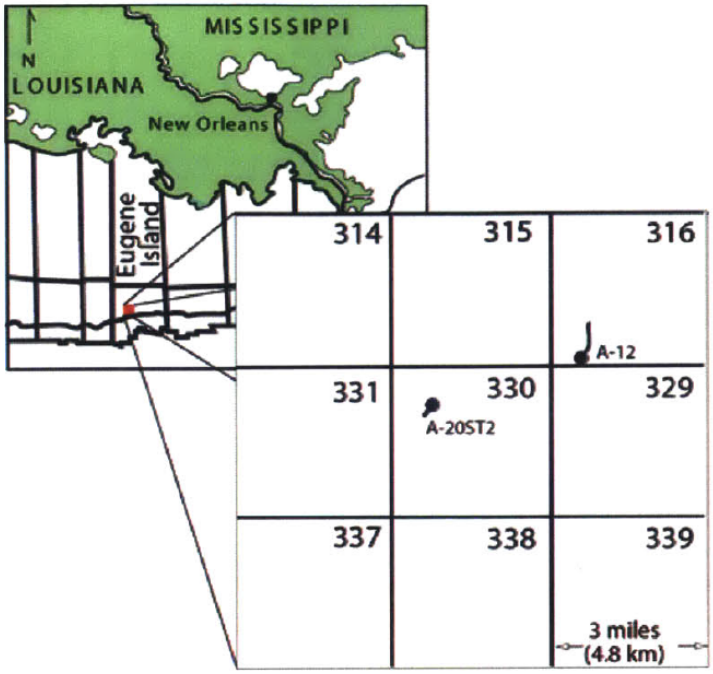

Figure 3-1: Source location of GoM-EI Material. It was cored from 2200-2500 meters below seafloor (Nordquist, 2015).

Figure 3-2: Ground and homogenized clay powder stored in 5-gallon buckets. Approximately half a bucket of powder was used in this research.

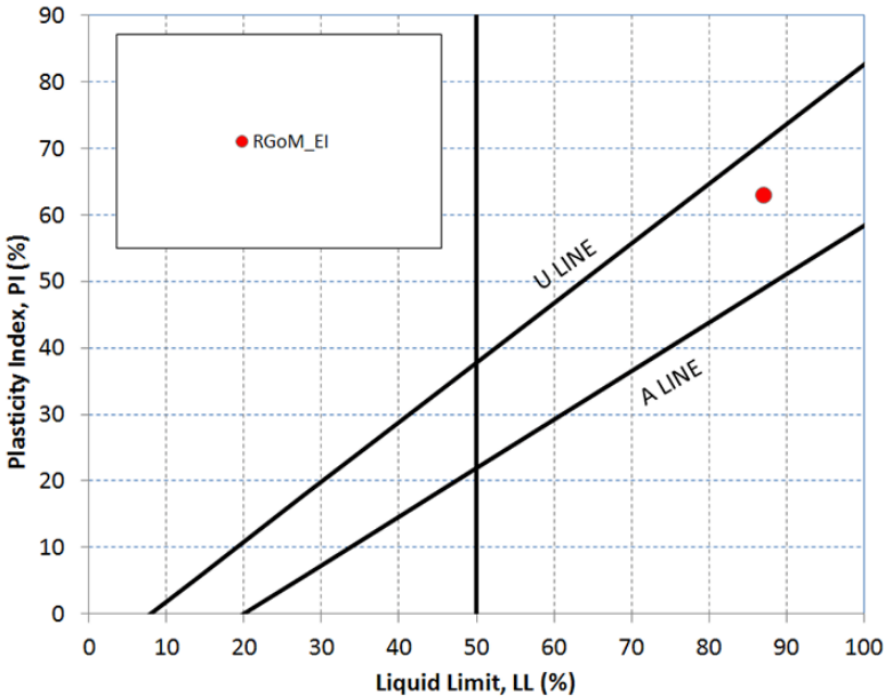

Figure 3-3: Plasticity chart with RGoM-EI material (from UT GeoFluids website).

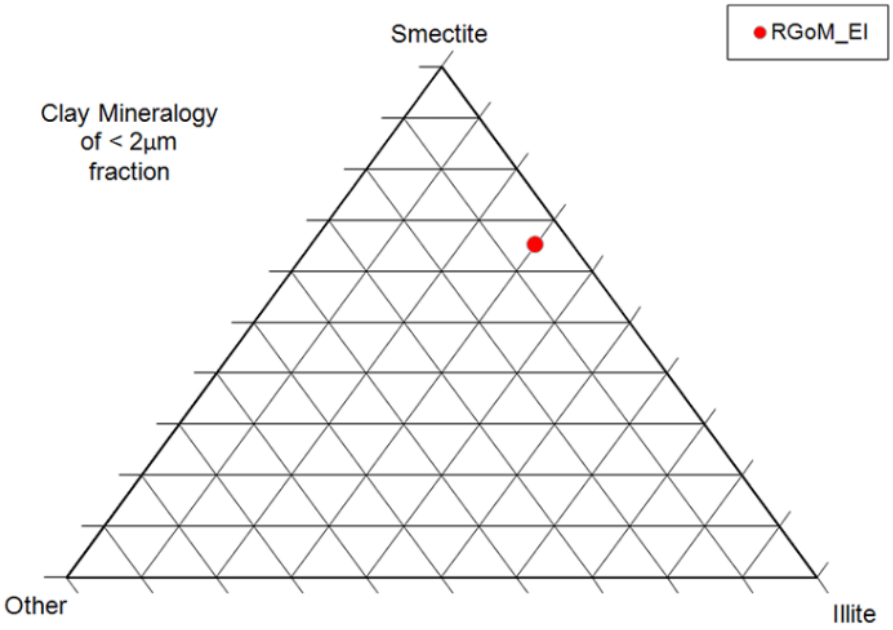

Figure 3-4: Clay fraction composition of GoM-EI material (from UT GeoFluids website).

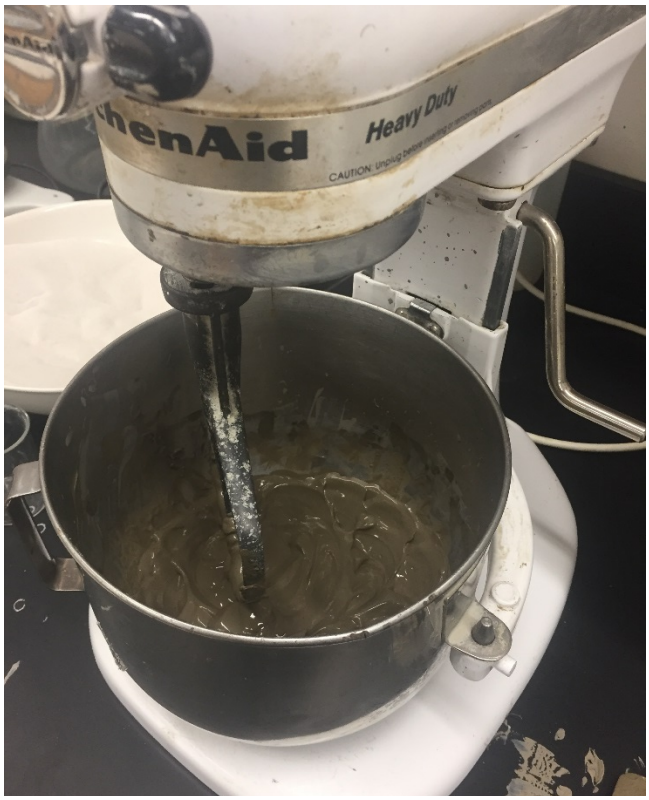

Figure 3-5: Mixture of clay powder, sea salt, and distilled water into a well-blended slurry.

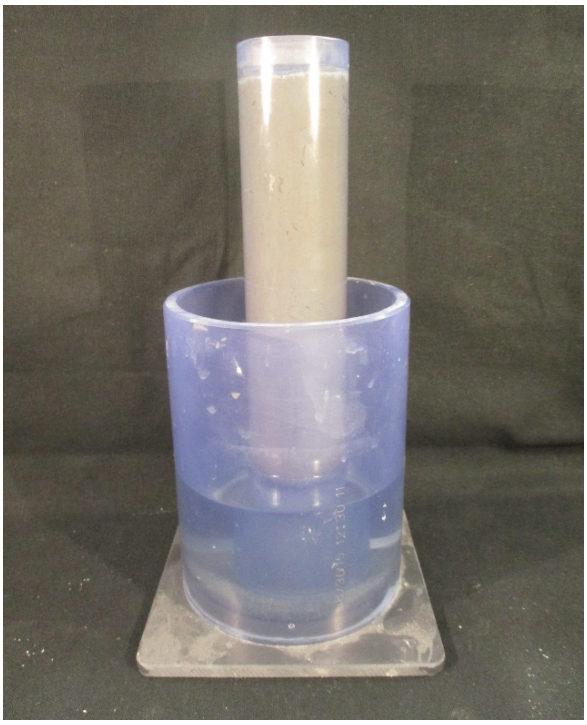

Figure 3-6: Typical resedimentation consolidometer set up.

Figure 3-7: Syringe method used to carefully tremie slurry into the rigid wall cylinder.

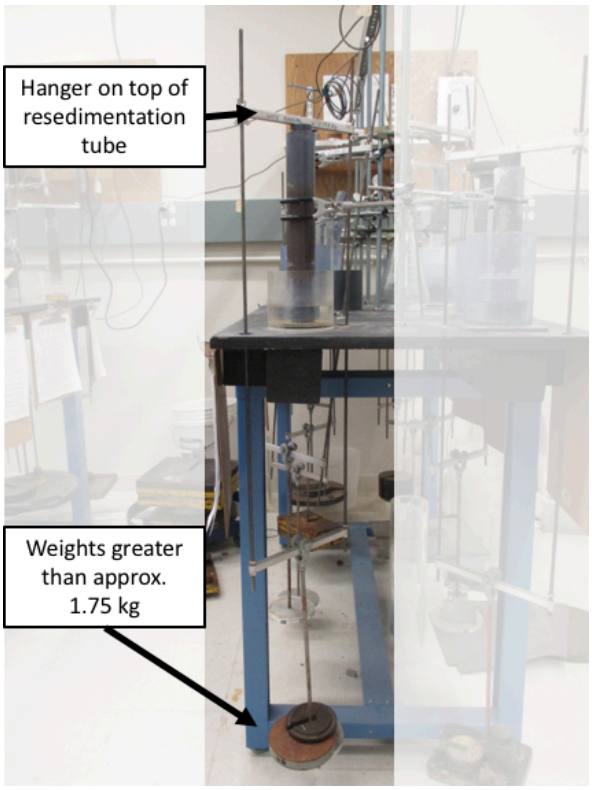

Figure 3-8: Hanger used to add load increments that are greater than 1.75 kg during resedimentation.

4 Equipment

4.1 Introduction

This chapter summarizes the equipment used for CRS tests and salinity measurements. Additionally, part of this research involved redesigning some of the computer control system components used in the TAG Lab, so there are also details regarding the newly designed components. Section 4.2 describes the CRS equipment, and Section 4.3 describes the electrical conductivity equipment. Transducers measure the physical parameters during tests and are briefly summarized in Section 4.4. Section 4.5 is an overview of the computer control system that allows experiments to be partially automated in the TAG Lab. Finally, Section 4.6 explains the data acquisition system that collects all data in the TAG Lab.

4.2 Constant Rate of Strain Equipment

The TAG Lab relies on Trautwein© CRS cells combined with a five ton Wykeham Farrance gear-driven load frames to run CRS tests. Two CRS cell set-ups, Cell 1 and Cell 2, are used in this research. Each CRS cell is outfitted with its own set of transducers used to measure important physical parameters during the test.

4.2.1 Standard CRS Set-up

The standard CRS set up, shown in Figure 4-1, contains five main pieces: the specimen ring, top cap, piston, base, and outer chamber. Additional accessory pieces and instructions for how to assemble everything together are outlined in the procedures section in Chapter 5.

- **Specimen Confinement Ring:** The confinement ring is a stainless steel ring that holds the physical specimen. The design of the ring was specially made by MIT researchers to house a small diameter specimen inside of Trautwein© cells. It

prevents the specimen from moving laterally so the test is truly one-dimensional. The inner diameter of the specimen chamber is 3.545 cm. The height of the specimen that goes into the chamber is 1.259 cm, so the aspect ratio is about 2.8. The outer diameter of the ring is 7.62 cm. The specimen ring sits tightly inside the outer Trautwein© chamber and on top of the cell base.

- **Base:** The base is 11.43 cm in diameter. It has two drainage ports. One port is attached to the pore pressure transducer and the other is attached to a pressure volume actuator (PVA) and is used to fill the cell during set-up and apply back pressure to the bottom of the specimen.
- **Outer Chamber:** The outer chamber seals the specimen off from the laboratory environment and seals the base pore fluid from the cell pressure. This separation of the base pore fluid and the cell pressure is what allows accurate measurement of the pore pressure. The outer chamber is made of different materials depending on testing requirements.
- **Piston:** The piston for the CRS is 1.905 cm in diameter and has a mass of about 2 kg. At the bottom of the piston a piston cap is screwed on that is just slightly smaller than the area of the specimen. This piston cap provides the loading surface. The piston moves up and down through a set of ball bearings that work to provide alignment for the piston and also reduce friction build up from moving up and down. The ball bearings should be greased every three or four tests to ensure the piston can move freely through its housing in the top cap.
- **Top Cap:** The top cap is required to hold the piston in place, exactly centered over the specimen. The top cap prevents any rotation or translation of the piston during loading. The opening in the top cap that the piston penetrates to make contact with the specimen is sealed using a rubber cup ring. The piston seal prevents the chamber from leaking and closes the chamber off from the outside laboratory environment.

4.2.2 Temperature Controlled CRS Tests – Cell 1

The temperature controlled CRS Cell was modified so the temperature of the cell could be held constant at elevated temperatures. The CRS cell used for the temperature related tests will be referred to as Cell 1. The outer chamber of Cell 1 was made of stainless steel, and a band heater was installed around the outside of this outer chamber. The band heater, a Tempco Duraband Barrel Band Heater, part number MBH00022, is made of a mica core able to heat up to approximately 425°C. The band heater is connected to a temperature control box designed for this research. Inside the temperature control box is a temperature controller that compares a thermocouple voltage reading to a set value and turns the heating element, the band heater, on or off to achieve the target value. The temperature controller is an Autotonics TX4S Series Temperature Controller, and the thermocouple is an Uxcell 3 mm x 200 mm x 1500 mm Type K thermocouple. The thermocouple was outfitted with the male component of a Swagelok connection. During set up the thermocouple is inserted into the vent opening in the CRS top cap. This way a pressure tight connection is made and the temperature measuring device is within the cell set-up. This CRS set-up (Figure 4-2) allows the CRS cell to be set and maintained at a certain temperature for the duration of the test.

The transducers for Cell 1 included two linear voltage displacement transducers (LVDTs), two pressure transducers, and one load cell. The load cell for Cell 1 is rated for up to 4,500 kgf (10,000 lbs), much higher than the load cell for Cell 2. Additionally, the entire test set-up is computer controlled and all of the transducers are connected to the central data acquisition system. The computer control set up is discussed in a subsequent section.

4.2.3 Salinity CRS Tests – Cell 2

The research related to understanding the salinity evolution primarily uses a different CRS set up, referred to as Cell 2. Cell 2 has an outer chamber made of translucent acrylic (the acrylic allows the inside chamber to be seen during testing). The transducers used for Cell 2 include: one LVDT, two pressure transducers, and one load cell. Finally, none

of this cell is computer controlled, but all of the transducers are connected to the central data acquisition system.

4.2.4 Load Frame

The load frames used for both cell setups are similar. A motor drives a set of gears that moves a pedestal that the CRS Cell sits on up or down to load or unload the specimen, respectively. The capacity of the load frame is 5 tons (10 klbs). Care must be taken to ensure that the load frame does not run out of stroke (the pedestal isn't too low or too high) during a test because this will break the load frame. The load frame is turned on by a two pole switch, the switch is either put into "FORWARD" or "REVERSE" mode which corresponds to loading or unloading.

4.3 Electrical Conductivity Equipment

To calculate the salinity of a liquid the TAG Lab uses the method of comparing an electrical conductivity reading to a calibration curve to determine the salinity. The electrical conductivity meter is a Fisher Scientific Accumet XL 20 with a Temperature Compensated Two-Cell Conductivity Probe (Figure 4-3). The calibration curve was created by Mark Zablocki in 2016 by following the procedure in Germaine & Germaine (2009). The calibration curve uses a reference solution of 1 g/L sea salt and is shown in Figure 4-4.

4.4 Transducer Calibration for CRS Cells

Transducers are an invaluable part of the experimental set up in the TAG Lab because they allow measurements to be made at times that nobody is in the lab, at the same time that other measurements are being made, and at any desired time increment. Additionally, if set up and calibrated correctly, the transducers provide more precision than measurements from manual devices (Germaine & Germaine, 2009).

Transducers convert a physical quantity to an electrical signal that is then recorded as a voltage. In the TAG Lab, these output voltages are recorded in the central data acquisition system. The pressure transducers, LVDTs, and load cells were all recalibrated prior to being used in this research with in house TAG Lab references. **Error! Reference s ource not found.** identifies the transducers that were used on each cell and the calibration data for each device.

4.5 Computer Control System

The TAG Lab is set up so most stations can operate under a computer controlled system. As discussed previously, CRS Cell 1 was completely computer controlled. The cell pressure held on the specimen is maintained at a constant value using a PVA and the load frame switched off once a certain stress level is achieved in the system.

The computer control system used in this research contains five parts: a computer, ARS Junction Box, computer control box, computer monitor, and a load frame junction box.

- **Computer:** The computer runs the Windows XP operating system. Using Microsoft QuickBASIC Version 4.50 and the BASIC language, multiple testing control programs were written to control the triaxial tests and CRS tests run in the TAG Lab. This research uses a revised 2017 CRS Program. The updated program includes code to interact with the load frame junction box.
- **ARS Junction Box:** The analog to digital and digital to analog converters use an old IBM ISA Interface configuration. The ARS Junction Box houses the ARS Card (developed by ARS technologies) which is an ISA to USB interface connector because the newer computers in the TAG Lab use the USB2ISO card.
- **Computer Control Box:** The computer control box is the main junction box between the computer program and the testing motors. For CRS tests, only the cell pressure is controlled, so there is one motor controller in the box. As part of this research, an updated version of previous computer control boxes was assembled with new ESCON motor controllers and a newly designed printed

circuit board (PCB) control card. More detail about the computer control box is provided in Section 4.5.1.

- **Computer Monitor:** Using the monitor allows the experimenter to monitor the test real time based on the engineering values that the computer calculates based on the transducer voltages.
- **Load Frame Junction Box:** The load frame junction box was designed for this research to shut the load frame off at a defined stress level. Because the tests were run to a final stress level that approaches the limit of the load cell it was important that the high stress level not be exceeded or else the load cell would be overloaded resulting in failure.

A diagram showing how the computer control system components interact is included as Figure 4-5.

4.5.1 Computer Control Box & Interface Control Card

During this research it was identified that an updated, more universal computer card needed to be designed and installed into the computer control boxes built for the TAG Lab. The existing control card is a handmade, soldered board, and across the lab the cards are not all identical. The variation between cards makes troubleshooting difficult and time consuming. Therefore, a new PCB card was designed using the same concept as the originals. The goal is to replace all of the controls cards in the lab with this new one to make everything standard and have the same capabilities.

The computer control card directs voltage commands from the computer to the correct motor controller to cause a physical change in the experiment. The universal card can accommodate up to three motor channels with a fourth one available for other uses, usually a relay. The PCB card was designed in the program Eagle 7.7.0. Using the software, all of the electronic components (example: 25-pin connectors or 16 pin ribbon cable connectors) are drawn schematically and with the appropriate connections between components. Figure 4-6 shows the circuit diagram schematically drawn in Eagle

for the designed card and identifies the major components. When the schematic is finished the software converts it to a properly scaled board drawing with the associated electronic components. The electronic components are then physically located and arranged within the board boundaries. Finally, based on the physical arrangement of electrical components and the electronic connections drawn in the schematic, the software auto routes the location of conductive tracks for the physical board. The resulting board layout is saved to a series of Gerber files and sent to a manufacturer for production, the TAG-R2 card was manufactured by Advanced Circuits in Colorado. The result is a number of identical PCB boards that are then "stuffed" with the necessary components when they are ready to be installed into a box. For the designed "TAG-R2" control card, the components are (4) 16 pin sleds, (5) 14 pin sleds, and a 25 pin connector. The (4) 16 pin sleds are for ribbon connectors, (4) of the 14 pin sleds are for DIP 171 Relays, the fifth 14 pin sled is for an IC7407 chip, and the 25 pin connector is for the connector that comes from the computer to the control box.

Inside the computer control box (Figure 4-7) there is: the "TAG-R2" control card, one ESCON 50/5 Servo controller, an Autotonics W50NT500 power supply, and all the associated wiring for the one motor channel. The computer control box can operate in either "Manual" or "Computer" control mode. The manual mode allows the user to bypass the computer signals and control the motor using a potentiometer that is on the front panel of the box. For most of the test, however, the box is set to computer control.

The cell pressure is controlled by a feedback loop through Motor Channel 1 in this computer control box (Figure 4-7). The cell pressure transducer records a voltage based on the physical pressure in the cell and sends it to the computer program. The computer program uses an input calibration factor and zero voltage reading to convert the measured voltage into an engineering value of the cell pressure. The engineering value is compared to the defined target value, and then the computer sends a signal through

the control box for the PVA to adjust appropriately. The PVA reacts to either push more water into the cell to increase the cell pressure or pull water out to lower it.

This computer control box also controls the Load Frame Junction Box through Channel 4 to turn the load frame on or off by comparing the current load to a target value. The voltages from the load cell and cell pressure transducers are used to calculate a stress value in engineering units based on their respective calibration factors and zero values. Section 4.5.2 describes how the load frame junction box works.

4.5.2 Load Frame Junction Box

The load frame junction box contains a manual switch, AC/DC converter, relay, a power inlet for the box to be powered, and a power outlet to plug in the load frame. The box is plugged into the 120V wall outlet, which provides power that goes to the AC/DC converter. If the box is in manual control then this power is provided directly to the outlet that energizes the load frame. The load frame then operates as if it were plugged into the wall as this outlet is always “hot” in manual control. However, when the box is in computer control then a signal comes in from Channel 4 of the computer control box and either energizes or deenergizes the relay in the box. If the relay is energized then a switch closes so the outlet that the load frame is plugged into is connected to power. If the relay is not energized then the switch is open so the outlet is not powered and therefore the load frame remains off. The control signal is based on a comparison between the current calculated stress in the system and the target value. This control loop is the reason the load frame automatically shuts off when the test reaches a target stress level and prevents the load cell from being overloaded. Figure 4-8 is a circuit diagram of the load frame junction box.

4.6 Data Acquisition System

All data in the TAG Lab are collected by a central data acquisition system. There are 200 total channels connected to the TAG Lab central data acquisition system. CRS Cell 1 uses

channels 80-86 and CRS Cell 2 uses channels 132-137. All of the data collection channels are connected to a Hewlett Packard HP3497A data acquisition unit connected to a PC with a Windows interface used to create data files. When setting up a data file the user has the option to choose which channels should be recorded, how many data entries should be recorded before terminating the file, and at what time interval. The data are stored on the computer hard disc and then transferred to USB sticks for subsequent analyses.

Table 4-1: List of electronic transducers and relevant calibration information for transducers used with CRS Cells 1 and 2.

Transducer ID	Type	Capacity	Calibration Factor, CF	R^2	Date	Calibrated by
CRS Cell 1 Transducers						
G90	LVDT	-	2.464 cm/(V/V)	0.999997	12/12/2016	ARP
L-91	LVDT	-	3.4566 cm/(V/V)	0.999995	6/2/2017	ARP
D6146	pressure transducer	140 kgf/cm^2	-7276.1 $kgf/cm^2/(V/V)$	0.99998	11/20/2016	ARP
PT9222505	pressure transducer	140 kgf/cm^2	9052.2 $kgf/cm^2/(V/V)$	0.99997	12/27/2016	ARP
AE13295	load cell	4500 kgf	1508168 kgf/(V/V)	0.99998	6/17/2016	ARP
CRS Cell 2 Transducers						
H-90	LVDT	-	2.49 cm/(V/V)	0.99998	9/13/2017	ARP
C03154	pressure transducer	200 kgf/cm^2	-699.9 $kgf/cm^2/(V/V)$	0.999999	11/20/2016	ARP
2590-0006	load cell	225 kgf	-43199.9 kgf/(V/V)	0.9998	9/26/2017	ARP
CAS	load cell	1100 kgf	376236 kgf/(V/V)	0.9999995	12/11/2017	ARP
8222502	pressure transducer	200 kgf/cm^2	-697.4 $kgf/cm^2/(V/V)$	0.999997	10/19/2017	ARP

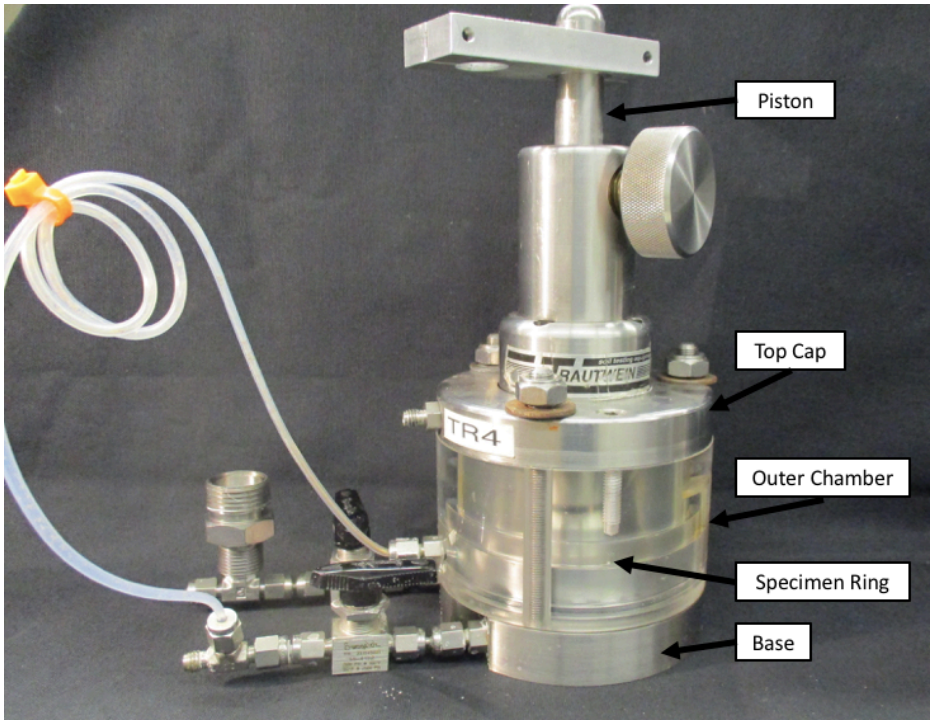

Figure 4-1: Standard CRS cell set-up with the five main components labeled.

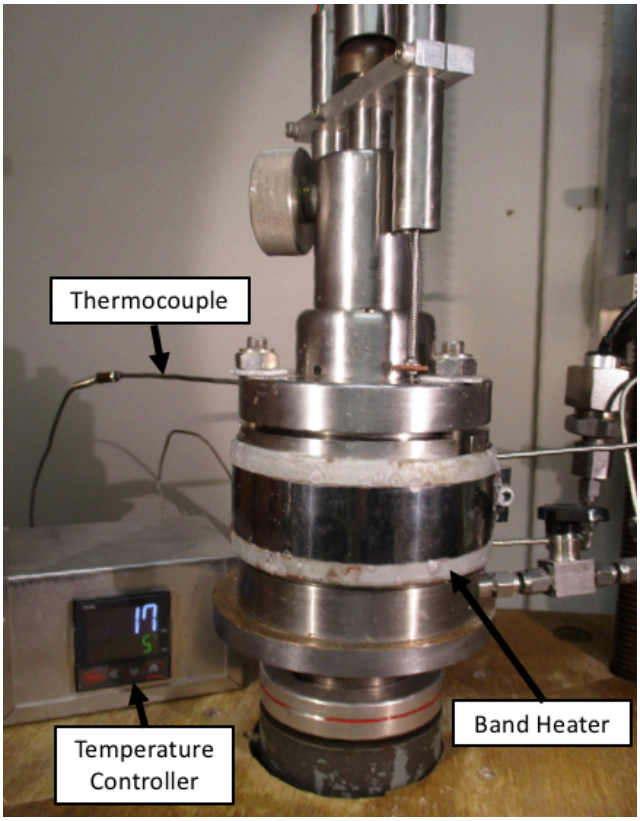

Figure 4-2: Temperature controlled CRS Cell is a standard cell plus a band heater, temperature control box, and thermocouple.

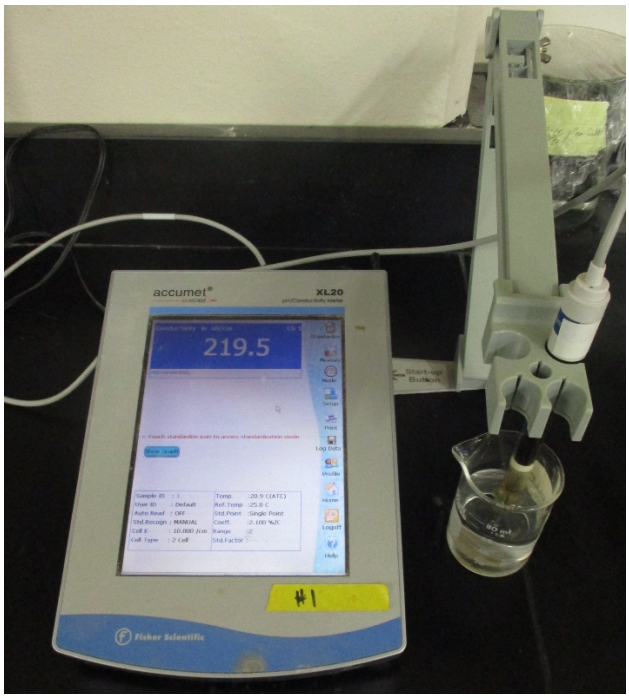

Figure 4-3: Electrical conductivity meter, Fisher Scientific Accumet XL 20, used in the salinity research.

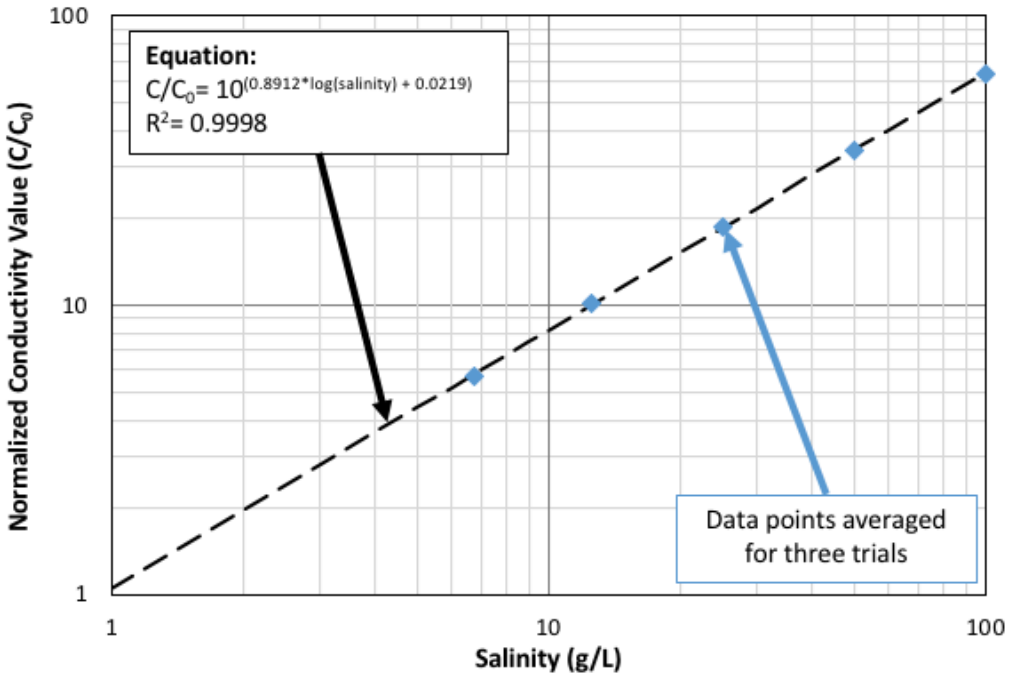

Figure 4-4: Calibration curve used to convert from normalized electrical conductivity to salinity. Calibration done by M. Zablocki in 2016 with sea salt as the reference salt.

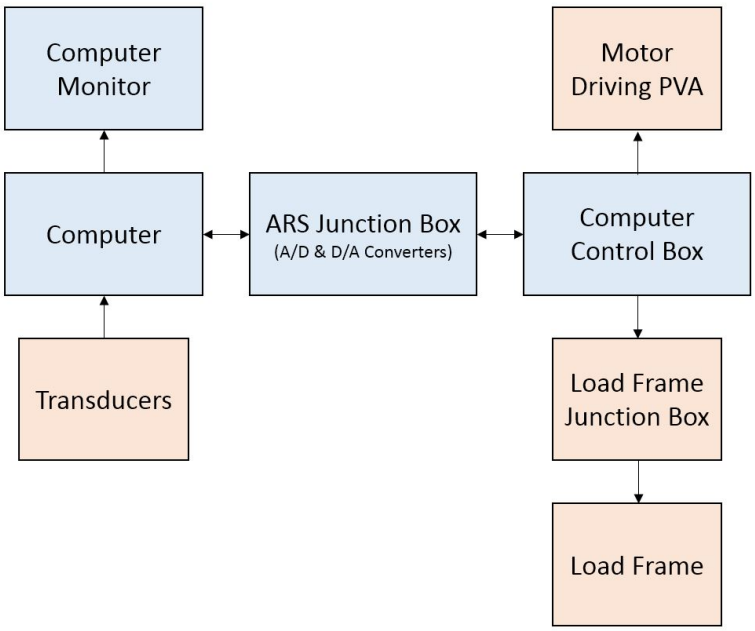

Figure 4-5: Overview of the computer control system. Blue boxes indicate the component is one of the main four items used at all TAG Lab stations and the orange are ancillary components used at the CRS station.

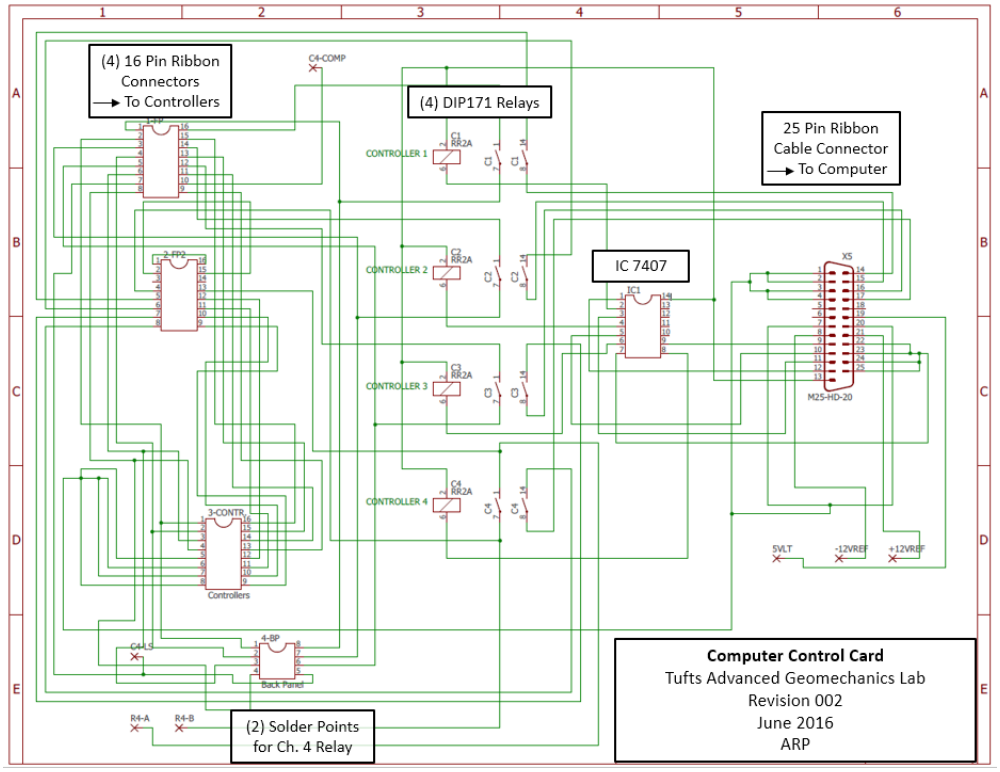

Figure 4-6: Circuit diagram schematic for the interface control card, "TAG-R2". All the interface control cards were updated to the PCB version, "TAG-R2".

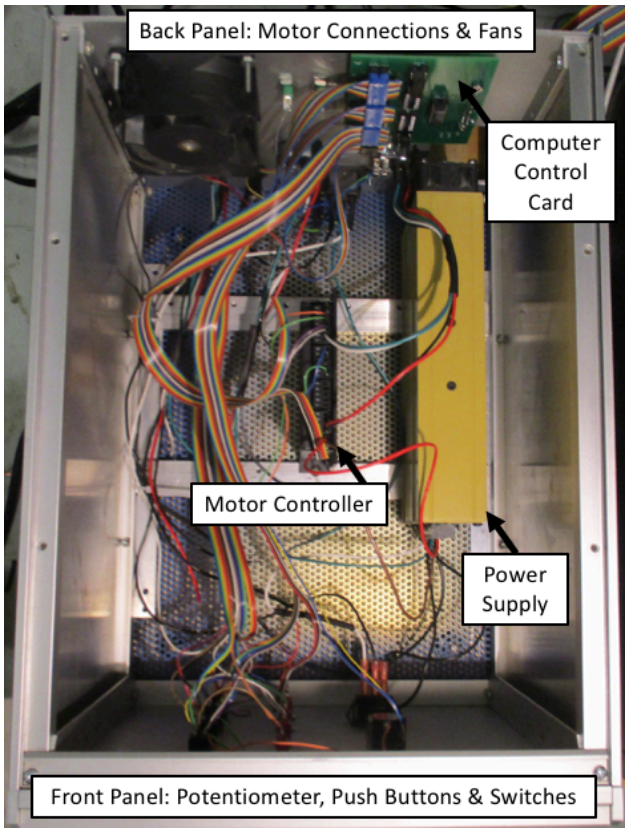

Figure 4-7: Inside the updated computer control box with major components labeled. There is only one motor controller in the CRS computer control boxes.

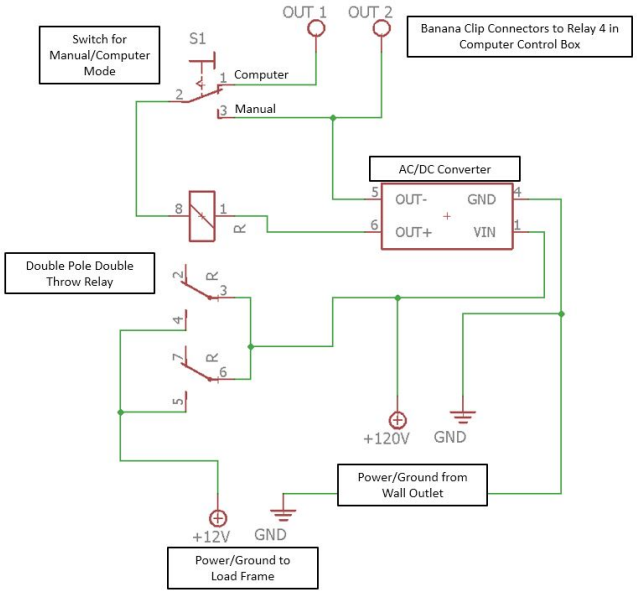

Figure 4-8: Circuit diagram of load frame junction box designed to cut power to the load frame when a target stress value is achieved.

5 Procedures

5.1 Introduction

This chapter outlines the procedures step by step and explains the analysis methods for all types of experiments used in this research. Section 5.2 outlines how to run a CRS test. The CRS tests follow the standard procedure that is used in the TAG lab which is also outlined in great depth in Nordquist (2014). This procedure strongly resembles ASTM D4186 – Standard Method for One-Dimensional Consolidation Properties of Saturated Cohesive Soils Using Controlled Strain Loading. Section 5.3 summarizes the experimental method for salinity testing. Section 5.4 explains how to analyze CRS data collected by the central data acquisition system. This analysis also follows the general steps of ASTM Standard D4186. Finally, Section 5.5 explains how to analyze the salinity data. The guidelines outlined in Germaine and Germaine (2009) are followed for the salinity related research because there is no ASTM Standard.

5.2 Constant Rate of Strain Test Set-up

This section includes detailed instructions for setting up a constant rate of strain experiment to test a saturated, fine-grained specimen. The procedure is sub-divided into the following six sections: Preparations, Specimen Trimming, Cell Set-up, Saturation and Backpressure the Specimen, Loading, and Disassembly.

5.2.1 Preparations

1. Disassemble the CRS apparatus and confirm all parts are present (Figure 5-1).
2. Set the gears to the desired strain rate (Table 5-1 and Figure 5-2).
3. Collect the following materials:
    a. Wire saw
    b. Long razor blade
    c. Wax paper (about 2 in x 2 in)

d. Plastic disc
e. Trimming turntable
f. Calipers
g. Confinement ring
h. Small diameter top and bottom porous stones (after cleaned in the Ultrasonic Cleaner)
i. One piece of filter fabric (nanofilament filter fabric)
j. Large diameter base porous stone (after cleaned in the Ultrasonic Cleaner)
k. Spacer tool
l. Trimming tools
m. Three water content tares
n. CRS test data sheet

4. Obtain the mass of the following:
    a. Three water content tares
    b. Lightly greased confinement ring with one filter fabric
    c. Top and bottom porous stones, surface saturated dry (SSD)
    d. Spacer tool
5. Obtain the following dimensions:
    a. Confinement ring height
    b. Confinement ring diameter
    c. Filter paper thickness
    d. Height of spacer tool

5.2.2 Specimen Trimming

All of the specimen included in this research are from prepared resedimentation tubes. The following steps list how to trim a specimen extruded from the resedimentation tube:

1. Extrude approximately 1 inch of the resedimented material out the bottom of the resedimentation tube. Use a PVC spacer to push the material out gently.

2. Lay the tube on its side and cut off the 1 inch piece using the wire saw (Figure 5-3).
3. Place the specimen on the piece of wax paper that is on top of the plastic disc.
4. Note on the resedimentation record where in the tube the test specimen comes from. This record is helpful for identifying the origin of the specimen in the resedimentation tube, particularly for salinity analyses.
5. Place the specimen on the wax paper and plastic disc on the trimming turn table. Center it as best as possible.
6. Hold the confinement ring in the top of the trimming turntable. Use two small C-clamps to clamp the confinement ring into the turntable.
7. Lower the confinement ring down close to the specimen (but do not touch yet). Adjust the specimen position to be concentric with the confinement ring (Figure 5-4).
8. Slowly lower the confinement ring to meet the specimen surface. As the confinement ring touches the surface it will begin to cut into the material. Gently advance the confinement ring through the material. As it advances, scrape away the outside material from the cutting shoe with a trimming tool.
9. Collect some of the material that is cut away and collect in one of the water content tares. Note on the CRS data sheet the label of the tare that contains the trimmings.
10. Continue lowering and cutting until the confinement ring is almost all the way down the specimen (about 1/16 in should be left).
11. Carefully remove the confinement ring with the soil from the turntable. Leave the plastic disc behind, but the wax paper will likely stick to the clay.
12. Mount the confinement ring in a vice to hold it still. Using the wire saw, cut the excess material off the cutting shoe end of the confinement ring. Put this slice of material in a second water content tare and note on the CRS data sheet that this tare has the top slice.

13. Use a razor blade to cut another layer off of the material in the confinement ring. Clean the confinement ring by wiping away any soil that was smeared while cutting.
14. Place the filter paper on top of the material in the confinement ring
15. Push the spacer tool into the confinement ring. This will cause material to be extruded from the bottom of the confinement ring (Figure 5-5).
16. Using the wire saw, cut the extruded material from the confinement ring and clean the confinement ring again. Put the removed material in the third water content tare and note on the CRS data sheet that this tare has the bottom slice.
17. Use the razor blade to cut another layer from the material at this end of the confinement ring. Clean the confinement ring by wiping away any soil that was smeared while cutting.
18. Record the mass of the confinement ring with the sediment, filter fabric, and spacer tool (Figure 5-6).
19. Record the mass of the water content tares with the wet soil, and then place the tares in the oven to dry.

5.2.3 Cell Set-up

After trimming the specimen into the confinement ring, set up the CRS cell by following these steps:

1. Place the larger porous stone into the depression in the CRS base. The depression should be filled with water at all times to ensure that the pore pressure line is saturated (Figure 5-7).
2. Place the bottom porous stone, SSD, on the bottom of the confinement ring and push it up in about 1/2 of the way. The stone should be placed so the larger diameter side is in contact with the specimen. Note, there is no filter fabric used on the bottom of the specimen because there should be no flow on this side.

3. Concentrically place the confinement ring, bottom porous stone, specimen, filter fabric, and acrylic spacer set up onto the base. Push the confinement ring down so it makes contact with the CRS Cell base.
4. Remove the acrylic spacer and place the top porous stone, SSD, in the confinement ring on top of the specimen and filter fabric. There is a slight bevel to the porous stone, the larger diameter side should be touching the filter fabric.
5. Measure the distance from the top of the confinement ring to the top of the porous stone with calipers. This value is used only as a reference and not in the calculations.
6. Grease a square O-ring and place it around the confinement ring on the base Figure 5-8).
7. Remove the cup ring from inside the top cap piston channel and clean and lightly grease it. In order to remove the ring you may need to breakdown the three piece top cap assembly (Figure 5-9). Reassemble the three piece top cap assembly.
8. Retract the piston all the way and secure it in that position.
9. Place the cell outer chamber on the base with the confinement ring, specimen, porous stones, and filter fabric inside. To do this line up the three threaded rods with the channels in the outer chamber.
10. If the top cap isn't already attached to the outer chamber, place the top cap on top of the CRS cell chamber and base set up, again using the threaded rods for alignment.
11. Tightly screw the top cap down to the base. Place a washer between the nut and the top cap before tightening the nut.
12. Carefully, place the CRS cell in the load frame (Figure 5-10).
13. Slowly unsecure the piston while holding it (do not let it drop). Lower the piston until it touches the top porous stone. This contact isn't visible, but with a light tap it should be apparent when contact is made.
14. Lock the piston in the position of contact with the specimen.

15. Record the zero voltage from the load cell (there should be no contact between the load cell and CRS cell yet).
16. Insert a moment/shear break between the piston and the load cell (Figure 5-11).
17. Raise the pedestal on the load frame so the load cell comes in contact with the moment/shear break on top of the CRS cell. Look at the load cell output voltage to see when contact is made.
18. Record the “seated zero” voltage vale for the load cell.
19. Record the zero voltages for the LVDTs.
20. Fill the reservoir attached to the PVA with water that is the same salinity as the specimen (usually 80 g/L in this research).
21. Open the valves connecting the reservoir to the cell chamber and fill the chamber with the saline water. All the air in the system should get flushed out through the drainage port in the top cap.
22. When water starts dripping out of the top cap drainage port, close the port. Cap it either with a Swagelok plug connection or the thermocouple Swagelok connection (depending on the CRS cell) (Figure 5-12).
23. Record the zero voltages for the pore pressure and cell pressure transducers. The zeros should be recorded while the cell is still connected to atmospheric pressure through the cell pressure line.
24. Log the CRS Test in the “CRS TEST” Binder. Use the next open line in the log book to determine the test number, “CRS####”.

5.2.4 Saturation and Backpressure the Specimen

A constant cell pressure must be put on the specimen for the duration of this test. The cell pressure is usually 5 ksc, or about 0.5 MPa. In CRS Cell 1 a computer control system holds the cell pressure using a PVA, but in CRS Cell 2 a manual system with an air pressure regulator controls the cell pressure. The purpose of applying cell pressure is to force any trapped air in the specimen and porous stones into solution in the surrounding fluid and

deair the lines. If using CRS Cell 1 follow the steps below, if using CRS Cell 2 skip to the next set of instructions.

1. Turn on the computer control system: the computer control box, computer, and monitor.
2. Use DOSBox to start the QuickBasic program and open the “CRS Set-up” file for the station being used.
3. Input the correct transducer “zero” voltages and calibration factors. The zeroes need to be normalized by the input and confirm the calibration factors are in the units specified by the computer control program.
4. Use the backpressure program to set a cell pressure on the system. This allows a certain cell pressure to be set for a specified time increment. Specify a couple of steps of cell pressure between 1 and 5 ksc, usually 1, 3, 5, and hold each step for at least 10 minutes. Don’t press start yet.
5. Create a data acquisition file on the central data acquisition system. Set the file for the appropriate channels and to record every 3 minutes.
6. Start the computer control program and switch the computer control for motor 1 to “Computer”.
7. Set the temperature controller to the appropriate temperature for the test. If the temperature set is higher than room temperature this will turn the band heater on.
8. Monitor the back pressuring process with the data acquisition system set to record data every three minutes.
9. Allow the cell to sit overnight, at least 8 hours, to come to temperature and pressure equilibrium.

If the CRS cell being set up is Cell 2, there is no computer control system to control the cell pressure. Therefore, the flowing steps are followed to saturate and back pressure the specimen:

1. Create a data acquisition file on the central data acquisition system. Set the file for the appropriate channels and to record every 3 minutes.
2. Close the valve that connects the screw pump to the PVA. Fill the screw pump with saline water to match the salinity of the specimen.
3. Close the valve that connects the screw pump to the reservoir of water and open the valve that connects the screw pump to the PVA.
4. Screw the pump in until the PVA is full of water. Close the valve connecting the PVA to the screw pump.
5. Use the manual regulator to slowly increase the pressure in the system to 5 ksc. Use the voltage meter to determine when the cell pressure transducer is reading the number of millivolts that corresponds to 5 ksc based on the zero value and calibration factor.
6. Allow the cell to sit overnight, at least 8 hours, to come to pressure equilibrium.

5.2.5 Loading

Once the CRS apparatus is set up, the specimen is loaded to a desired stress level by the following steps:

1. Set the gears and transmission to the desired strain rate. The proper gear configuration is determined using Table 5-1. The strain rate must be high enough to develop excess pore pressures that can be measured by the pore pressure transducer, but low enough that the flow doesn't affect the soil fabric (Nordquist, 2015). The strain rate used in this research is about 0.3%/hour.
2. Confirm the data acquisition system is recording every 3 or 4 minutes and has a sufficient number of readings left.

If CRS Cell 1 is used, the maximum stress level can be set using the control system. Follow steps 3-5 below:

3. Escape out of the backpressure program and start the CRS Consolidation Program.

4. Enter the maximum stress level as the target stress. For the load cell used in this research it is 40 MPa (400 ksc). Start the program.
5. Switch the load frame junction box into computer control mode.

CRS Cell 2 does not have computer control to turn the load frame off at a particular stress level. In this case, skip steps 3-5 above and continue with 6 below:

6. Close the valve connecting the cell pressure to the bottom of the CRS Cell, this isolates the pore pressure transducer.
7. Engage the transmission and start the motor to begin vertical compression.
8. Load the specimen to the desired stress level. Especially in CRS Cell 2 be sure not to over load the pore pressure transducer or the load cell. Take care to monitor the experiment and make sure everything is going as expected throughout the test.
9. Shut off the motor at the desired stress level. For Cell 1 the power to the load frame will be switched off at the correct stress level, however, the switch on the load frame should be switched to the "OFF" position at a time that's convenient once this happens.

5.2.6 Disassembly

1. Obtain the mass of two tares for water content measurements
2. Gather the following: small razor blade, squirt bottle of distilled water, calipers.
3. Record all of the transducer readings before disassembly.
4. Lock the piston.
5. Switch the computer control box to the neutral mode, out of computer control mode.
6. Unload the specimen. Use the hand wheel on the load frame to manually unload.
7. Open the valve to connect the pore pressure valve to the rest of the system, and open the valve to connect the cell pressure line to the room. This will release the cell pressure and bring the entire cell to atmospheric pressure.
8. Retire the data acquisition data file.

9. Unscrew the nuts that connect the top cap to the CRS chamber and base.
10. Close the cell pressure line valve so the reservoir above the PVA does not run dry.
11. Remove the CRS Cell from the load frame and place it on a lunch tray.
12. Remove the top cap.
13. Remove the CRS outer chamber. This will release the cell fluid that filled the chamber into the lunch tray.
14. Drain the water that is trapped above the specimen within the confinement ring.
15. Remove the confinement ring, specimen, filter paper, and porous stone set up.
16. Dry off any excess water and obtain a mass of the confinement ring, specimen, porous stones, and filter fabric.
17. Remove the specimen from the confinement ring. It is easiest to rest the ring on two spacers, put a metal cylinder on top of the specimen that protrudes out of the confinement ring, and tap on it with a rubber mallet to push out the specimen (Figure 5-13).
18. Put the entire specimen in one of the tares mass earlier and measure and record the wet mass of the specimen plus the tare.
19. Using the razor blade, scrape out any material that was left behind in the confinement ring or sides of the stone and put it in the other water content can. The squirt bottle can help to spray any of the excess material away.
20. Dry both tares for 24 hours at 105°C to obtain the dry mass.
21. Store the compressed, dry specimen in a labeled plastic bag.

5.3 Salinity Test Procedure

The salinity testing is performed on a test specimen that comes out of the CRS cell after being compressed to a predetermined stress. The disassembly steps for the CRS test is slightly different because only half of the final specimen is oven dried (to find the final water content of the CRS test) and the other half is left wet for the salinity tests. Therefore, an additional step, Step 18, is added to “CRS Disassembly” that reads:

18a. Cut the specimen in half. Store one half wet in a plastic bag until it is ready to be used for a salinity test and put the other half in one of the water content tares.

Once the specimen is ready to be used for a salinity test the following steps, after Germaine & Germaine (2009), are followed:

5.3.1 Preparations

1. Gather the following materials:
    a. Four centrifuge test tubes
    b. Squirt bottle full of distilled water
    c. Empty 250 mL glass beaker
    d. Salinity test data sheet
    e. 10 mL glass beaker
    f. Paper towels
    g. Pressurized air in a can
    h. 250 mL beaker of 1 g/L sea salt water (reference solution)
    i. 250 mL beaker of distilled water
    j. Electrical conductivity probe
    k. Eight water content tares
    l. Trimming tool (scoop)
2. Record the mass of the eight water content tares.
3. Tare the scale with the 250 mL glass beaker on it. The beaker is used to hold the test tubes upright on the scale while they are filled with water/soil.
4. Mass each test tube with its cap independently, M_c.
5. Cut the CRS specimen into four representative samples. Two samples will come from the half that was oven dried, and two will come from the half that is still wet.
6. Add one sample to each test tube (should be ~15 grams of material).
7. Mass each test tube with its cap and the soil, M_{tc}.

8. Add approximately 15-30 grams of distilled water to each test tube. The final mass of each test tube, cap, water, and soil system needs to be within 1% of each other so the mass is balanced when in the centrifuge.
9. Record the mass of each test tube, cap, water, and soil, M_{twc}.
10. Shake each test tube rigorously for about 30 seconds (Figure 5-14).
11. Allow the test tubes to sit overnight so all clay particles dissociate and water is absorbed.
12. After 12-24 hours shake the test tubes rigorously again.
13. Place all four test tubes in the centrifuge. They should sit in pairs that are directly opposite each other.
14. Run the centrifuge at about 5000 rpm for 20-30 minutes.

5.3.2 Conductivity Measurements

After the test tubes go through the centrifuge, a mostly clear liquid should sit above the separated solids as shown in Figure 5-15. The following procedure is followed to measure the electrical conductivity of the clear liquid:

1. Decant the supernatant liquid from one tube into the 10 mL glass beaker.
2. Measure the conductivity of the distilled water. To make sure the probe is working correctly and is clean, this value should be very low (10-100 µS).
3. Wipe off the probe and pat dry with paper towel. The pressurized air can be used to force out any water that is left stuck in the probe.
4. Measure and record the conductance of the 1 g/L sea salt solution, this is the reference solution, C_0.
5. Clean the probe with distilled water and dry.
6. Measure the conductance of the distilled water. Confirm the probe is reading 10-100 µS again. Dry the probe.
7. Measure and record the conductance supernatant solution, C_c.
8. Clean the probe with distilled water and dry.

9. Measure the conductance of the distilled water. Confirm the probe is reading 10-100 μS again. Dry the probe.
10. Repeat steps 4-10 two more times for this sample of supernatant liquid.
11. Pour of the supernatant liquid from the 10 mL glass beaker to one of the water content tare. Measure and record the mass of the tare plus the supernatant.
12. Repeat steps 1-11 for the remaining three test tubes.
13. Place all of the tares with supernatant in the oven for 24 hours to dry.
14. Empty the sediment from each test tube into a water content tare. Use a trimming tool to scrape the material off the tube side. Distilled water can be used to rinse out the sediment as well.
15. Oven dry the tares for 24 hours at 105°C.
16. Record the mass of the tares with the dry material.

5.4 CRS Analysis

This section explains how to use the data collected by the central data acquisition system during a CRS experiment to interpret the measurements. The CRS test analysis has two main parts. First, an Excel document developed by previous TAG Lab researchers, "CRS Phase Relationships", calculates the initial and final conditions of the test specimen. Then, a QuickBasic program calculates the engineering values based on the transducer data.

To begin the analysis, transfer the appropriate data file from the central data acquisition system to a USB stick and then to a personal computer. The following files pertain to the analysis process:

- CRS####.dat – raw data file transferred from central data acquisition system
- QB.exe – QuickBasic executable program
- CRSQB2.bas – QuickBasic CRS Analysis Code
- CRS####.red – reduction file input into CRSQB2 that contains all transducer zeroes, calibration factors, and specimen dimensions

- CRS####.res – results file output from CRSQB2 that has engineering values

5.4.1 Specimen Phase Relations

First, input the data on the CRS Test Datasheet to the CRS Phase Relationships Excel sheet to determine the specimen properties. The calculations in the Excel sheet mimic those outlined in D4186 (ASTM Standard D4186, 2014), but add the necessary equations to account for a saline pore fluid.

The measured values on the CRS data sheet that are used in the subsequent calculations are defined below:

1. $m_{t,i}$= total wet mass of initial specimen inside the confinement ring with the recess tool and filter paper (g)
2. m_{c+fp} = mass of confinement ring and one filter fabric (g)
3. m_r = mass of recess tool (g)
4. m_{tf+t1} = mass of final wet specimen inside water content tare 1 (g)
5. m_{t1} = mass of empty water content tare 1 (g)
6. m_{df+t1} = mass of final dry specimen inside water content tare 1 (g)
7. $m_{extr+t2}$ = mass of dry extraneous washings inside water content tare 2 (g)
8. m_{t2} = mass of empty water content tare 2 (g)

Relevant dimensions of the specimen include the initial height and the area. The initial height of the wet specimen, h_i (cm), is typically a constant. It is calculated as the total height of the specimen ring minus the height of the recess tool minus the thickness of one filter fabric. The area of the specimen, A (cm^2) is also a constant; it is calculated using the standard area of a circle equation, $A = \frac{\pi}{4} d^2$, where d is the diameter of the specimen ring in centimeters.

The above measured values provide the information needed to calculate all the specimen properties. First, calculate the initial wet mass of the specimen, M_{ti} (g), using Equation 5-1 below:

$$M_{ti} = m_{t,i} - m_{c+fp} - m_r \qquad (5-1)$$

Then, calculate the water content of the final specimen, w_f (%), with Equation 5-2 below:

$$w_f = \frac{m_{tf+t1} - m_{df+t1}}{m_{df+t1} - m_{t1}} \times 100 \qquad (5-2)$$

Compute the total dry mass, M_{df} (g), of the final specimen using Equation 5-3 below. The total dry mass is the mass of the soil grains and the salt at the end of testing.

$$M_{df} = \frac{m_{tf+t1} - m_{t1}}{1 + \frac{w_f}{100}} + m_{extr+t2} - m_{t2} \qquad (5-3)$$

Next, calculate the initial wet density, ρ_t (g/cm^3), and initial dry density, ρ_d (g/cm^3), of the specimen with Equations 5-4 and 5-5 below.

$$\rho_t = \frac{M_{ti}}{h_i \times A} \qquad (5-4)$$

$$\rho_d = \frac{M_{df}}{h_i \times A} \qquad (5-5)$$

The second part of this research focuses on how the salinity changes during compression. Therefore, to be complete, it is important to consider that the mass of the salt at the beginning of the experiment is different than the mass of the salt at the end of the

experiment. The following calculations continue to mirror the calculations in D4186, but include considerations for salt.

First, calculate the final mass of water, M_{wf} (g), using Equation 5-6:

$$M_{wf} = M_{df} \times \frac{w_f}{100} \qquad (5-6)$$

Then calculate the final mass of salt, $M_{salt,f}$ (g), with Equation 5-7. This calculation relies on the assumption that the pore fluid salinity has not changed since the beginning of the test and remains at whatever the batched/testing salinity is.

$$M_{salt,f} = \left(\frac{s}{\rho_{sw}}\right)\left(\frac{1000\ cm^3}{1\ Liter}\right)M_{wf} \qquad (5-7)$$

Where:
- s = salinity of pore fluid at beginning of test (usually batch salinity) (g/L)
- ρ_{sw} = density of salt water with concentration s at testing temperature (g/cm^3)

Now the mass of the soil grains, M_s (g), is calculated with Equation 5-8. This value is assumed to be a constant throughout the test, there should be no loss or gain of soil during compression.

$$M_s = M_{df} - M_{salt,f} \qquad (5-8)$$

The volume of grains, V_s (cm^3), is calculated based on this mass of solids using Equation 5-9:

$$V_s = \frac{M_s}{\rho_w G_s} \quad (5-9)$$

Where:
G_s = specific gravity of soil grains
ρ_w = density of water at 20°C (0.99821) (g/cm^3)

Then, using the volume, the height of the solids, h_s (cm), is calculated using Equation 5-10:

$$h_s = \frac{V_s}{A} \quad (5-10)$$

The mass of the soil grains is used to calculate the initial conditions of the specimen. The initial mass of fluid, M_{fi} (g), initial fluid volume, V_{fi} (cm^3), and initial mass of salt, $M_{salt,i}$ (g), are all values of interest and calculated in Equations 5-11, 5-12, and 5-13 respectively.

$$M_{fi} = M_{ti} - M_s \quad (5-11)$$

$$V_{fi} = \frac{M_s}{\rho_{sw}} \quad (5-12)$$

$$M_{salt,i} = (V_{fi} * s)(\frac{1\ Liter}{1000\ cm^3}) \quad (5-13)$$

The final three parameters to calculate the phase relationships, void ratio, e, porosity, n, and degree of saturation, S (%). Typically void ratio and porosity are ratios of volumes, however, since the area of the test specimen remains constant it is convenient to compare heights instead. All three parameters are calculated for the initial conditions of the specimen. Below, Equation 5-14 calculates the initial void ratio:

$$e_i = \frac{h_i - h_s}{h_s} \quad (5-14)$$

Equation 5-15 is the general equation for calculating porosity based on void ratio:

$$n_i = \frac{e_i}{1 + e_i} \qquad (5-15)$$

Finally, calculate the initial degree of saturation with Equation 5-16:

$$S = \frac{V_{fi}}{(A \times h_i) - V_s} * 100 \qquad (5-16)$$

This concludes all the phase relationships calculated using the CRS Phase Relationships Excel document. Review the calculated values to confirm that all the measurements make sense, for example the initial saturation is about 100% and the void ratio is in a reasonable range.

5.4.2 Engineering Value Calculations

During the experiment the central data acquisition system collects voltage readings from all of the transducers connected to the cell at the specified time increment. Usually this time increment is around 3-5 minutes. The tests last between 5-7 days, and this leads to the creation of thousands of data points for analysis. Analyzing these data using a QuickBasic program reduces calculation time and helps to keep files consistent and organized. The program can be broken into two phases 1) Transducer to engineering values 2) Engineering values to experimental values.

Transducer to Engineering Values

As discussed previously, transducers record voltages which then need to be converted to meaningful engineering values. The following section describes what each transducer measures and how it is used to calculate an engineering value. In all of the following discussion V_{out} is defined as the output voltage (reading) from a particular transducer and V_{in} is defined as the input voltage from the power supply to the transducer (usually

around 5.5 V). All of the equations used to convert voltages to engineering values have a parallel set up to Equation 5-17:

$$\begin{matrix} Engineering \\ Value \end{matrix} = \begin{matrix} Calibration \\ Factor \end{matrix} \times \left(\begin{matrix} Normalized\ Voltage \\ Reading \end{matrix} - \begin{matrix} Normalized\ Zero \\ Voltage\ Reading \end{matrix} \right) \qquad (5-17)$$

The specific equation for each transducer is outlined in this section. LVDTs are used for measuring the vertical displacement of the piston during testing. They are tightly attached to the piston with the end of the shaft touching the top cap. In order to improve the displacement accuracy, two LVDTs are used opposite each other on the top cap. The results from the two are averaged into one displacement value; this method reduces the effect of any skewness in the measurements due to the top cap not being exactly horizontal. The zero for the LVDT reading is recorded after the specimen has been loaded into the cell, the top cap screwed tightly to the base, and the piston put into contact with the porous stone.

The uncorrected displacement, δ_u (cm), based on each of the LVDT's is calculated based on Equation 5-18:

$$\delta_u = CF_{LVDT} * \left(\frac{V_{out}}{V_{in}} - \frac{V_{out,zero}}{V_{in,zero}} \right) \qquad (5-18)$$

Where:
δ_u = uncorrected displacement (cm)
CF_{LVDT} = LVDT calibration factor (cm/(V/V))
$V_{out,zero}/V_{in,zero}$ = normalized output voltage from LVDT at zero height (V/V)

δ_u is defined as the uncorrected displacement because it is the total displacement that the LVDT's are measuring which is not necessarily the displacement of the specimen. The issue of apparatus compressibility is discussed later.

Pressure transducers measure the pore pressure of the specimen through the outlet in the base of the CRS and the cell pressure in the CRS chamber. The cell pressure, σ_c, is calculated using Equation 5-19:

$$\sigma_c = CF_{CP} * \left(\frac{V_{out}}{V_{in}} - \frac{V_{out,zero}}{V_{in,zero}}\right) \qquad (5-19)$$

Where:
σ_c = cell pressure (kgf/cm^2)
CF_{CP} = LVDT calibration factor ((kgf/cm^2)/(V/V))
$V_{out,zero}/V_{in,zero}$ = normalized output voltage from cell pressure transducer at atmospheric pressure (V/V)

One comment to recognize is the units used in the laboratory during testing are different than the units used in analysis and to report results. In the lab the pressure transducers are used to calculate a pressure value in kilograms-force per square centimeter, kgf/cm^2 or ksc. In analysis and all of the figures included in future chapters the ksc value is converted to the more conventional Pascal unit (or typically Megapascal). The conversion factor for ksc to MPa is 1 ksc equals 0.098 MPa. Similarly, in the laboratory the engineering units for the load are typically kilogram-force, kgf. The conversion for kgf to Newton (N) is 1 kgf equals 9.806 N.

Next the base pressure engineering value needs to be equated to the cell pressure engineering value after backpressure saturation is complete and right before the cell pressure valve is closed for loading. Do this by modifying the $V_{out,zero}$ value for the pore pressure transducer so that u_b calculated in Equation 5-20, below, is equal to σ_c from above.

$$u_b = CF_{PP} * \left(\frac{V_{out}}{V_{in}} - \frac{V_{out,zero}}{V_{in,zero}}\right) \qquad (5-20)$$

Where:
u_b = base pressure (kgf/cm^2)
CF_{PP} = pore pressure calibration factor ((kgf/cm^2)/(V/V))
$V_{out,zero}/V_{in,zero}$ = normalized output voltage from pore pressure transducer at atmospheric pressure (V/V)

Then, update the u_b values with the new $V_{out,zero,adjusted}$ value using Equation 5-21:

$$u_b = CF_{PP} * \left(\frac{V_{out}}{V_{in}} - \frac{V_{out,zero}}{V_{in,zero}} \right) \quad (5-21)$$

Where:
u_b = base pressure (kgf/cm^2)
CF_{PP} = pore pressure calibration factor ((kgf/cm^2)/(V/V))
$V_{out,zero,adjusted}/V_{in,zero}$ = normalized output voltage from pore pressure transducer at atmospheric pressure using the adjusted zero value (V/V)

Finally, calculate the uncorrected axial force using the load cell data and Equation 5-22:

$$f_{a,u} = CF_{loadcell} * \left(\frac{V_{out}}{V_{in}} - \frac{V_{out,zero}}{V_{in,zero}} \right) \quad (5-22)$$

Where:
$f_{a,u}$ = uncorrected axial load (kgf)
$CF_{loadcell}$ = load cell calibration factor (kgf/(V/V))
$V_{out,zero}/V_{in,zero}$ = normalized output voltage from load cell at zero load (V/V)

These four fundamental measurements are calculated for every line of data and then used in the subsequent calculations which are used to calculate parameters to analyze the test. First, however, two corrections need to be made to proceed. The uncorrected axial force needs to be corrected by adding the weight of the piston and subtracting the force due to the cell pressure acting on the area of the piston. Calculate the net axial force, f_a (kgf), the force actually felt on the specimen using Equation 5-23:

$$f_a = f_{a,u} + W_p - A_p \sigma_c \quad (5-23)$$

Where:
W_p = weight of piston (kgf)
A_p = area of the piston (cm^2)

The second correction is due to the apparatus compressing during compression tests and is discussed in the next section.

Apparatus Compressibility

When a CRS cell is loaded to high stress levels, some of the cell pieces compress ever so slightly which results in a larger deformation reading than the specimen actually experiences. To determine the apparatus compressibility correction equation, four load-unload cycles are run on the CRS cell with a steel dummy specimen. If it is assumed the steel dummy specimen does not compress at all then any deformation during this test is due to the apparatus compressing. The displacement and load are recorded with the transducers, just as in a normal test. After the test, the first cycle of data is discarded and then a polynomial regression is fit for the data of the three last loading cycles. The regression was done using MATLAB's best fit line function and splitting the data into two load ranges. The data with the best fit line equations is included in Figure 5-16 and the compressibility constants are listed in Table 5-2.

The change in specimen height due to apparatus compressibility, $\delta_{ac,n}$ (cm), Equation 5-24 is used:

$$\delta_{ac,n} = \left(af_{a,u,n}^3 + bf_{a,u,n}^2 + cf_{a,u,n} + d\right) - \left(af_{a,u,i}^3 + bf_{a,u,i}^2 + cf_{a,u,i} + d\right) \qquad (5-24)$$

Where:
- a, b, c, d = apparatus compressibility factors given in Table 5-2.
- $f_{a,n}$ = vertical force for current line of data (kgf)
- $f_{a,i}$ = vertical force for first line of data (kgf)

Using the apparatus compressibility calculated from Equation 5-24 the change in specimen height, Δh_n (cm), can be calculated using Equation 5-25:

$$\Delta h_n = \delta_{u,n} - \delta_{ac,n} \qquad (5-25)$$

Additionally, since some of this research is related to temperature and heating up the entire CRS cell, analyzing how the cell shrinks or swells with changes in temperature was also required. The data acquisition system does not record the temperature of the device during the test, so there is no calibration correction done based on this information. This

is reasonable because the reaction to temperature is elastic and reversible and each test is held at a constant temperature so there are no changes throughout the test. The cell compressibility due to temperature is included in Figure 5-17. This calibration was done by setting up the cell exactly as done for a real test except using the dummy specimen. Then it is placed in the load frame with about 320 kg of load on top. Then the heating band was cycled on and off to see how the cell deformed with the heating and cooling cycles.

Physical Properties

The following physical properties are calculated using the QuickBasic program, CRSQB2.bas. They are each calculated for every line of data, n lines, with line 1 being the first line of data.

The specimen height, H_n (cm), is calculated using Equation 5-26:

$$H_n = h_i - \Delta h_n \qquad (5-26)$$

The porosity for each line is calculated using Equation 5-27:

$$n_n = \frac{H_n - h_s}{H_n} \qquad (5-27)$$

Similarly, the void ratio is calculated using Equation 5-28:

$$e_n = \frac{H_n - h_s}{h_s} \qquad (5-28)$$

The axial strain of the specimen, $\varepsilon_{a,n}$ (%), is calculated using Equation 5-29:

$$\varepsilon_{a,n} = \frac{h_i - H_n}{h_i} \times 100 \qquad (5-29)$$

The axial strain rate (hr^{-1}) is calculated using Equation 5-30:

$$\dot{\varepsilon}_n = \left(\frac{\Delta h_{n+1} - \Delta h_{n-1}}{h_i}\right)\left(\frac{1}{t_{n+1} - t_{n-1}}\right)\left(\frac{3600\ sec}{1\ hr}\right) \qquad (5-30)$$

Where:

t_n = time that reading was taken (seconds)

Stress & Pressure

The pore pressure transducer measures the pressure at the bottom of the specimen. This is the location assumed to have the maximum pore pressure during loading. The maximum pore pressure is calculated as the difference between the pore pressure reading and the cell pressure, since the entire system is under that cell pressure. Compute the base excess pore pressure, Δu_b (ksc), with Equation 5-31:

$$\Delta u_{b,n} = u_{b,n} - \sigma_{c,n} \qquad (5-31)$$

The total vertical stress, $\sigma_{a,n}$ (ksc), on the specimen is calculated using Equation 5-32:

$$\sigma_{a,n} = \frac{f_{a,n}}{A} + \sigma_{c,n} \qquad (5-32)$$

The vertical effective stress is the parameter of more interest for the analysis in this research and is calculated by subtracting the average excess pore pressure from the total vertical stress, Equation 5-33:

$$\sigma'_{a,n} = \sigma_{a,n} - \frac{2}{3}\,\Delta u_{b,n} \qquad (5-33)$$

The average excess pore pressure is calculated using linear theory developed by Wissa et al. (1971).

Permeability & Compressibility

The final set of calculations are to evaluate the permeability and compressibility values that are of interest. First calculate the hydraulic conductivity, $K_{v,n}$ (cm/s), using Equation 5-34 (ASTM Standard D4186, 2014):

$$K_{v,n} = \left(\frac{\dot{\varepsilon}_n h_n h_i \rho_{sw}}{2\Delta u_{b,n}}\right)\left(\frac{1\ kg}{1000\ g}\right) \qquad (5-34)$$

Where:

ρ_{sw} = density of salt water at test temperature (g/cm^3)

Then, compute the permeability, k (m^2), from the hydraulic conductivity using Equation 5-35:

$$k_{v,n} = \left(\frac{K_{v,n}\left(\frac{1\ m}{100\ cm}\right)\mu}{\rho_{sw}\left(\frac{100\ cm}{1\ m}\right)^3\left(\frac{1\ kg}{1000\ g}\right)g}\right) \qquad (5-35)$$

Next, calculate the volume compressibility, $m_{v,n}$ (m^2/kN) using Equation 5-36:

$$m_{v,n} = \left(\frac{\varepsilon_{n+1} - \varepsilon_{n-1}}{\sigma'_{a,n+1} - \sigma'_{a,n-1}}\right)\left(\frac{1.0}{100\ \%}\right) \qquad (5-36)$$

The second term in this factor is converting strain from a percent to a decimal format. Finally, calculate the coefficient of consolidation, $c_{v,n}$ (m^2/s), using Equation 5-37:

$$c_{v,n} = \frac{k_n}{m_{v,n} \cdot \gamma_w} \qquad (5-37)$$

5.5 Salinity Analysis

The electrical conductivity measurements need to be analyzed to determine the salinity of the pore fluid in the specimen at the end of the CRS test. The following analysis is similar to the procedure outlined in Germaine & Germaine (2009). First, each measurement of the supernatant solution is normalized by the measurement of the salinity of the reference solution, this gives three values of C/C_0 for each supernatant fluid. Then, the three trials are averaged to give one representative value for each fluid. That average value of C/C_0 is compared to a calibration the calibration curve shown in Figure 4-4 to determine the salinity of the supernatant solutions, SS. This is the "measured salinity value" or the salinity of the supernatant. The SS value must be adjusted because the supernatant is diluted compared to the water that came from the specimen. There are two slightly different calculation procedures followed to calculate this adjustment depending on if the specimen that originally went into the test tube was oven dried or not. Usually there are two test tubes that were set up using wet material and two test tubes using dry material. The calculations for the test tubes with wet material are identified in Equations 5-38 to 5-40.

First, calculate the mass of water, M_w (g), in the wet soil that was added to the centrifuge tube using Equation 5-38:

$$M_w = (M_{tc} - M_c) * \frac{w_N}{100} / (1 + \frac{w_N}{100}) \qquad (5-38)$$

Where:
M_{tc} = mass of tube, cap, and soil
M_c = mass of tube and cap
w_N = natural water content of specimen added to centrifuge tube

Then, calculate the "artificial water content", w_c, of the soil in the centrifuge tube using Equation 5-39. The artificial water content, w_c, is the water content of the moist soil, w_N, plus the added water, so w_c should be a higher value than w_N.

$$w_C = \frac{M_w + M_{twc} + M_{tc}}{M_{tc} - M_c - M_w} * 100 \qquad (5-39)$$

Where:
M_w = mass of water in soil specimen in tube
M_{twc} = mass of tube, cap, soil, and water
M_{tc} = mass of tube, cap, and soil
M_c = mass of tube and cap
w_N = natural water content of specimen added to centrifuge tube

Finally, calculate the salinity of the actual specimen, RSS, using Equation 5-40:

$$RSS = SS * \frac{w_C}{w_N} \qquad (5-40)$$

If the initial specimen was oven dried then follow Equations 5-41 to Equation 5-45. First calculate the mass of water in the test tube using Equation 5-41.

$$M_{wa} = M_{twc} - M_{tc} \qquad (5-41)$$

Then, use Equation 5-42 to calculate the mass of solids in the tube:

$$M_{solids} = M_{tc} - M_c \qquad (5-42)$$

Calculate the mass of salt in the test tube, M_{salt}, using Equation 5-43:

$$M_{salt} = \frac{SS * M_{wa}}{\rho_w * 1000 \frac{cm^3}{Liter}} \qquad (5-43)$$

Where:
ρ_w = density of water at room temperature that measurements are made

Next, the mass of water that was in the sample (before oven drying) that was put in the test tube needs to be calculated using Equation 5-44. This is based on the water content that was calculated after the half of the CRS specimen was oven dried.

$$M_w = w_N * M_{solids} \quad (5-44)$$

Finally, the interpreted specimen salinity is calculated by relating the calculated mass of salt to the mass of water in the pore space before being oven dried using Equation 5-45:

$$RSS = \frac{M_{salt} * \rho_w * 1000 \frac{cm^3}{Liter}}{M_w} \quad (5-45)$$

Where:

ρ_w = density of water at room temperature that measurements are made

Interpreted specimen salinity is a term developed in the TAG Lab to refer to the end result of the calculation above. More discussion about the term and why it is defined this way instead of pore fluid salinity is discussed in Chapter 7.

Table 5-1: Strain rate for different gear configurations (Nordquist, 2014).

[in/min]	[cm/sec]	[sec^{-1}]	[hr^{-1}]	Theoretical [%/hr]	Actual [%/hr]
0.000024	0.0000010	0.000001	0.00465	0.46	0.3
0.000032	0.0000014	0.000002	0.00619	0.62	
0.000048	0.0000020	0.000003	0.00929	0.93	
0.000072	0.0000030	0.000004	0.01394	1.39	
0.000096	0.0000041	0.000005	0.01858	1.86	
0.00012	0.0000051	0.000006	0.02323	2.32	
0.00016	0.0000068	0.000009	0.03097	3.1	
0.00024	0.0000102	0.000013	0.04645	4.65	
0.00036	0.0000152	0.000019	0.06968	6.97	
0.00048	0.0000203	0.000026	0.0929	9.29	
0.0006	0.0000254	0.000032	0.11613	11.61	
0.0008	0.0000339	0.000043	0.15484	15.48	
0.0012	0.0000508	0.000065	0.23226	23.23	
0.00018	0.0000076	0.000010	0.03484	3.48	
0.0024	0.0001016	0.000129	0.46452	46.45	

Table 5-2: Compressibility coefficients used in Equation 5-24. These coefficients are also noted in the appropriate equations in Figure 5-16.

Compressibility Calibration Equation Constants	
log(Normal Force [kg]) < 2.4	
a	-0.0026
b	0.0135
c	-0.0265
d	-0.0009
log(Normal Force [kg]) > 2.4	
a	-0.0052
b	0.0354
c	-0.0843
d	0.0474

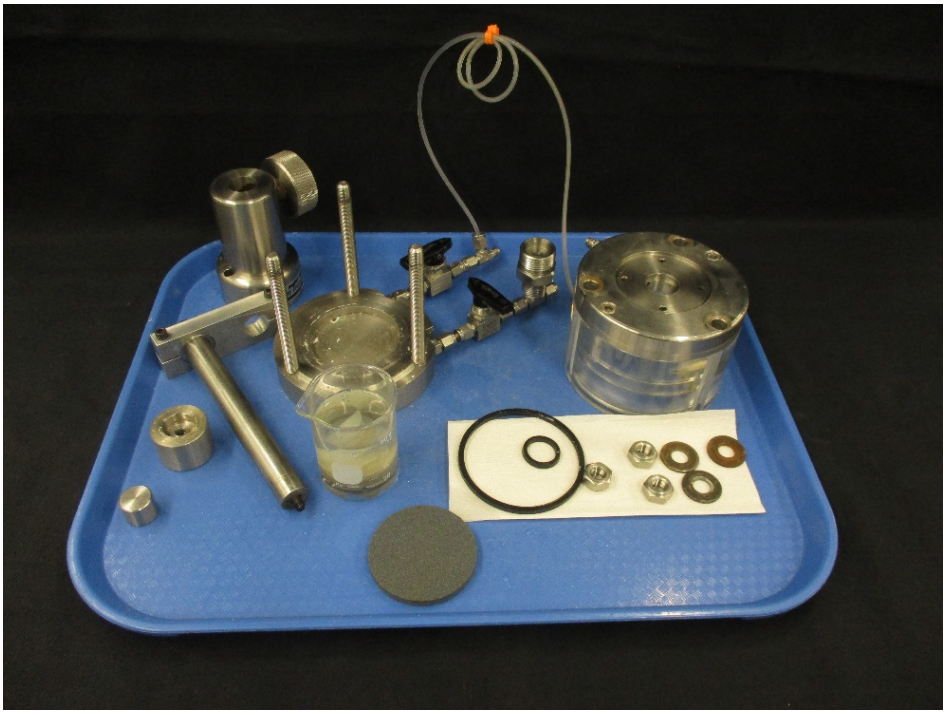

Figure 5-1: CRS disassembled pieces

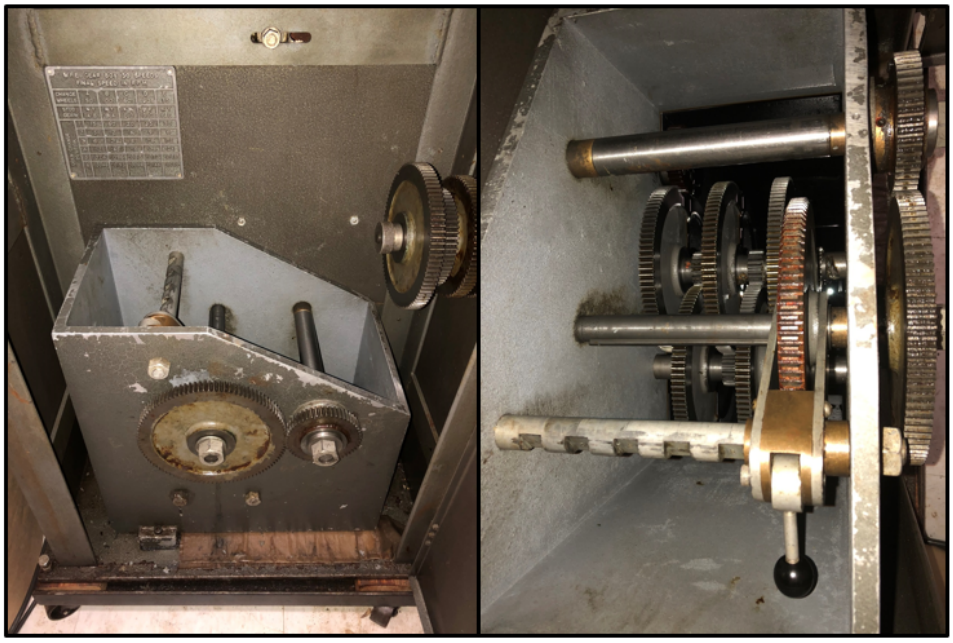

Figure 5-2: Interchangeable load frame gears. The left is looking from outside the load frame door, and the right view is looking down into the gear box.

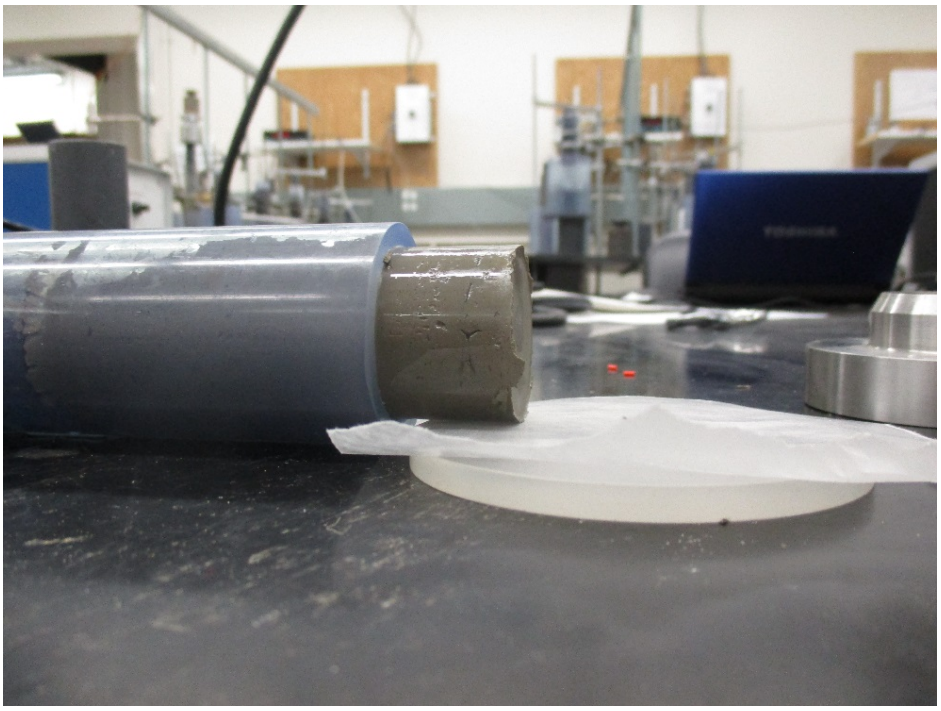

Figure 5-3: Extruding a sample of resedimentation tube for compression test.

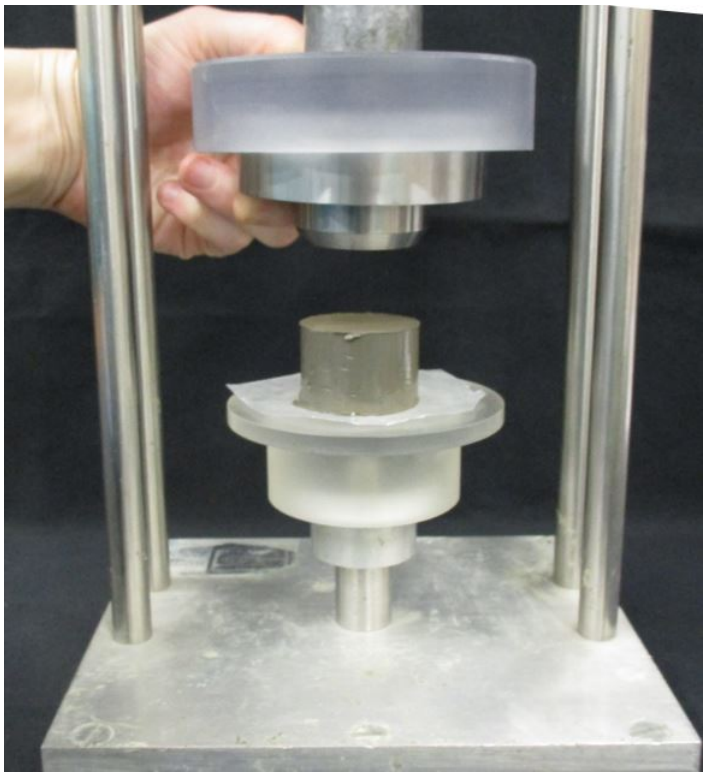

Figure 5-4: Align the clay sample to be concentric with the confinement ring.

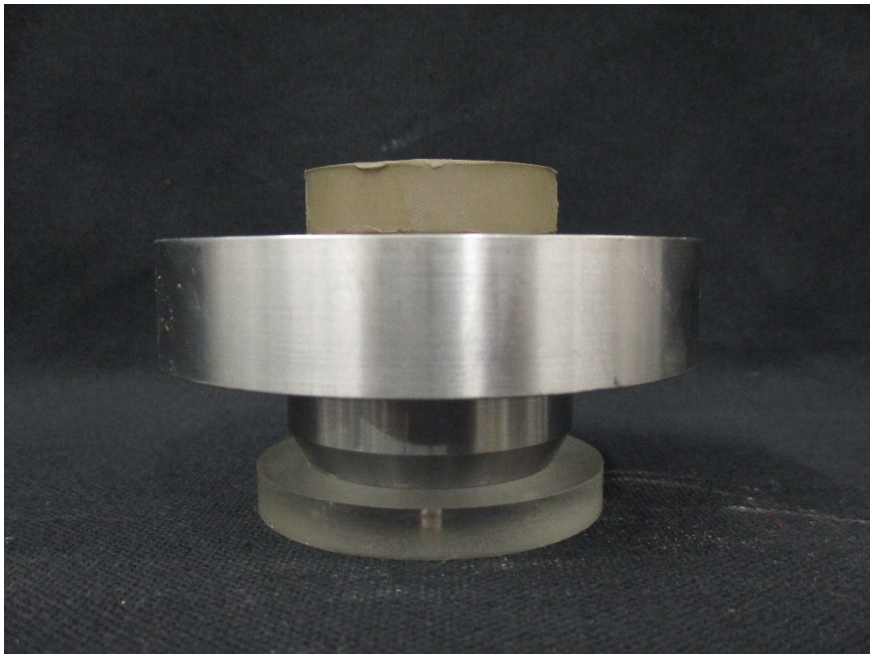

Figure 5-5: The acrylic spacer is pushed into the confinement ring which extrudes some of the specimen on the opposite end.

Figure 5-6: The confinement ring, filter paper, acrylic spacer set up.

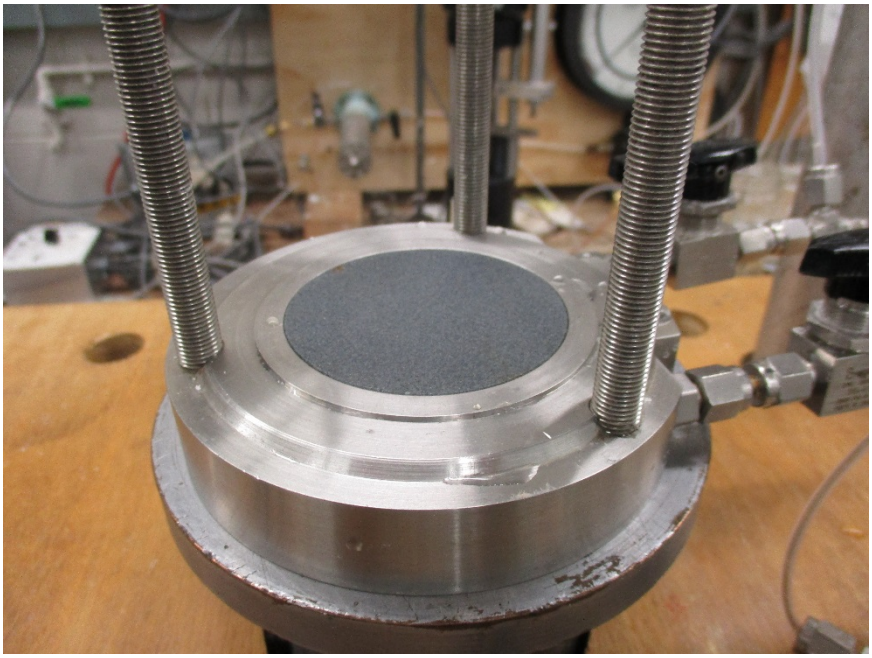

Figure 5-7: Large porous stone in the base of CRS cell.

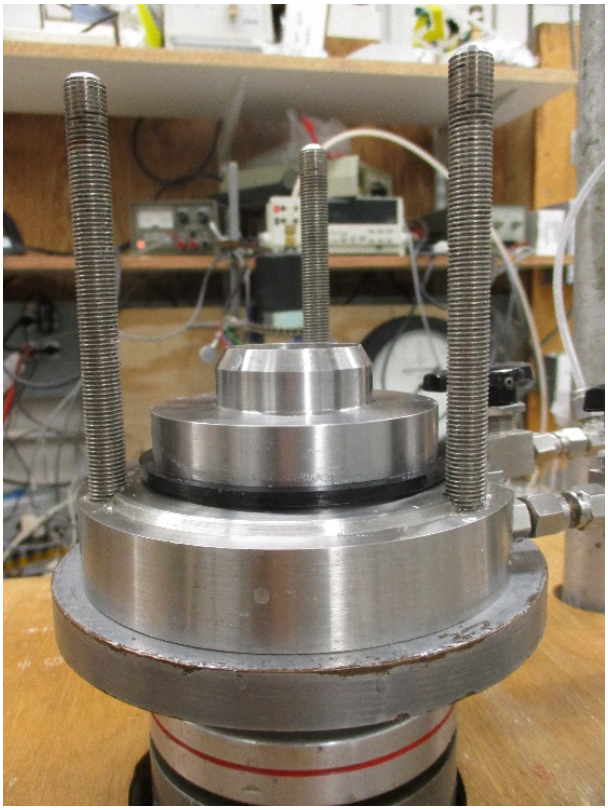

Figure 5-8: Confinement ring with square O-ring on CRS base.

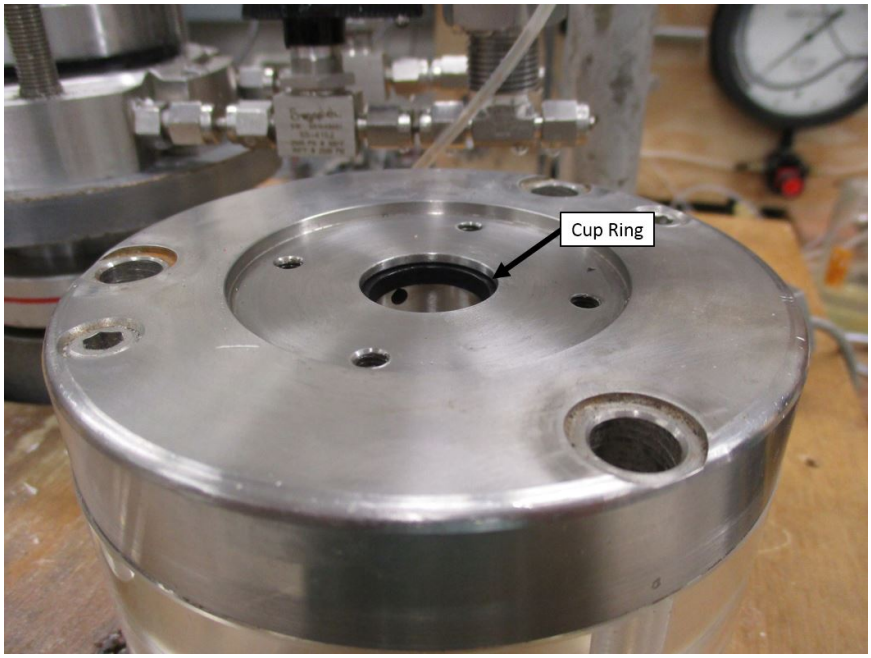

Figure 5-9: Cup ring that seals the channel for the piston to move through.

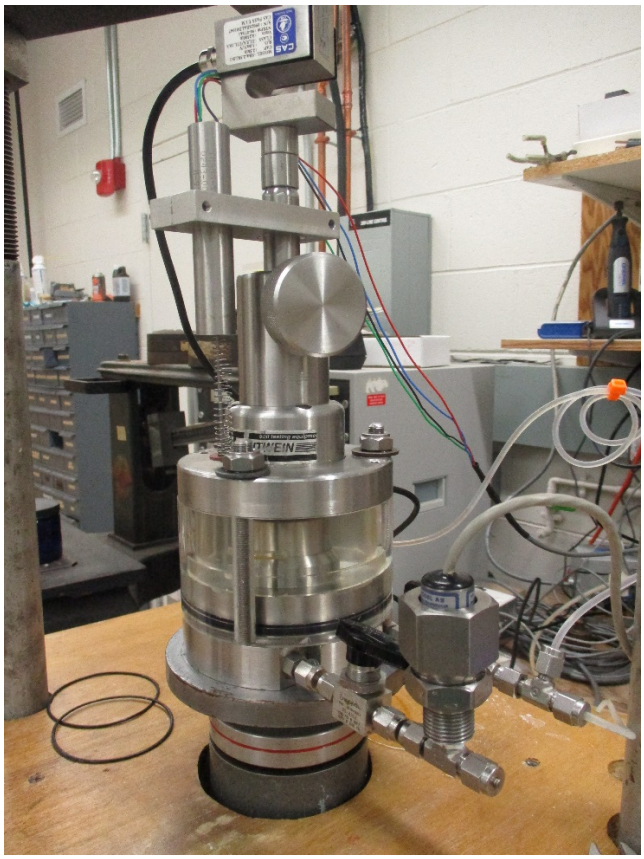

Figure 5-10: CRS Cell all set up on the load frame.

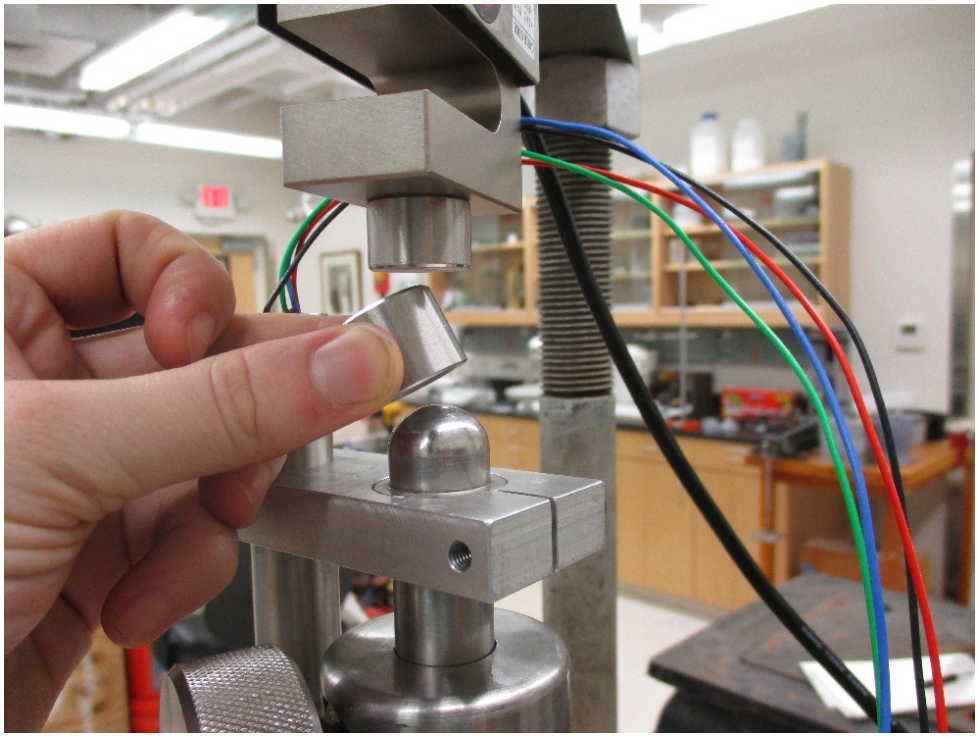

Figure 5-11: Moment/shear break put on the top of the piston.

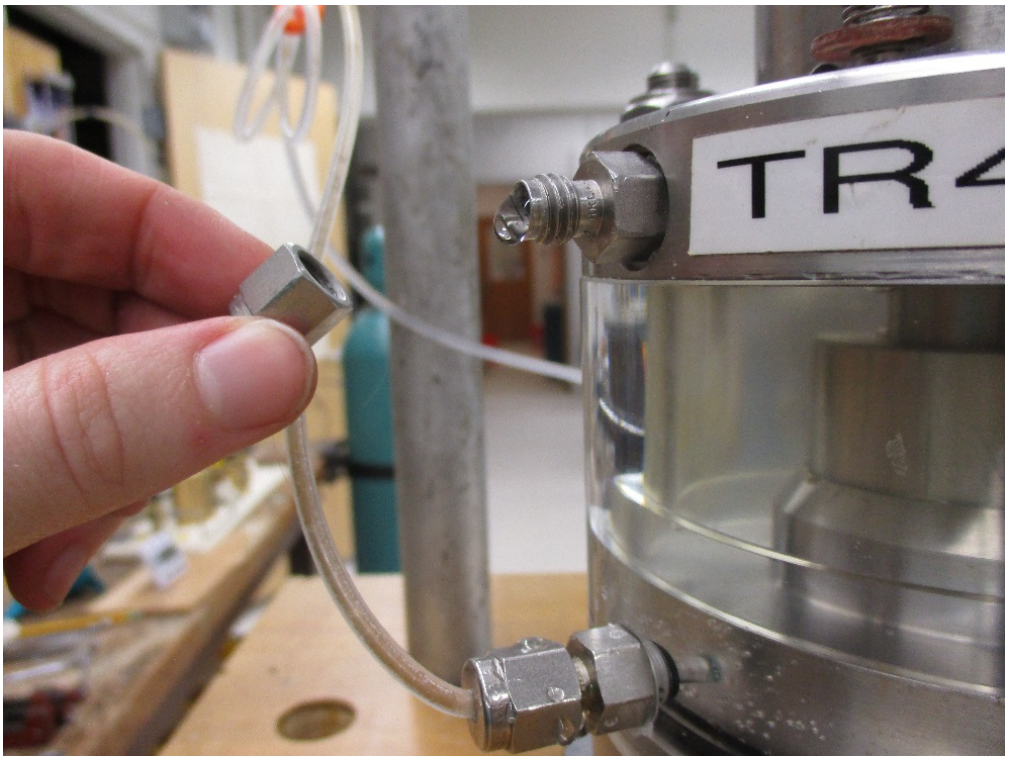

Figure 5-12: Swagelok connection on vent outlet (for CRS Cell 1 it is a thermocouple outfitted with female Swagelok).

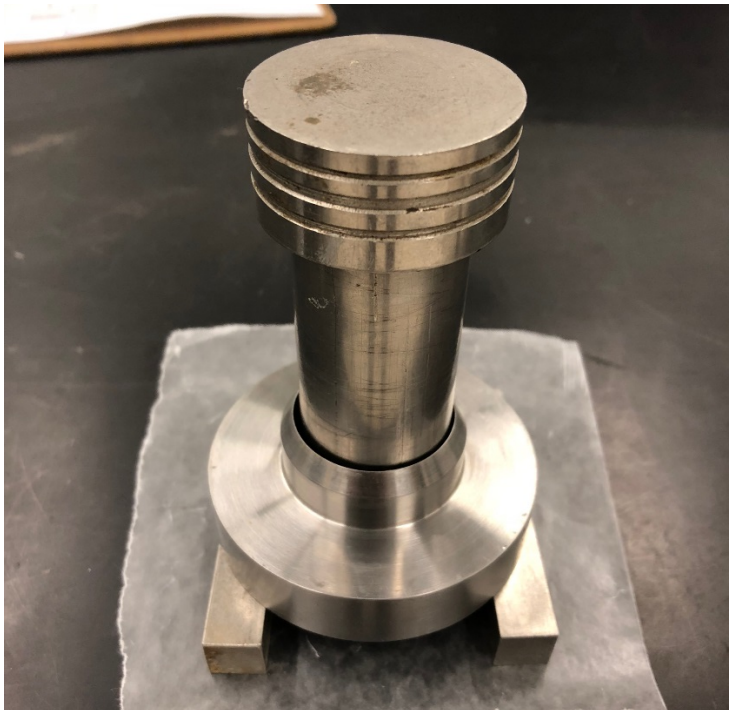

Figure 5-13: Removing compressed specimen from the confinement ring.

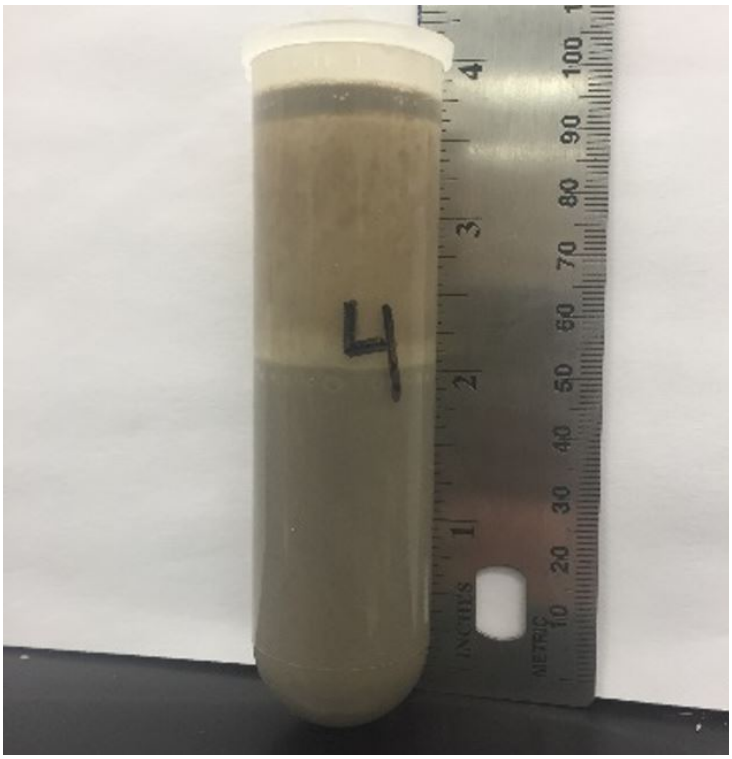

Figure 5-14: Test tube filled with water and specimen.

Figure 5-15: Test tubes after spinning in the centrifuge. The soil particles drop out leaving salt water as the supernatant.

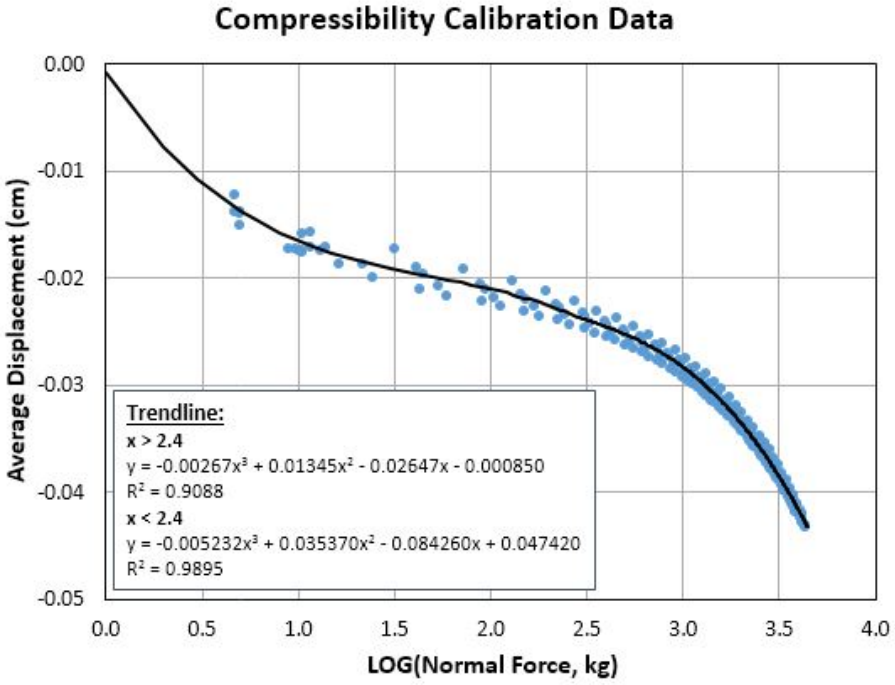

Figure 5-16: Compressibility calibration data used in the calculation for specimen deformation.

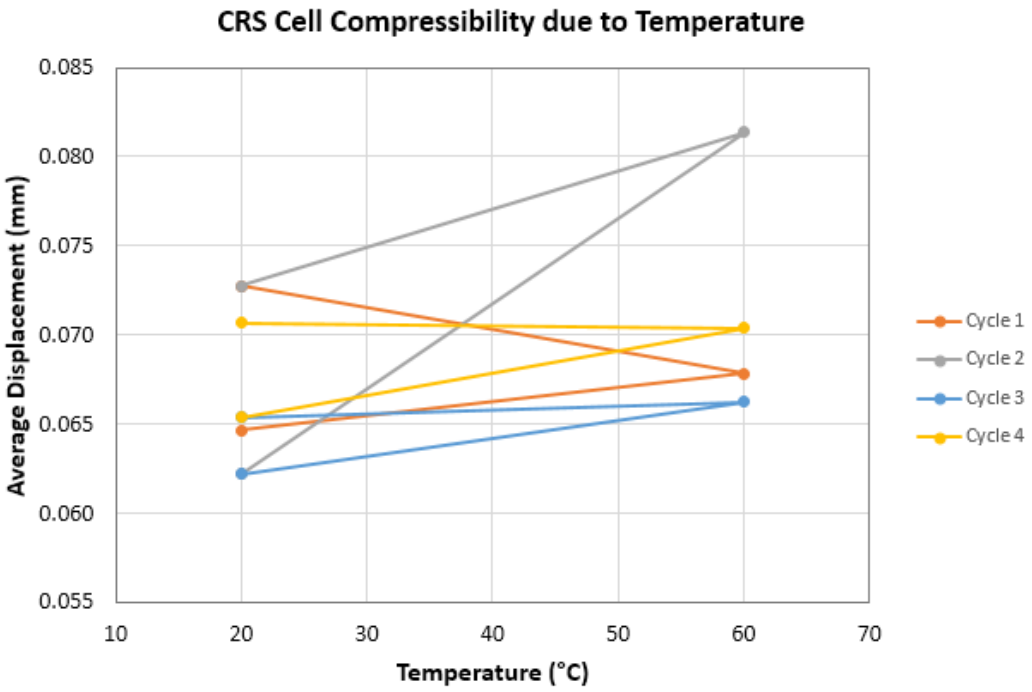

Figure 5-17: Temperature compressibility data

6 Influence of Temperature on CRS Compressibility Results

6.1 Introduction

This chapter summarizes the results from eleven constant rate of strain tests that were run to compare compression properties of RGoM-EI at different temperatures. Table 6-1 lists all the CRS tests and notes which tests were used for understanding the effect of temperature versus the ones used in the salinity research presented in Chapter 7. Room temperature tests were run at approximately 20°C and elevated temperature tests were run primarily at 60°C, but one was at 40°C. The 60°C temperature value was chosen so there is a significant increase in temperature from room temperature, but not high enough that the pore fluid or cell fluid is susceptible to boiling.

Section 6.2 analyzes the compression curves and related compression properties and Section 6.3 evaluates the permeability results. Section 6.4 discusses the conclusions from these results. Table 6-2 summarizes the results from all the experiments.

6.2 Compression Behavior

6.2.1 Compression Curves

The compression behavior is first analyzed using a traditional compression curve plot, a fabric density parameter (void ratio or porosity) versus effective stress. The majority of the plots included here have the primary y-axis as porosity, n. This convention is used because the porosity versus vertical effective stress for RGoM-EI is more linear than the void ratio versus effective stress plots.

There is one unique test included in this research, CRS1510. This CRS test is most similar to the test run on Arctic Silt discussed in Chapter 2. The temperature of the CRS cell, and

thus the specimen, changed between load and unload cycles during this single test. First, the specimen was loaded and unloaded at room temperature, then heated to 60°C and loaded and unloaded again, and finally cooled back to room temperature for one last load-unload cycle. The resulting compression curve is included as Figure 6-1. The curve is plotted vertical stress (not effective) versus void ratio. The vertical effective stress is not plotted because there was an issue with the pore pressure transducer that prevented the collection of accurate pore pressure measurements during the test. However, any developed pore pressures were likely very small, so the test can be reasonably understood by the total stress values.

As the name suggests, CRS tests are strain rate controlled experiments. For tests using RGoM-EI Nordquist (2016) uses a strain rate of 0.3% strain per hour. This research uses the same value. The strain rate must be high enough that excess pore pressures develop, but low enough that the flow due to the pore fluid being squeezed out does not disturb the soil fabric.

In the compression curve for CRS1510, Figure 6-1, a slight shift exists between the room temperature (blue) cycles and the hot (red) load-unload cycle, particularly at the lower stress range around 1 MPa. This supports the hypothesis that there is a shift in the compression curve with changing temperature that previous literature studies also support. On the other hand, at the higher stress level of about 10 MPa there is no shift between the blue and the red curve. Based on this one curve, the effect of temperature on the compression curve is unclear. During the UT GeoFluids Consortium Meeting 8.0, sponsoring researchers suggested that changing the temperature rapidly during a test of one specimen could be artificially affecting the way the clay fabric has set up. An additional challenge to the test protocol of varying temperature during one test is the cell apparatus expands and contracts as a result of the rapid heating and cooling (Figure 5-19). The expanding and contracting affects the LVDT reading and thus the strain measurement which must be accurately accounted for when reducing the raw data. The

sponsors suggested running each test at a single temperature and comparing them instead of changing the temperature midway. For these reasons, CRS1510 was the only test run using the changing temperature test protocol.

Ten more CRS tests were run to study the effect of temperature on compression properties. Five test specimen were compressed at 20°C, four at 60°C, and one at 40°C. These ten compression curves are plotted in Figure 6-2. In all the figures, compression curves that are a shade of red indicate it is an elevated temperature test, and shades of blue indicate a room temperature test. There is one outlier in Figure 6-2, the room temperature test CRS1522. The compression curve for this test is included in Figure 6-2, but is omitted from the rest of the analysis and figures. CRS1522 was run at 20°C, and therefore, should match all other room temperature tests from this research program and be similar to the ones run by previous GeoFluids members. Clearly the slope is different than all the other curves, and additionally the porosity reaches about 0.15. It would take an effective stress greater than 40 MPa to bring the porosity lower than 0.2. Exactly what caused this test to be an outlier is uncertain, however, it is excluded from the analysis because the curve is not representative of the room temperature compression behavior.

Figure 6-3 includes the nine experimental compression curves and a regression line fit to all of the data. The line is fit to the data between the stress range of 0.1 to 40 MPa, this is the range that represents the virgin compression line (VCL). There is a pretty strong linear-log relationship between the porosity and vertical effective stress with an R^2 value of 0.994 for all of the data.

Next the data are split into two subgroups to analyze, a set of five elevated temperature tests and one set of four room temperature tests. The 40°C test is plotted on the "heated" figure (Figure 6-4), however, the data from that test was not included in the data set used to determine the regression line equations. Figure 6-4 shows all elevated

temperatures hot tests and Figure 6-5 includes the room temperature ones. Each set has good repeatability with R^2 values greater than 0.9, but the room temperature tests are slightly more repeatable with an R^2 value of 0.998. Figure 6-6 compares just the two trend lines. There is a small divergence at greater stress levels, for example at a vertical effective stress of 20 MPa based on the 20°C line the porosity is 0.257 and based on the 60°C line the porosity is 0.242. This is a difference in porosity of 0.015.

An application of the experimental results is shown in Figure 6-7 and Figure 6-8. These two figures are porosity versus depth curves that were calculated based on the buoyant unit weight of RGoM-EI and the experimental compression curves. The buoyant unit weight of RGoM-EI is calculated based on the specific gravity, G_s, the unit weight of 80 g/L sea salt water, and the void ratio (which changes with depth). The buoyant density is integrated with depth to calculate the stress at discrete depth intervals. This calculated stress is then compared to the compression curve to determine the porosity expected at that stress. Then this porosity can be plotted as a function of depth. Based on Figure 6-7 there is not much of a difference between the curve calculated based on the average elevated temperature regression line (from Figure 6-4) and the one from the room temperature tests (from Figure 6-5). At shallow depths the lines lie right on top of each other and at the deeper depths, 5250 meters, the difference is less than 0.01 porosity units. Figure 6-8 plots the porosity versus depth curve based on the compression lines for the two most different elevated temperature tests. Figure 6-4 shows all of the elevated temperature tests and it is clear that CRS1533 lies at the upper bound of compression curves and CRS1517 is at the lower bound. The slope of these two compression curves are used to create the two porosity versus depth curves in Figure 6-8. The difference in the porosity depth profiles for the two elevated temperature tests at a depth of about 5250 meters is about 0.04 porosity units, greater than the difference between the two average profiles in Figure 6-7. Based on these two plots it is clear that the scatter in the elevated temperature tests is much greater than the room temperature ones, but there is a very minor shift in the curve comparing the two sets of data (Figure

6-7). The minor shift seen in Figure 6-7 is in the direction expected based on the literature discussed in Chapter 2 and the field measurements. The hotter curve sits at a lower porosity than the room temperature curve for a given depth.

The data from this research are also compared to compression data from previous research on RGoM-EI material. All previous compression tests on RGoM-EI were tested at room temperature, so this comparison verifies the room temperature trend. Figure 6-6 includes all of the test data for this research, a trendline developed by Nordquist (2014) based on his collected data, and the published compression data for RGoM-EI on the UT GeoFluids website. The trendline for this research matches the GeoFluids database well and converges with it at higher stress levels. There is a large difference between the reported lines from the research by Nordquist and data from this research; there is a divergence between the two data sets at high stress levels. No clear explanation is evident for the difference between the two research data sets because they all use specimen of RGoM-EI created through the resedimentation process. However, the resedimentation source material for this research and the research by Nordquist is from different buckets of clay powder. Although the buckets were sent to a processing facility to be mixed, one hypothesis for the difference is perhaps there is variation between the different storage buckets.

6.2.2 Compressibility and Coefficient of Compressibility

Volume compressibility, m_v (m^2/kN), and the compression ratio, CR, are two parameters derived from the compression curves. m_v is defined as the change in strain divided by the change in effective stress, $\Delta\varepsilon/\Delta\sigma'$, and instructions for calculating m_v are included in Chapter 5. CR is the slope of the virgin compression line in a strain versus log effective stress space; it is the change in strain per log cycle of stress. CR is defined in Equation 6-1 below:

$$CR = \frac{\Delta\varepsilon}{\Delta \log(\sigma'_v)} \qquad (6-1)$$

Where:
Δε = change in strain in decimal format

Figure 6-10 shows the volumetric compressibility versus porosity for all experiments. There is some variability between the different curves, however, no systematic variability exists between the elevated temperature and room temperature tests. Figure 6-11 is the same volumetric compressibility data against vertical effective stress (instead of porosity). The curves in Figure 6-11 match each other much better than in the previous figure. This is likely due to errors in the initial measurements of the CRS specimen before compression, which are used to calculate porosity values. When the data is compared against vertical effective stress the specimen dimension measurements are not relied on and the variability between curves is much lower.

Similar to Figure 6-10, Figure 6-12 shows the compression ratio, CR, for all tests against vertical effective stress. Often times in soil mechanics CR is reported as a constant value for a material. Figure 6-12 shows that there is a change in CR with stress level (as the stress level increases CR decreases). Therefore, in Table 6-2 the CR value for each test is reported for two different stress ranges (when applicable). Again, for CR there is no difference between the CR values for elevated temperature tests and those for the room temperature tests.

6.3 Permeability Measurements

During CRS tests, data are collected so the permeability can be calculated as a function of porosity. Section 5.4.2 includes instructions for how to calculate permeability and Figure 6-12 shows the permeability data for all of the tests in this research (again excluding CRS1522) with a regression line fit to the experimental data. It is important to note that the calculation for permeability accounts for temperature effects on the

dynamic viscosity and density of water. The appropriate constant values are used in the calculations for 20°C, 40°C, and 60°C tests.

The figures display the regression line equations in the format of Equation 6-2 below:

$$log_{10}(k) = \gamma(n - 0.5) + log_{10}(k_{0.5}) \qquad (6-2)$$

Where:
γ = slope of the regression line
$k_{0.5}$ = permeability at a porosity of 0.5

The regression line is of this format based on correlation information in Casey (2014). His results show the permeability of a soil at a porosity of 0.5 gives the best correlation with the liquid limit of the material (Casey, 2014).

The permeability data is split up into two more figures, one for the room temperature tests and one for the elevated temperature tests. Figure 6-14 shows the five elevated temperature tests and the regression line fit through the data in the same format as Figure 6-13. Comparing the regression line in Figure 6-14 to the regression line for the room temperature tests in Figure 6-15, the difference in the $k_{0.5}$ values based on the hot and cold correlation lines is $1x10^{-18}$. However, the difference in $k_{0.5}$ just between elevated temperature tests is about $5x10^{-18}$ so the difference between the two sets of data is much smaller. Similar to Figure 6-6, Figure 6-16 compares the two different temperature regression lines. The elevated temperature regression line is shifted slightly higher than the room temperature line at higher porosities, but the two converge at lower porosities (higher stress levels).

6.4 Discussion of Temperature Compression Results

The results of this research suggest that temperature may have a minor effect on the compression properties of clay material, but not as significant an effect as the literature

suggests. While there is a slight shift in the compression curves and the resulting porosity versus depth curves, the scatter between compression curves of the same temperature tests is as great as the difference between the average room temperature compression curves and elevated temperature curves.

The conclusion of this research is different than what is reported in the literature where there is a more significant and clear effect of temperature. It is important to restate that all of the CRS tests included in the results were on RGoM-EI material that was batched to a salinity of 80 g/L sea salt. Therefore, perhaps the effect of temperature on compression properties of clay is specific to the type of clay. In the literature studies included in Chapter 2, the materials tested include an illite material, silt, and Newfield clay from New York. The plasticity index of these materials (all saw a shift in the compression curve) are on either side of the plasticity index of RGoM-EI so it seems unlikely it's directly linked in plasticity. No information is given regarding the pore fluid salinity used in the literature experiments though. Using 80 g/L pore fluid salinity (as in this research) collapses the double layer which may reduce the sensitivity to temperature. The double layer thickness has an effect on how adjacent clay particles interact with each other, attracting or repelling each other. These interactions affect compressibility properties at low stress levels (Horan, 2012) which may be impacting the temperature sensitivity.

The conclusion of this research is, therefore, that temperature has a minor effect on the compression curve but no effect on compression properties or permeability of RGoM-EI at a pore fluid of 80 g/L and in the stress range of 0.1-40 MPa.

Table 6-1: List of all CRS tests performed for research in this thesis (some are for the salinity research discussed in Chapter 7).

Test No.	Date Started	Temp. (°C)	Analyzed for Temp. Effects	Salinity Measurements	Station	Notes
CRS1510	1/23/2017	-	Yes	-	Station 9	Different test protocol
CRS1517	4/24/2017	60	Yes	-	Station 9	
CRS1518	5/6/2017	60	Yes	-	Station 9	
CRS1521	6/9/2017	20	Yes	-	Station 9	
CRS1522	7/12/2017	20	Yes	-	Station 9	Porosity outlier
CRS1526	8/16/2017	20	Yes	-	Station 9	
CRS1529	9/7/2017	20	Yes	-	Station 9	
CRS1530	9/18/2017	60	Yes	-	Station 9	
CRS1532	9/27/2017	40	Yes	-	Station 9	
CRS1533	10/5/2017	60	Yes	-	Station 9	
CRS1535	10/23/2017	20	No	Yes	Manual	
CRS1536	10/30/2017	20	Yes	-	Station 9	
CRS1534	10/18/2017	90	No	-	Station 9	PVA problem
CRS1537	11/4/2017	20	No	Yes	Manual	
CRS1539	12/2/2017	20	No	Yes	Manual	Load cell broke
CRS1541	12/12/2017	20	No	Yes	Manual	
CRS1540	12/9/2017	20	No	Yes	Manual	

Table 6-2: Summary of results for all CRS tests related to the temperature effect.

Test No.	Resed No.	Initial Conditions					Maximum Stress			Final	CR	
		w_i (%)	e_i (-)	S_i (%)	γ_d (g/cm^3)	γ_t (g/cm^3)	σ'_{vm} MPa	ε_a (%)	e_f (-)	w_f (%)	0.1-1 MPa (-)	1-10 MPa (-)
CRS1517	RS547	48.49	1.38	104.27	1.184	1.8	9.63	41.71	0.39	21.00	0.26	-
CRS1518	RS547	49.47	1.486	98.89	1.132	1.736	28.19	49.14	0.26	19.04	0.26	0.16
CRS1521	RS547	48.09	1.342	106.37	1.198	1.824	29.03	46.17	0.26	15.52	0.24	0.17
CRS1522	RS550	57.32	1.652	103.78	1.059	1.725	39.11	54.66	0.20	16.11	0.22	0.15
CRS1526	RS550	56.06	1.673	100.11	1.051	1.695	38.50	52.25	0.27	17.14	0.25	0.15
CRS1529	RS550	50.88	1.552	97.52	1.1	1.709	38.27	49.65	0.28	16.18	0.27	0.16
CRS1530	RS551	59.57	1.804	98.94	1.001	1.657	39.38	55.11	0.26	16.07	0.27	0.14
CRS1532	RS551	56.85	1.712	99.28	1.035	1.681	17.93	49.91	0.36	16.52	0.24	0.16
CRS1533	RS551	56.18	1.694	99.11	1.043	1.684	40.10	52.68	0.27	17.63	0.28	0.16
CRS1536	RS551	51.61	1.55	99.08	1.101	1.72	38.93	50.01	0.27	16.33	0.25	0.16

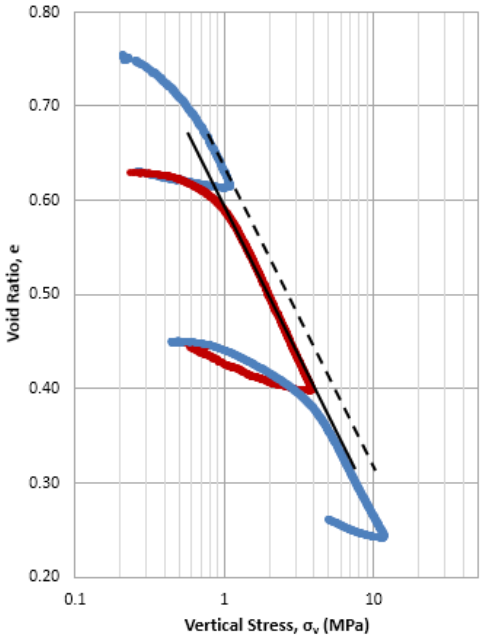

Figure 6-1: Compression curve for CRS1510. There are two load-unload cycles at 20°C (blue curves) and one load unload cycle at 60°C (red curve).

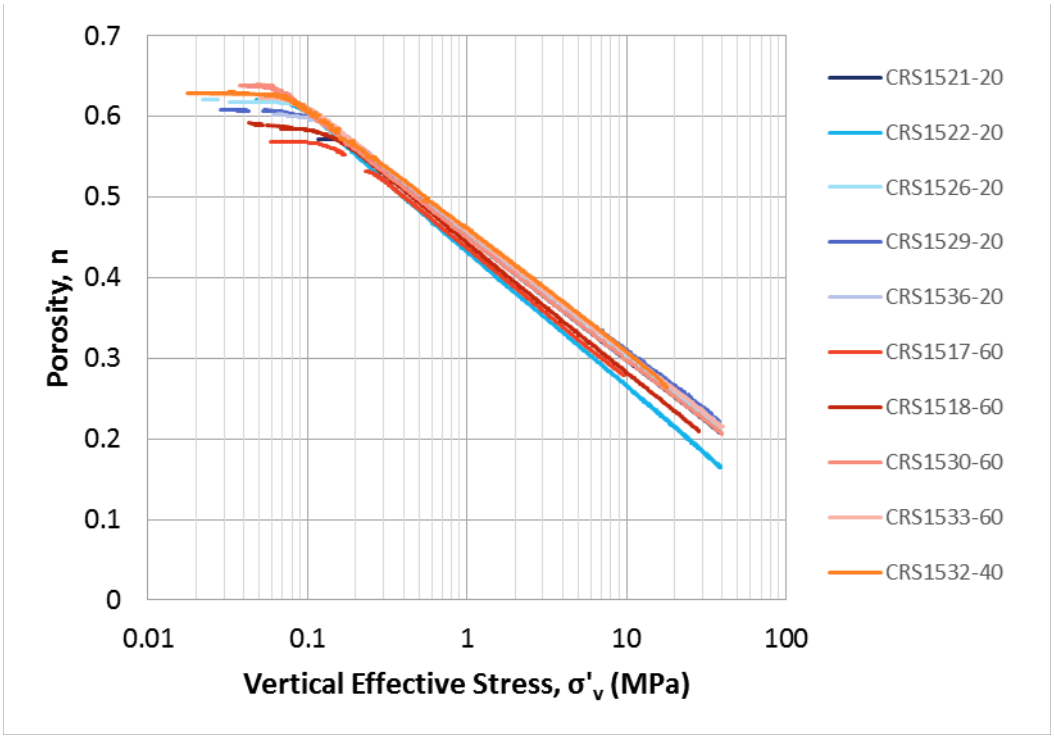

Figure 6-2: Ten compression curves run at single temperatures, five at 20°C, four at 60°C, and one at 40°C. CRS1522 is the outlier and removed for all subsequent analyses.

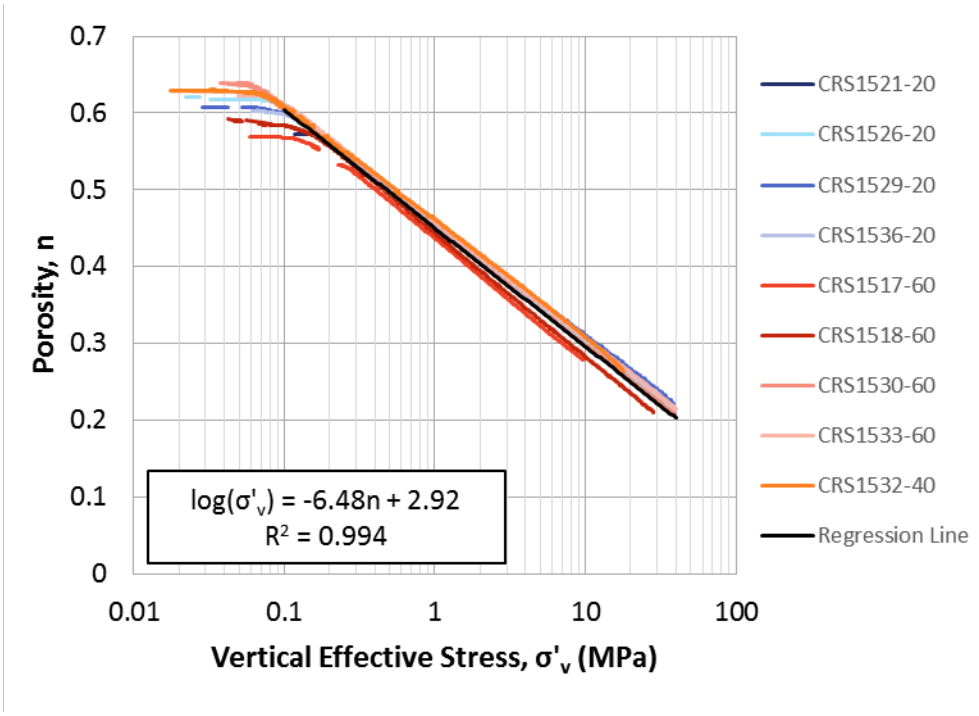

Figure 6-3: Compression curves used for analyses with the regression line fit to all of the data (room temperature and elevated) and regression equation.

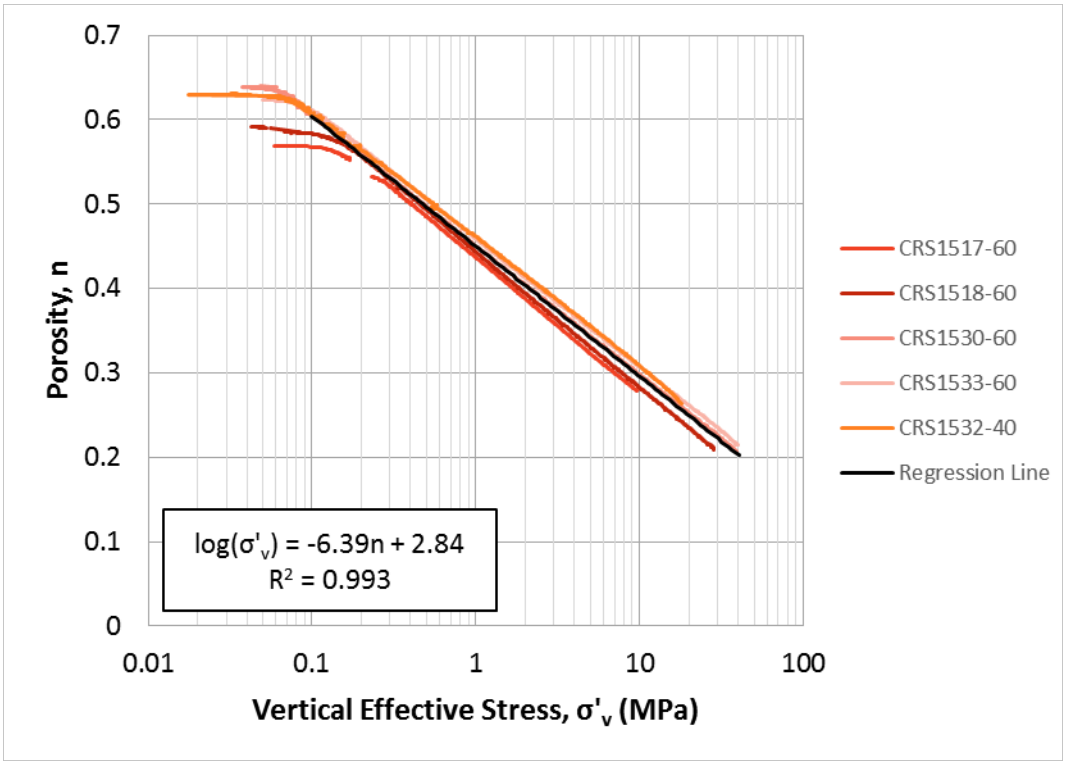

Figure 6-4: Elevated temperature test compression curves with regression line and equation included.

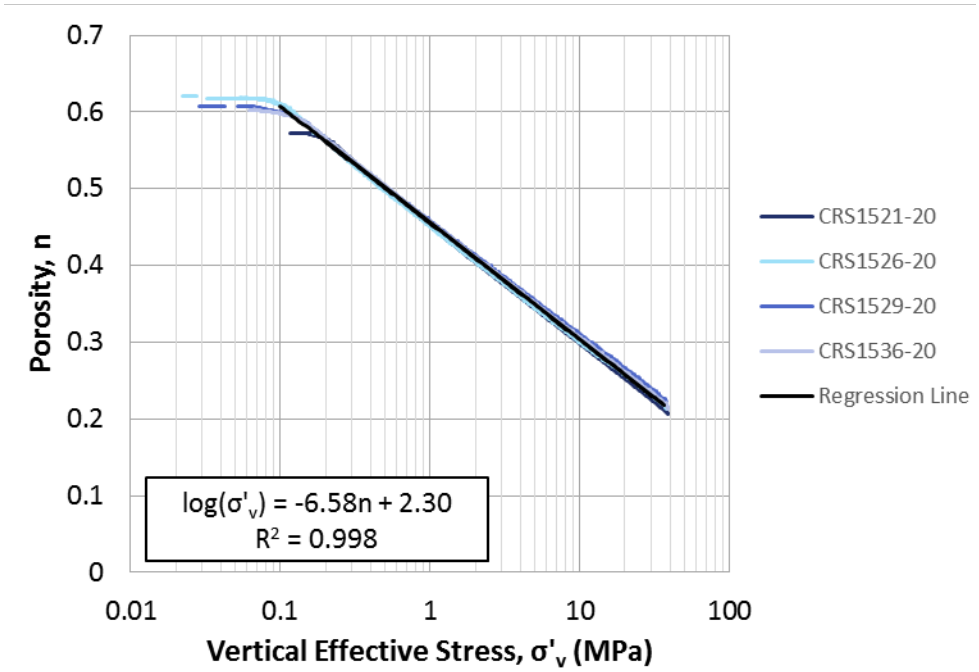

Figure 6-5: Room temperature, 20°C, test compression curves with regression line and equation included.

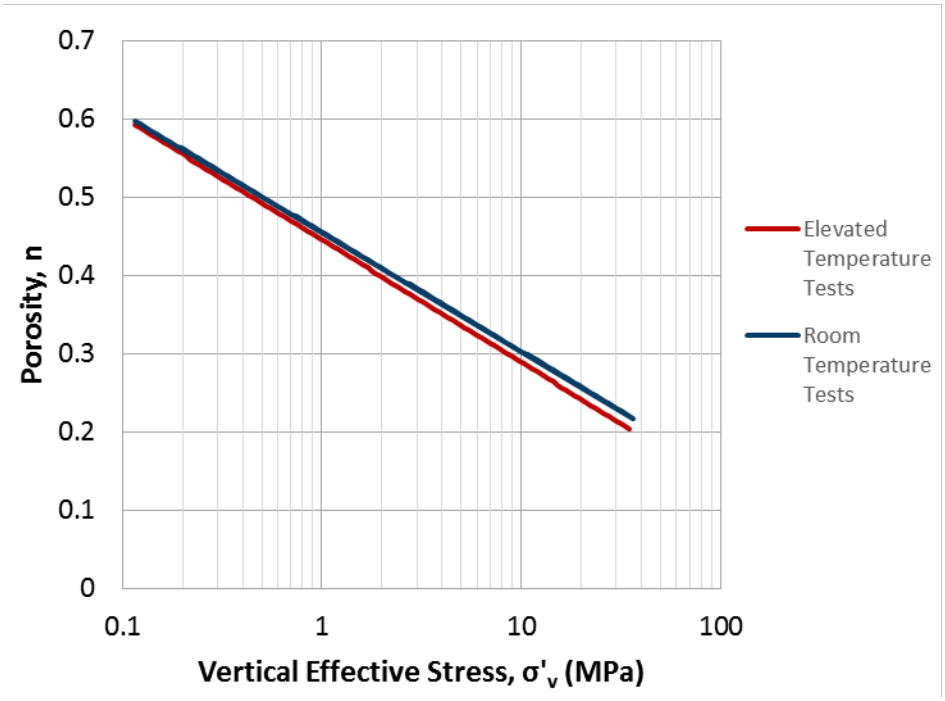

Figure 6-6: Comparison of regression lines fit to the elevated temperature test data and the room temperature test data.

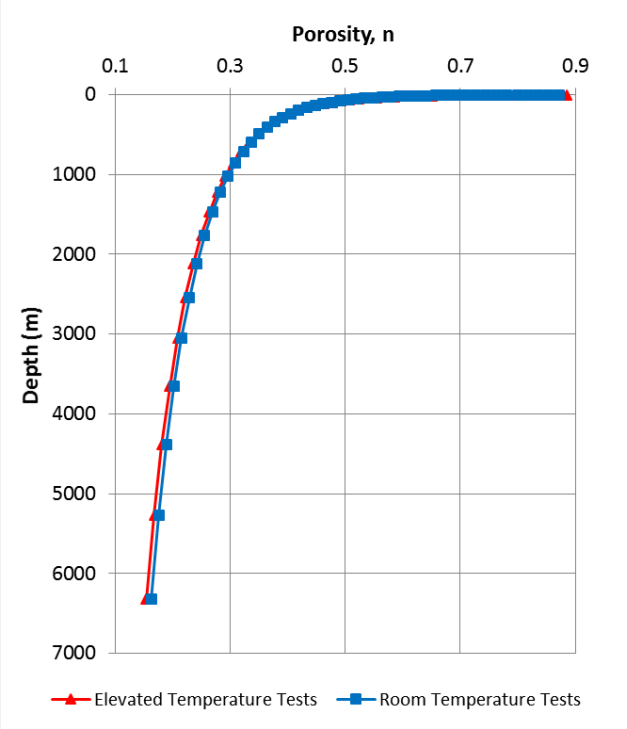

Figure 6-7: Comparison of porosity versus depth curve based on the regression line for the elevated temperature tests and the regression line for the room temperature tests.

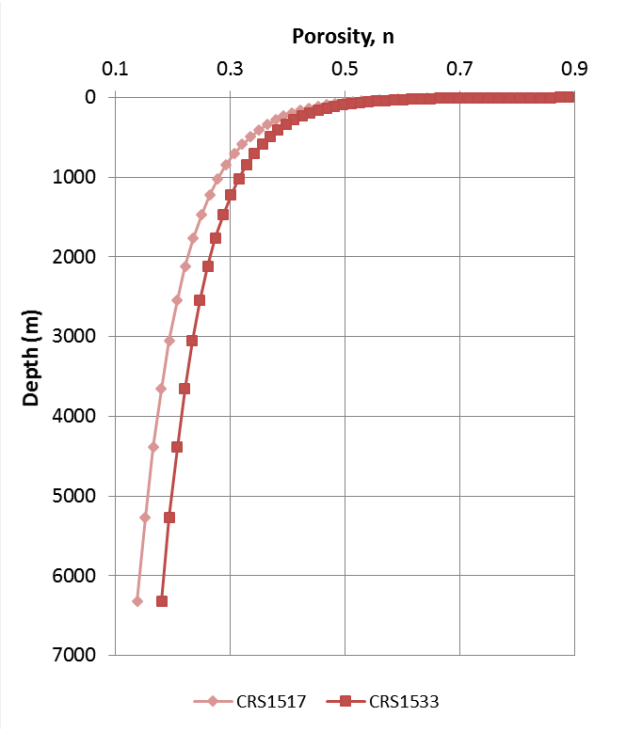

Figure 6-8: Comparison of porosity versus depth curves for the two elevated temperature tests that had the greatest difference between compression curves.

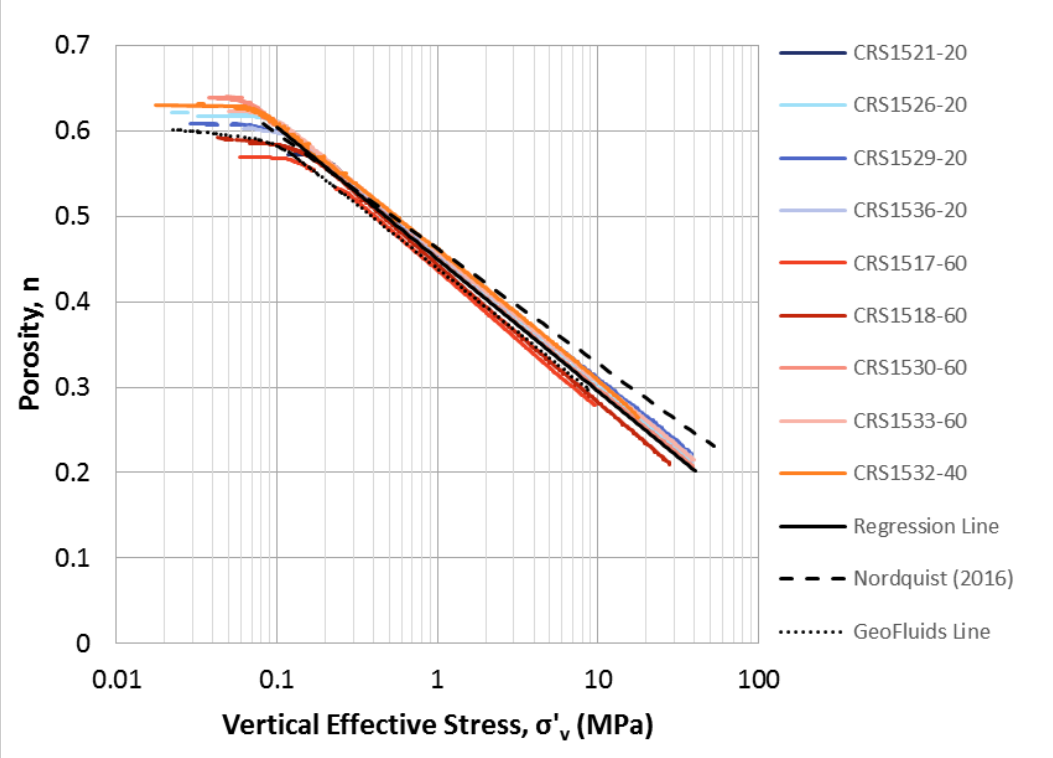

Figure 6-9: Comparison of compression curves from this research to regression line from research by Nordquist and published RGoM-EI data in the GeoFluids database.

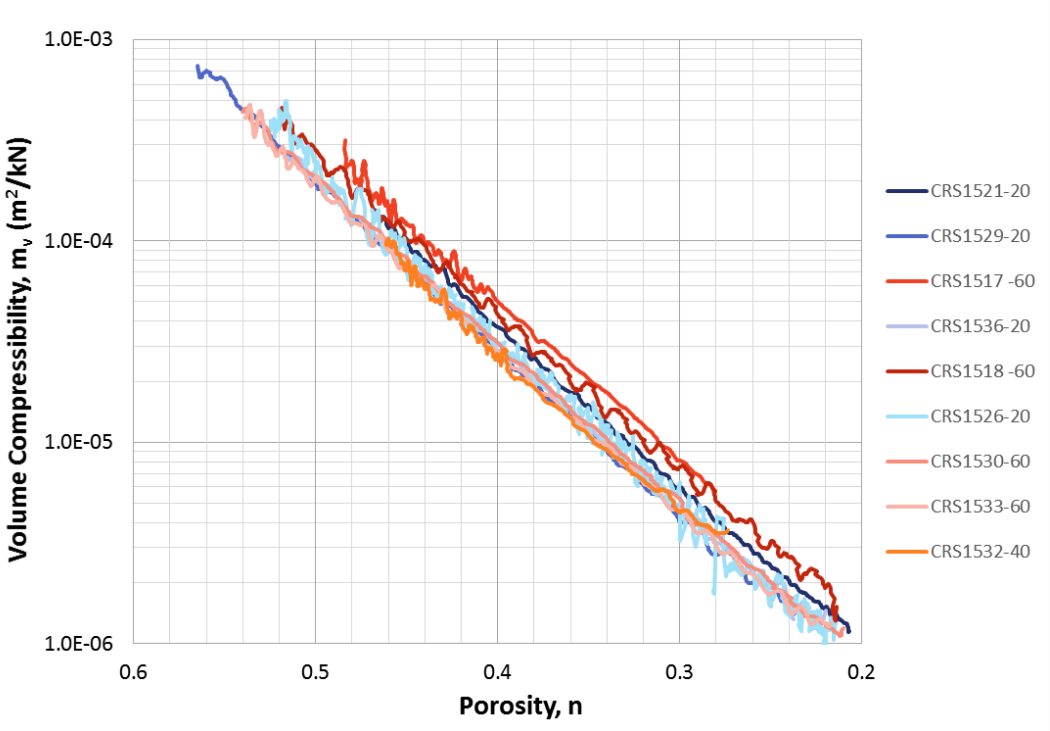

Figure 6-10: Volume compressibility, m_v, versus porosity curves.

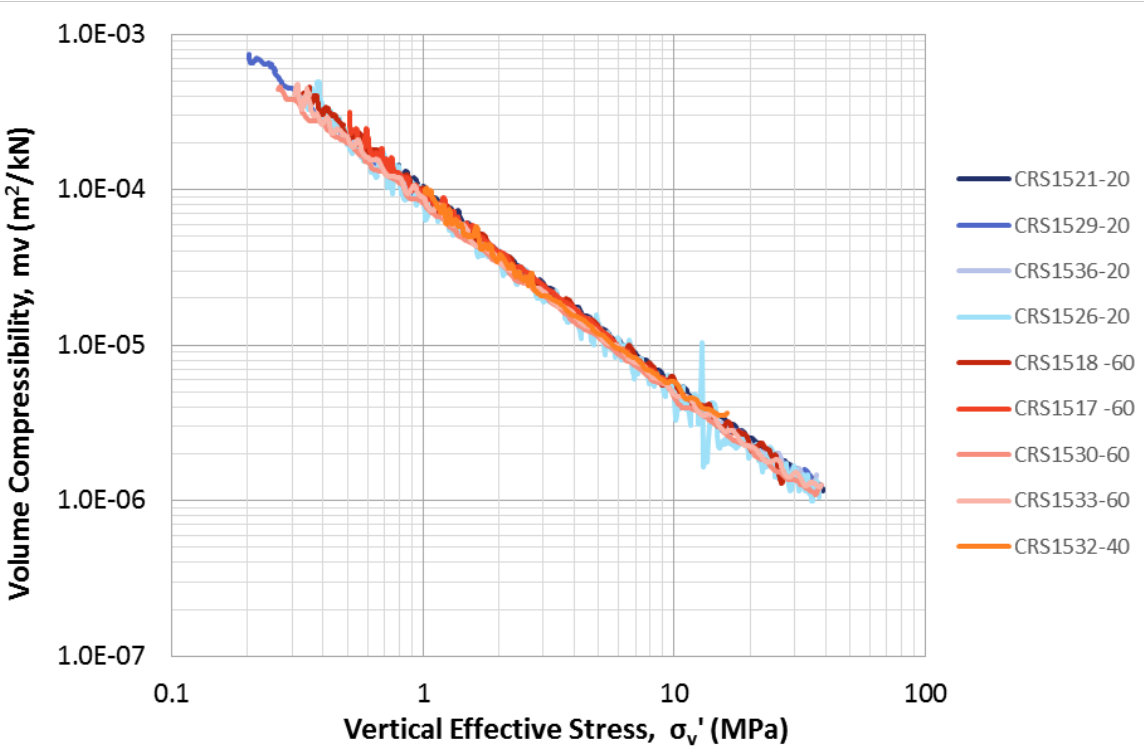

Figure 6-11: Volume compressibility, m_v, of all tests versus vertical effective stress.

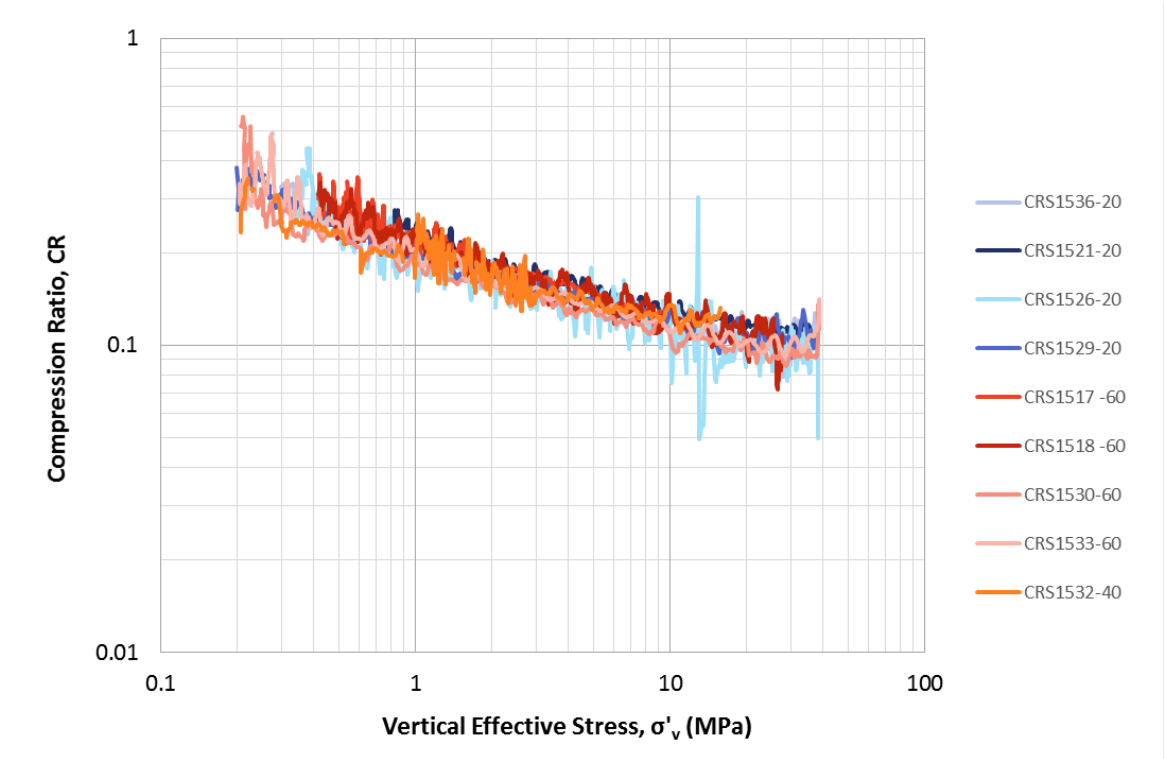

Figure 6-12: Compression ratio, CR, for all tests.

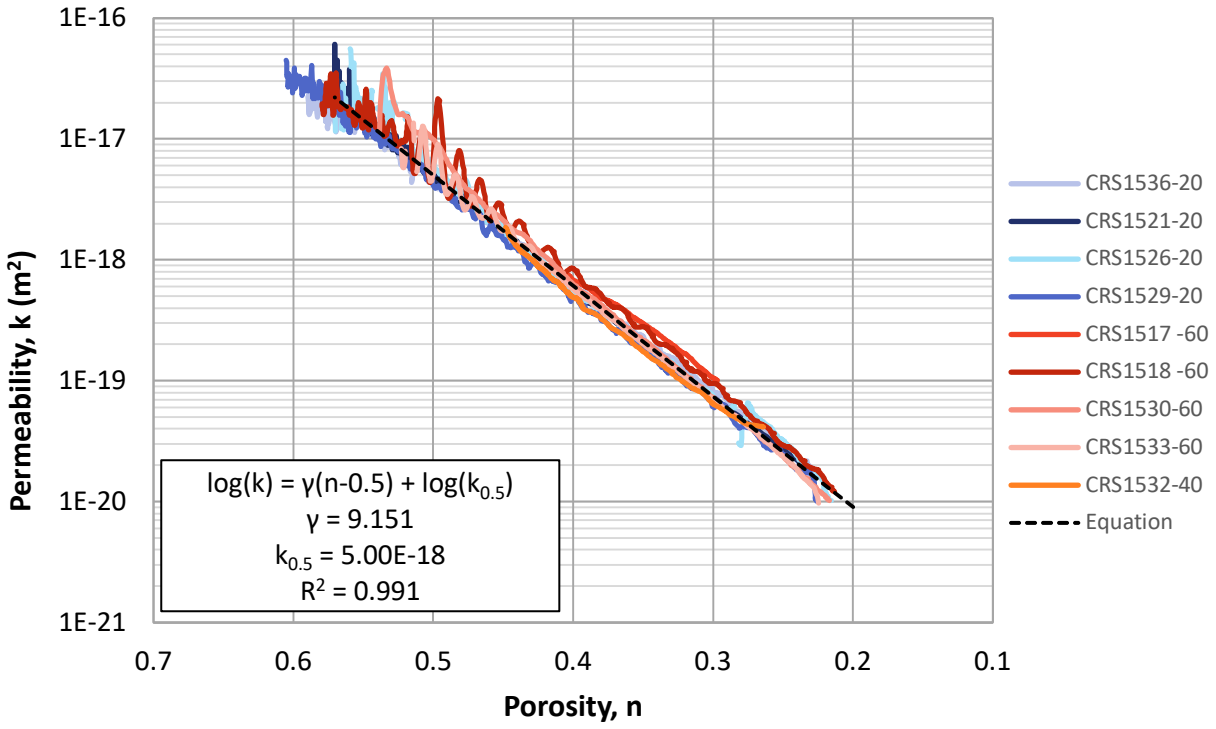

Figure 6-13: Permeability data for all compression tests with regression line fit to all the data.

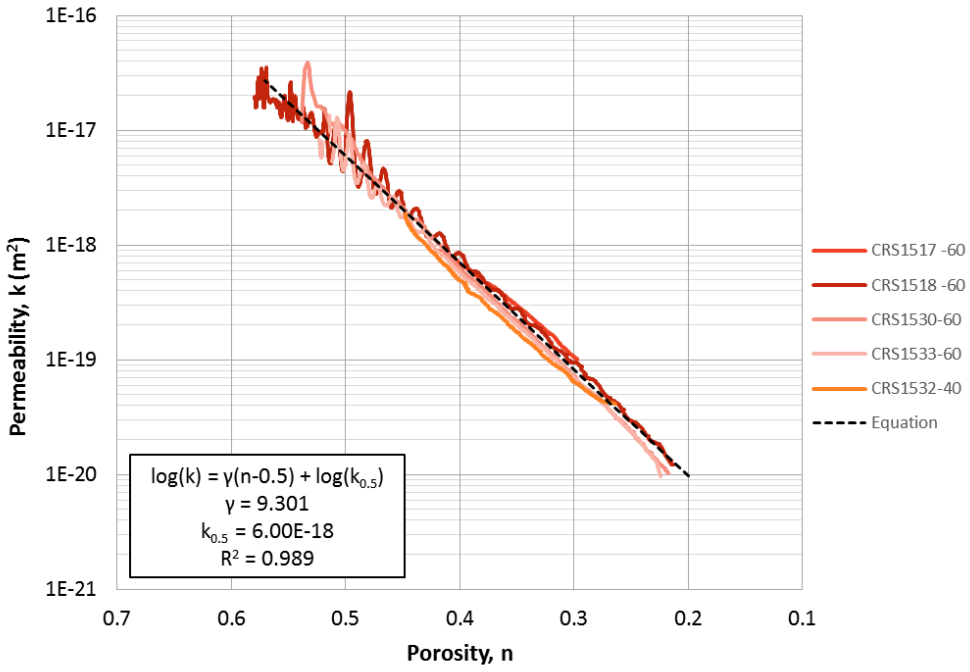

Figure 6-14: Permeability data and correlation for elevated temperature tests.

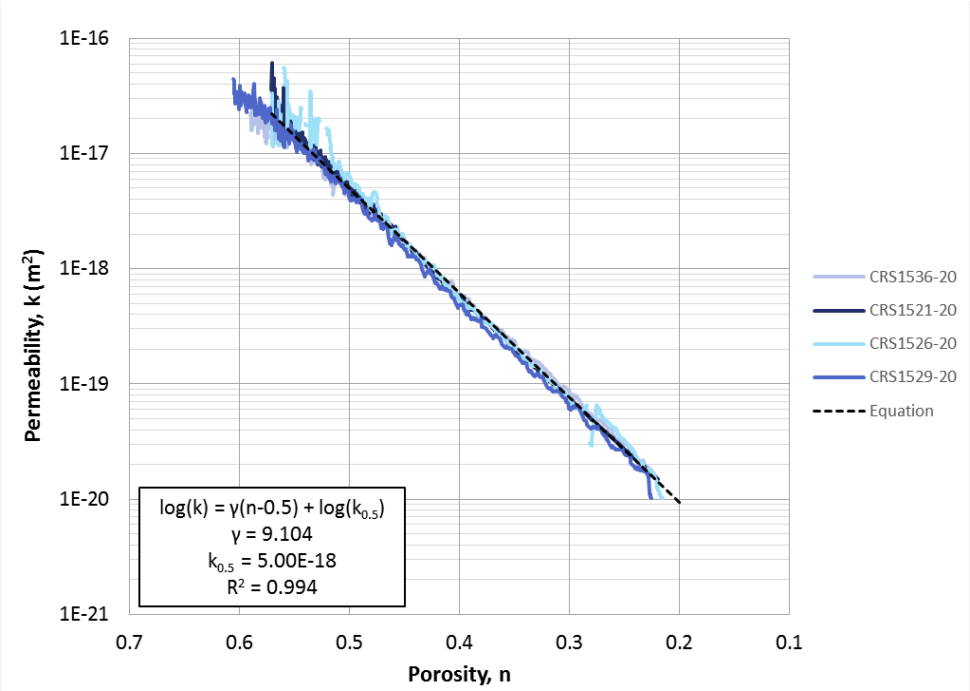

Figure 6-15: Permeability data and correlation for room temperature tests.

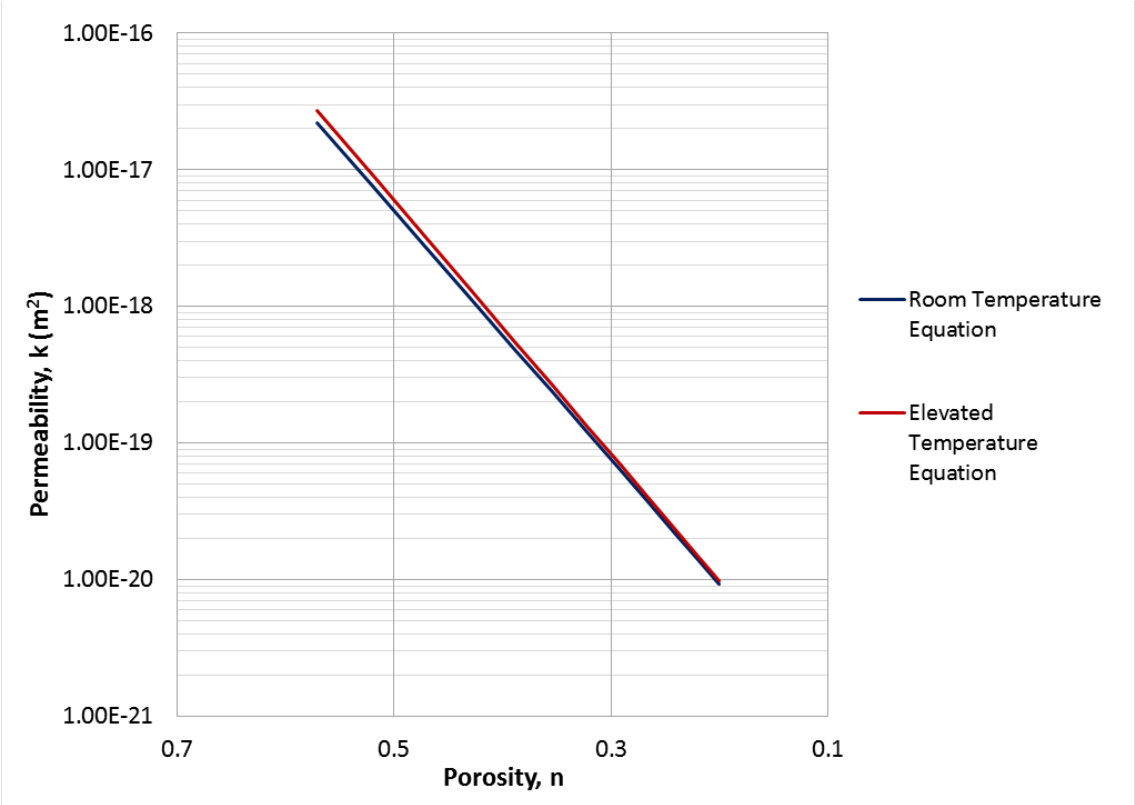

Figure 6-16: Comparison of regression lines fit to permeability data for room temperature and elevated temperature tests.

7 Salinity Results and Model Development

7.1 Introduction

This chapter summarizes the results from the investigation of the effect of compression on pore fluid salinity. Section 7.2 outlines experimental results and discusses the trends in the data from eighteen salinity experiments. Section 7.3 explains the "Interpreted Pore Fluid Salinity" model developed to predict the salinity of a sample of clay material at a specified stress level.

7.2 Salinity Results

Eighteen salinity test results are included in this research. The total includes six tests on batched slurries prepared for resedimentation tubes (before being incrementally loaded), eight CRS specimens compressed to various stress levels, and five slices from resedimentation tubes (after being incrementally consolidated to 0.01 MPa). The following sections discuss the results of these tests. Section 7.2.1 focuses on the salinity of the slurries and Section 7.2.2 summarizes the results for the CRS test specimens and resedimentation slices.

7.2.1 Salinity of a Slurry and Error Evaluation

The purpose of measuring the salinity of the resedimentation slurries prior to resedimentation was twofold: to evaluate the error and variability associated with the measurements and to measure the salinity of the slurries at the lowest experienced stress level. Five of the six slurries were batched to a water content of 120% and a target pore fluid salinity of 80 g/L. One slurry, S_SLURRY4, was batched with distilled water so the only salt in the mixture is the salt contained in the dry clay powder.

Table 7-1 lists all of the slurry salinity tests.

The salinity of the slurries batched to the target value of 80 g/L sea salt and 120% water content are measured to quantify the variability between test tubes. To understand the variability and precision of the salinity measurements the following statistical calculations are based on ASTM Standard E691-18: Standard Practice for Conducting an Interlaboratory Study to Determine the Precision of a Test Method (2018).

For each slurry salinity test, four test tubes of the slurry from the same batch are made (the slurry is well blended after the resedimentation mixing process so all test tubes should contain identical material). As instructed in Section 5.3.2, three independent measurements are made of the supernatant that comes from each of the four tubes. The three measurements are made on the same sample of the decanted supernatant. The measurements are used to determine an SS value, the salinity of the supernatant using Figure 4-4. Then, an RSS value, the salinity of the pore fluid is calculated with Equation 5-40 or Equation 5-45. The average of the three RSS values associated with one test tube is used as the representative salinity value for that tube. Using the average RSS values, there are then four average values per salinity test, one from each test tube. The average of the four test tube averages is used as the representative salinity value for the test specimen. Figure 7-1 to Figure 7-3 show the results for the test of S_SLURRY5a.

Figure 7-1 is a bar graph of the three RSS values based on the three independent measurement trials for Test Tube 3. The three values shown on this graph, 92.62 g/L, 93.95 g/L, and 91.65 g/L, are then averaged to determine the average salinity of Test Tube 3. This is the value used to plot the “5a Test Tube 3” bar on Figure 7-2. The error bar associated with the 5a Test Tube 3 bar in Figure 7-2 is the standard deviation of the three values shown in Figure 7-1, 0.597 g/L in this example. This process is repeated for the next three test tubes in the set. The final step is to average the four test tube averages to calculate a single representative salinity value for each specimen. The representative salinity values of each slurry salinity test, with their respective error

bands, are plotted in Figure 7-3. Figure 7-3 also has the average value of all slurry batches that were made to 80 g/L and 120% water content and the error band associated with these measurements. The error band on the orange bar, "AVERAGE", is the standard deviation of the reported salinity values for all the slurry tests, ± 8.15 g/L.

In subsequent plots of salinity data, there are error bands associated with each data point. Calculation of the error associated with the measurements relies on the results from S_SLURRY5a and S_SLURRY5b. The test tubes made for these two tests used material from the same batch of slurry, so there were eight identical tubes of that slurry. The same calculations as outlined in the previous paragraph are followed to determine the average salinity of each test tube (eight averages). The error bar on subsequent plots is then the coefficient of variation of those eight averages, 12.97%, multiplied by the average salinity for the subsequent tests. For example, the average of S_CRS1535 is 42.49 g/L and the error bar is ± 5.51 g/L.

7.2.2 Post CRS Test Specimen Salinity

This section interprets the results of the salinity tests on the CRS specimen and resedimentation slices. There are two types of specimen included, either specimen directly from the resedimentation tube at a stress level around 0.01 MPa or specimen after a CRS test. Testing the resedimentation tube slices along with the CRS test specimen allows direct comparison of the salinity of a specimen before and after compression. Table 7-2 lists the salinity tests included in this section.

Results of all the salinity tests listed in Table 7-2 are plotted in Figure 7-4. It is apparent from Figure 7-4 that the salinity decreases as the void ratio decreases. The resedimentation tubes used here are resedimented to approximately 0.01 MPa. The data from slices of resedimentation tubes are clustered in the 70 to 86 g/L range. The data points from slurry salinity tests are at a void ratio of 3.3. The data in the lower void ratio range, e less than 1.0, are from CRS tests stopped at predetermined stress levels

between about 1 and 40 MPa. Figure 7-5 is the same data as in Figure 7-4 but plotted versus effective stress instead of void ratio. Again, the salinity decreases with an increase in stress level.

A second way to look at the change is by plotting the pairs that directly represent before and after being put into a CRS apparatus for compression. Figure 7-6 shows the five pairs. The values at the higher salinity and higher void ratio are slices of material in the resedimentation tube adjacent to its partner CRS specimen. The lower point is the CRS specimen after compression. A total of five pairs were tested with before and after data. All of the resedimentation slices start at approximately the same salinity, and the slight variations do not carry into the after compression results. Specifically, CRS1537 has a higher starting salinity than CRS1541. However, since CRS1537 is compressed to a lower void ratio than CRS1541, the resultant salinity is lower than CRS1541.

Another subset of the data from Figure 7-4 is plotted in Figure 7-7. This shows all of the measurements on specimen that originate from the same resedimentation tube, RS480. The trend of salinity decreasing with stress level is true for this set of data, but in this data set another layer of information is available. Figure 7-8 is a diagram of where, vertically, in the resedimentation tube the specimen was. It is interesting that there is no pattern, based on this set of data, of salinity versus tube location, particularly for the resedimentation slices. The slice from the tube that is associated with CRS1537 is in the middle of the other two resedimentation slices for CRS1540 and CRS1535, but has the highest salinity of 87 g/L. One explanation could be that based on the order of testing, the slices associated with CRS1535 would have been cut from the tube and then the tube replaced in the 80 g/L water bath until ready to test the next specimen. There is no consideration to how much time the resedimentation tube sat with the material that would later become CRS1537 at the bottom of the tube in contact with the porous stone and the 80 g/L salt water bath.

Overall, the results of this section provide clear evidence that the salinity of specimens decrease with increasing stress level. This research measures the salinity of the pore fluid left behind during a compression test (not the effluent liquid expelled during compression). The next goal is to develop a model to predict the salinity of clay at a particular stress level.

7.3 Salinity Model Development

This section discusses the development of the Interpreted Pore Fluid Salinity Model developed to predict the salinity of a clay element at a particular stress level. Section 7.3.1 explains the input parameters used to understand the clay mineral geometry. Section 7.3.2 explains how to use the inputs to evaluate how the clay geometry changes during compression. Section 7.3.3 applies the developed model to RGoM-EI, and Section 7.3.4 discusses recommendations for future work and compares this research to what is in the literature.

The basis of the developed model is an understanding of what physically happens at the clay particle scale during mechanical compression. A schematic of the hypothesis for what happens during a compression test is included as Figure 7-9. A single clay particle of RGoM-EI with its associated electrolyte and fluid is used to represent a unit element. In Figure 7-9a, the pre-compression clay particle is shown (for simplicity only half is shown and it would be mirrored over the "centerline"). The black arrows represent a vertical stress applied during compression. Figure 7-9b is the same clay particle system as Figure 7-9a during compression. Notice the only difference from Figure 7-9a is the reduction in size of the free pore fluid; the height of the free pore fluid changes from $h_{fpf,0}$ to h_{fpf}. During a compression test, water is squeezed out of the specimen, and the following model relies on the assumption that the water expelled comes from the free pore fluid volume. There is no change in the double layer water and the interlayer water until the stress level is so high that compression eliminates all of the free pore fluid. One important distinction to point out is there is a difference between pore fluid and free

pore fluid. Pore fluid is the total amount of water in the element, the sum of the double layer water, interlayer water, and free pore fluid water. The free pore fluid is the water labeled in Figure 7-9, and is a single component of the free pore fluid.

7.3.1 Physical Parameters

The first step in model development is to quantify the system parameters of interest and how they change with stress. Figure 7-9 provides a schematic with labels of the geometry of interest. Even though in a real system this should be a three-dimensional unit, in one-dimensional compression there is no change in area. The constant area allows the system to be simplified to a one-dimensional system and heights of components to be compared instead of volumes.

The model formulation requires seven main physical parameters which are mostly related to the geometry and physical properties of a clay particle and labeled in Figure 7-9. The inputs are listed and defined below:

1. Initial Void Ratio, e_0: The void ratio of the clay before compression begins. For CRS specimen, the "Physical Properties" section of Chapter 5 explains how to calculate void ratio based on the initial dimensions and water content.
2. Initial Salinity, s_0 (g/L): The salinity of the material at the initial void ratio. For a resedimented sample this is the salinity of the water mixed with the dry clay power plus the salts that already exist in the clay powder.
3. Thickness of Clay Layer, t_S (Å): Thickness of one of the physical clay layers (for example smectite layer in Figure 2-1 or t_S in Figure 7-9). The clay layer thickness is the sum of the tetrahedral and octahedral sheet thicknesses.
4. Thickness of Hydrated Clay Layer, t_{total} (Å): This is the thickness of one clay layer plus the associated interlayer water. In Figure 7-9, t_{total} is the sum of t_{IL} and t_S.
5. Number of Layers per Clay Particle, n_{layers}: XRD identifies the total thickness of one clay particle. The total thickness of one clay particle and the thickness of a hydrated clay layer are used to determine the number of layers per clay particle.

6. Thickness of Double Layer, t_{DL} (Å): The distance away from the clay particle surface that the double layer spans. The thickness depends on the salinity of the surrounding pore fluid. Figure 2-3 shows the relationship between the thicknesses of the double layer and pore fluid salinity. Figure 7-9 includes a label of t_{DL} for the RGoM-EI example particle.
7. Clay Fraction, CF (%): The percent of the bulk material that is actually clay size particles.

These seven inputs define the clay mineral geometry and initial material properties to quantify all of the dimensions shown in Figure 7-9. The thickness of the interlayer is calculated first with Equation 7-1.

$$t_{IL} = t_{total} - t_s \qquad (7-1)$$

The convention used in this research is “thickness” is referring to one single unit and its associated measurement, and “height” is used to refer to the total amount of a parameter in the specimen of interest. For example, if the thickness of the double layer is 5Å and there are two double layers per clay particle then the height of the double layer is 10Å. The next step is to quantify all the “heights”. Figure 7-10 is a schematic of the total element that identifies the heights of interest. A discussion of the sand component is included below. Equations 7-2 to 7-6 identify how to compute the heights based on thicknesses defined previously. First, the height of the interlayer water, h_{IL} (Å), is calculated with Equation 7-2 below:

$$h_{IL} = t_{IL} * \left(n_{layers} - 1\right) \qquad (7-2)$$

Then the total height of water within a particle, the “interwater”, h_{IW} (Å), is calculated with Equation 7-3. This includes the double layer and interlayer water but does not include free pore fluid.

$$h_{IW} = h_{IL} + 2 * t_{DL} \quad (7-3)$$

The third parameter is the height of clay solids, h_{clay} (Å), calculated using Equation 7-4:

$$h_{clay} = n_{layers} * t_s \quad (7-4)$$

Finally, it is important to consider that the specimen being compressed is not purely clay. The clay fraction is less than 100% meaning that there are some sand solids. Accounting for the sand solids is important because the sand contributes to the total amount of solids in the system, which affects the void ratio. The sand is omitted in Figure 7-9 because it doesn't have an effect on the clay specific behavior during compression, but it is included in Figure 7-10 because it is part of the entire element. The height of sand solids, h_{sand} (Å), is calculated using Equation 7-5:

$$h_{sand} = \frac{h_{clay}}{\left(CF/_{100}\right)} - h_{clay} \quad (7-5)$$

Where:

CF = clay fraction input value (%)

Now the height of the free pore fluid can be calculated. The initial free pore fluid height, $h_{fpf,0}$ (Å), is based on the height of the other parameters and the known initial void ratio. Equation 7-6 is used to calculate the $h_{fpf,0}$:

$$h_{fpf,0} = e_0 * \left(h_{sand} + h_{clay}\right) - h_{IW} \quad (7-6)$$

In the above equation, and for the rest of this chapter a "0" subscript indicates the value of a parameter at initial conditions and a subscript "n" indicates the values of the parameter at an "nth" time interval into a compression test.

7.3.2 Applying the Physical Parameters to Model Salinity Evolution

Section 7.3.1 identifies all the necessary physical parameters before compression. The next phase is to understand how these parameters change with compression. In a dry clay, adsorbed cations are tightly held by the negatively charged clay surface (Mitchell, 1976). The clay powder used to create the resedimented specimen for salinity experiments already contains the cations needed to satisfy the negative clay particle charge (they are so tightly attracted it is difficult to separate them). Additionally, there are likely cations in excess of the required amount to satisfy the charge and sea salt water is added to the powder to create the resedimentation slurry. All of the ions added in the sea salt water and any excess cations in the powder are in solution and dissolved in the free pore fluid. This means the free pore fluid salinity is actually higher than the target batch pore fluid salinity value. The actual free pore fluid salinity is calculated using Equation 7-7:

$$s_{fpf} = \frac{s_0 * (h_{fpf} + h_{iw})}{h_{fpf}} \qquad (7-7)$$

A key hypothesis to this model is the free pore fluid salinity does not change during compression, s_{fpf} is a constant value. This model assumes that the free pore fluid salinity is squeezed out at the salinity initially calculated, s_{fpf}, for the duration of the compression test (or until all of the free pore fluid water is squeezed out). While the salinity of the free pore fluid does not change, the amount of free pore fluid in the system does change with stress level. The change is uniquely related to the strain of the specimen. Equation 7-8 shows how to convert the strain in the system to the change in height of the specimen.

$$\Delta h_n = \varepsilon_n * (h_{fpf} + h_{iw} + h_{clay} + h_{sand}) \qquad (7-8)$$

Where:

ε = strain of the specimen during compression in decimal form

As mentioned previously, all of the change in height is due to the free pore fluid being expelled so the Δh_n is subtracted from the initial height of the free pore fluid, $h_{fpf,0}$ to get the height of the free pore fluid at any time, n, during the test. Equation 7-9 shows this calculation:

$$h_{fpf,n} = h_{fpf,0} - \Delta h_n \qquad (7-9)$$

Now, if the cations in the double layer and interlayer are both tightly attracted to the clay particle then they are inaccessible to any measurements (Mitchell, 1976). Therefore the only cations that are accessible to measurements are those in the free pore fluid. The salinity of the free pore fluid, calculated above (Equation 7-7), and the height of the free pore fluid are used to determine the mass of the "accessible" salt in the system, these salts (and thus cations) are the ones that contribute to salinity measurements. The calculated mass of salt is distributed to the entire volume of water in the specimen (determined when the specimen is oven dried) to calculate the salinity of the pore fluid. This calculated salinity value is defined as the "Interpreted Pore Fluid Salinity" (IPFS) and is calculated with Equation 7-10 below:

$$Interpreted\ Pore\ Fluid\ Salinity = \frac{s_{fpf} * h_{fpf,n}}{h_{fpf,n} + h_{il} + h_{dl}} \qquad (7-10)$$

The Interpreted Pore Fluid Salinity is defined as the mass of the mobile ions in the element divided by the total amount of pore fluid water. Analyzing Equation 7-10, s_{fpf}, h_{il}, and h_{dl} are all constants and $h_{fpf,n}$ decreases with increasing stress level. Therefore, the entire ratio is going to decrease as stress increases.

The developed model outputs an Interpreted Pore Fluid Salinity value for any given strain input. The Interpreted Pore Fluid Salinity values can be plotted against void ratio (which is a function of strain) to examine how the pore fluid salinity is expected to change through the course of a test.

7.3.3 Model Application to RGoM-EI

The Interpreted Pore Fluid Salinity model is applied using input values for RGoM-EI. First the seven input parameters are identified for the material of interest, RGoM-EI. Table 7-3 lists the values with related notes pertaining to sourcing the information. Figure 7-11 displays the calculated IPFS curve for the RGoM-EI material. For this curve, two notable inputs are the initial salinity is 80 g/L and the initial void ratio is 3.3. To evaluate the appropriateness of the model, the calculated IPFS values are compared to the eighteen data points from the actual measurements collected in the lab. Figure 7-12 shows the laboratory data are in reasonable agreement with the IPFS model prediction, suggesting it is an appropriate model. Unfortunately, by the end of this research only RGoM-EI specimen batched with a salinity of about 80 g/L are evaluated in the lab so there are no other data sets to compare with the model. However, the model inputs can be varied to see how the IPFS is expected to change based on changing certain parameters.

Figure 7-13 to Figure 7-16 are four graphs showing how the curve changes if an input parameter is changed from the RGoM-EI parameters. In all cases, the dashed black line represents the model output for RGoM-EI inputs (shown in Figure 7-11 and Figure 7-12). In Figure 7-13 the batched salinity value is altered and therefore so is the double layer thickness (since it's a function of salinity), but in the rest of the figures only one parameter is changed at a time. In Figure 7-13 it is obvious that changing the initial salinity moves the start of the curve, e equal to 3.3, to match that initial salinity input. This change dominates the model output. In order to understand what the effect of changing the double layer is, the curves are normalized by the initial salinity value and then compared in Figure 7-14. Increasing the initial salinity does not change the double layer as much as decreasing the initial salinity does, as seen by the spacing of the curves in Figure 7-14. This is because the double layer is already very small at a salinity of 80 g/L. From Figure 7-14 the trend is increasing the double layer thickness decreases the salinity at a given void ratio. In Figure 7-15, the trend is the lower the clay fraction (more sand) the less of a change in salinity as the specimen is compressed. This is because when

there is less clay in the system there is more free pore fluid, so more of the free pore fluid needs to be squeezed out (more compression) to affect the ratio used to calculate the IPFS. Varying the clay fraction also seems to have the largest effect on the slope of the curve. Finally, Figure 7-16 shows how decreasing the initial void ratio results in the curves shifting down. However, at a salinity of around 50 g/L all of the curves converge and follow the same path.

7.3.4 Recommendations

There is potential for this research to be expanded to create a more widely proven model. There are currently plans to test RGoM-EI material batched at different salinities to confirm the model matches the experimental results. Additionally, it would be beneficial to use a different type of clay with different particle geometry to be able to vary the hydrated clay thickness parameter and the ratio of interlayer water to free pore fluid.

Perhaps, more notably the next step needs to be rectifying the discrepancy between this research and what exists in the literature. In the research summarized in Chapter 2, Fitts and Brown (1999) measure the salinity of the pore fluid being expelled from specimen while being compressed and concludes that the salinity of the expelled fluid is decreasing during compression. The TAG Lab currently does not have a set up that allows the expelled pore fluid to be collected for analysis, so instead we measure the salinity of the entire specimen and pore fluid that is left behind after a test. Based on Figure 7-4 it is clear that this measurement also has a decreasing trend with stress level. The conundrum is, therefore, where is the salt? If the measurement of what is left behind decreases with stress level and the measurement of what is expelled decreases with stress level then there is a mass balance problem. There can't be a loss of salt in the system as a whole. There is a need for more research to close this loop.

Table 7-1: Slurry salinity tests

No.	Test ID	Date	Description	Batched Salinity (g/L)	Avg. Measured Salinity (g/L)
1	S_SLURRY1	9/21/2017	Slurry for Salinity Testing	80	91.55
2	S_SLURRY2	11/1/2017	Slurry for RS486	80	73.42
3	S_SLURRY3	11/20/2017	Slurry for RS488	80	78.17
4	S_SLURRY5a	2/13/2018	Slurry for RS570 - Part a	80	90.79
5	S-SLURRY5b	2/13/2018	Slurry for RS570 - Part b	80	88.19
6	S_SLURRY4	3/1/2018	Slurry for RS571	~7	7.87

Table 7-2: Salinity tests on compressed specimen either from resedimentation tubes or after CRS compression tests.

No.	Test ID	Date	Specimen Info	Avg. Measured Salinity (g/L)	Void Ratio	Stress Level (MPa)
1	S_CRS1526	8/28/2017	CRS1526 Test Specimen	35.28	0.26	38.50
2	S_CRS1529	9/16/2017	CRS1529 Test Specimen	45.51	0.27	38.30
3	S_CRS1530	10/12/2017	CRS1530 Test Specimen	39.90	0.24	39.40
4	S_RS551A	10/10/2017	Slice of RS551 for CRS1530	72.02	1.70	0.01
5	S_CRS1535	11/16/2017	CRS1535 Test Specimen	42.49	0.46	5.23
6	S_CRS1537	11/29/2017	CRS1537 Test Specimen	66.24	0.87	2.27
7	S_RS480A	11/29/2017	Slice of RS480 for CRS1537	87.01	1.60	0.01
8	S_RS480C	12/20/2017	Slice of RS480 for CRS1540	77.60	1.60	0.01
9	S_CRS1540	12/20/2017	CRS1540 Test Specimen	60.59	0.71	1.31
10	S_RS480B	12/13/2017	Slice of RS480 for CRS1535	85.02	1.60	0.01
11	S_RS486A	12/12/2017	Slice of RS486 for CRS1541	81.02	1.60	0.01
12	S_CRS1541	1/2/2018	CRS1541 Test Specimen	68.50	0.93	0.53
13	S-CRS1543	4/3/2018	CRS1543 Test Specimen	44.67	0.82	0.91

Table 7-3: Inputs for salinity prediction model for GoM-EI

Input	Value	Notes
Initial Void Ratio	1.6	Approximate void ratio of specimen in resedimentation tube at a stress of about 0.01 MPa
Initial Batch Salinity (g/L)	80	GoM-EI Material In-situ salinity
Number of Sheets per Clay Particle	3	XRD Analysis by previous TAG Lab researchers
Thickness of Hydrated Particle (Å)	18	Fitts, 1999
Thickness of Clay Sheet (Å)	9.6	Mitchell, 1976
Thickness of Double Layer (Å)	2.6	Based on relationship shown in Figure 2-3
Clay Fraction (%)	44	XRD and Particle Size Distribution, published on UT GeoFluids website

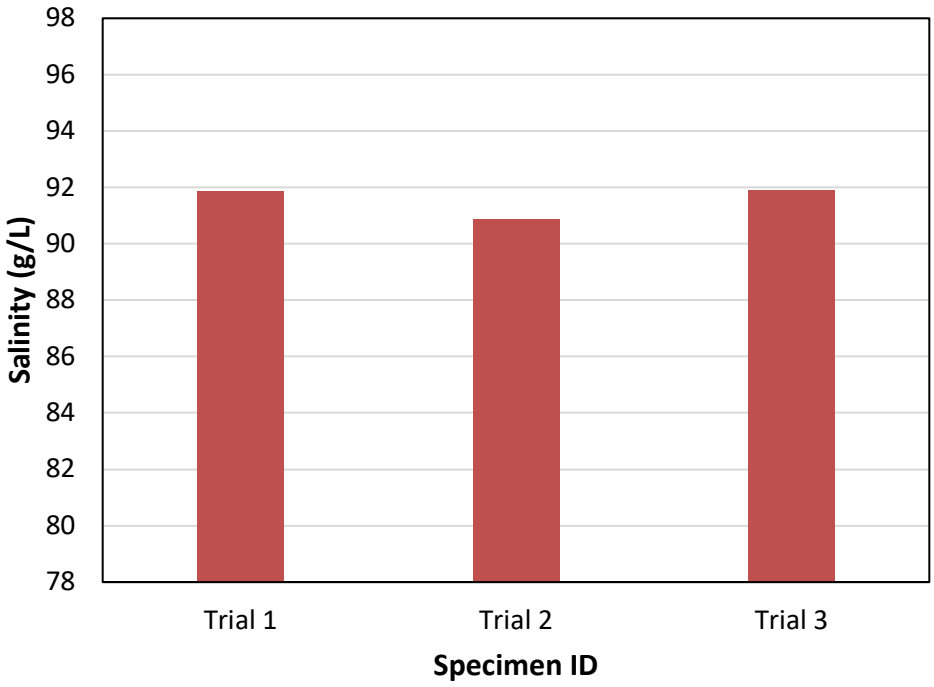

Figure 7-1: Three RSS values based on three independent measurements of one sample of the supernatant from Test Tube 3 for S_SLURRY5a

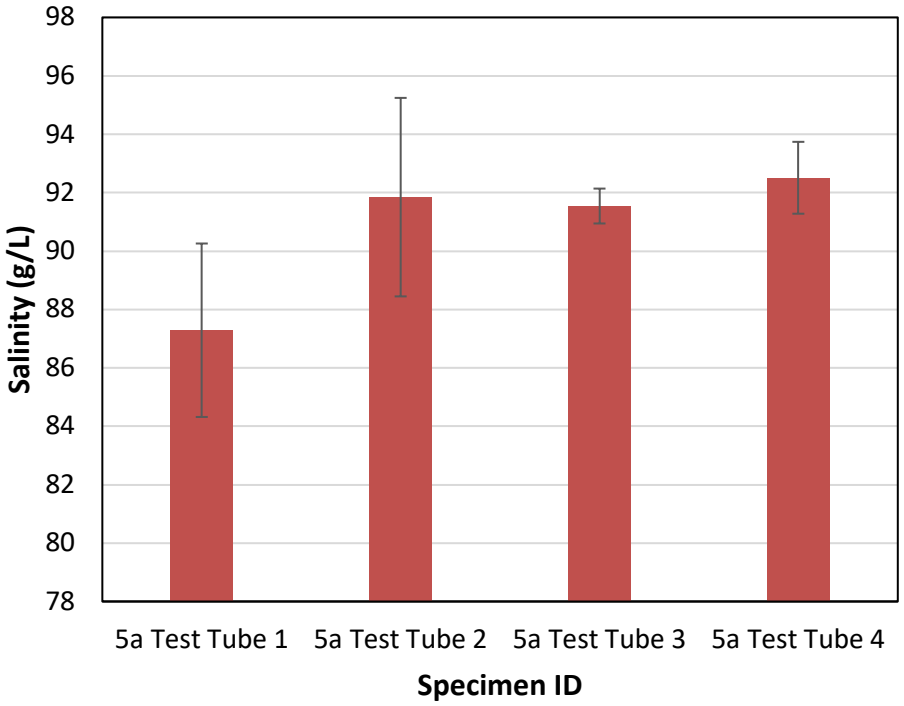

Figure 7-2: Average salinity value for each test tube for S_SLURRY5a test. Each bar is the average of the three measurements made for that tube (shown for Test Tube 3 in Figure 7-1).

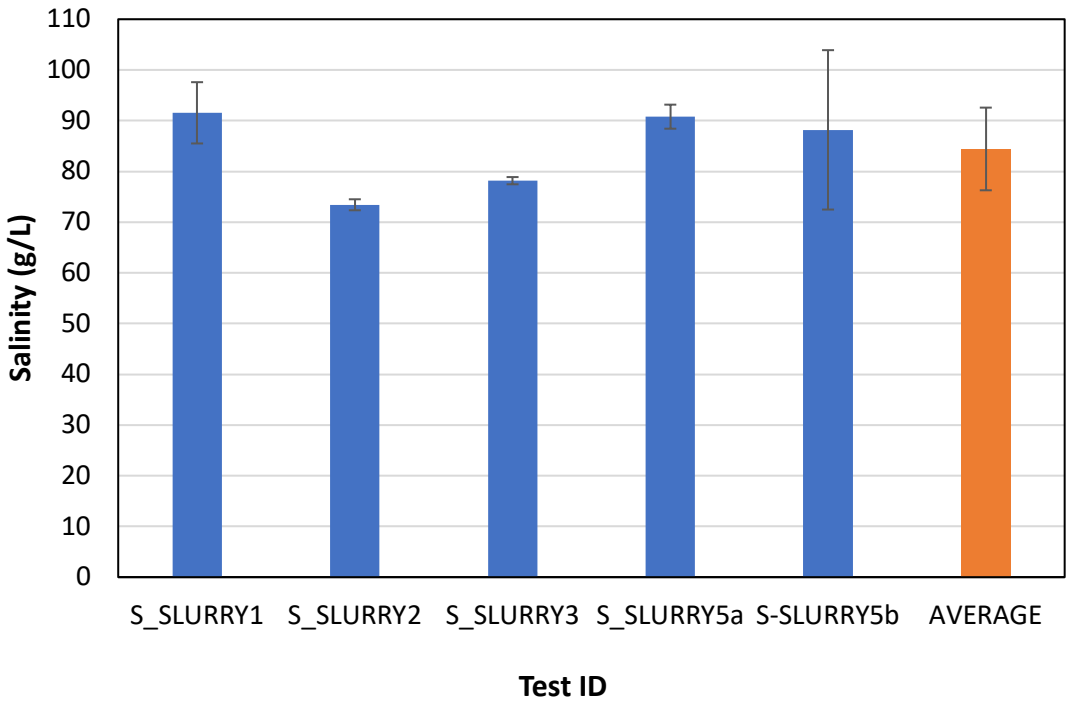

Figure 7-3: Average salinity value for all 80 g/L slurry specimen. Each bar is the average of the four test tubes made for that test with the standard deviation included as the error bar.

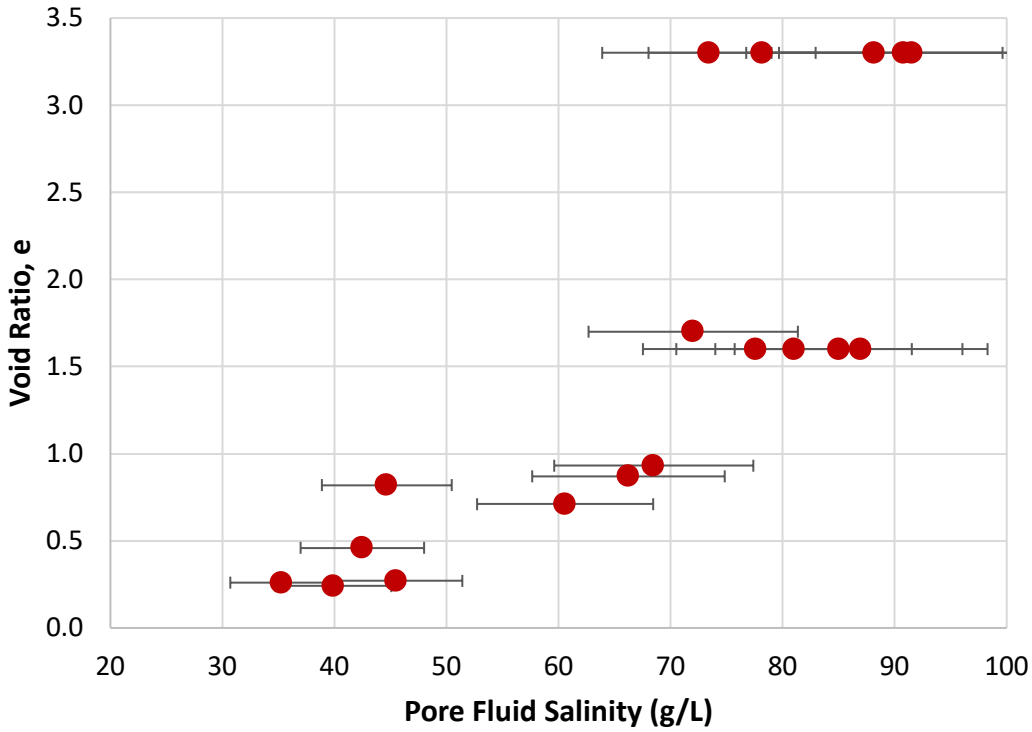

Figure 7-4: Data from all salinity tests on slurries, resedimentation slices, and CRS test specimen plotted versus void ratio.

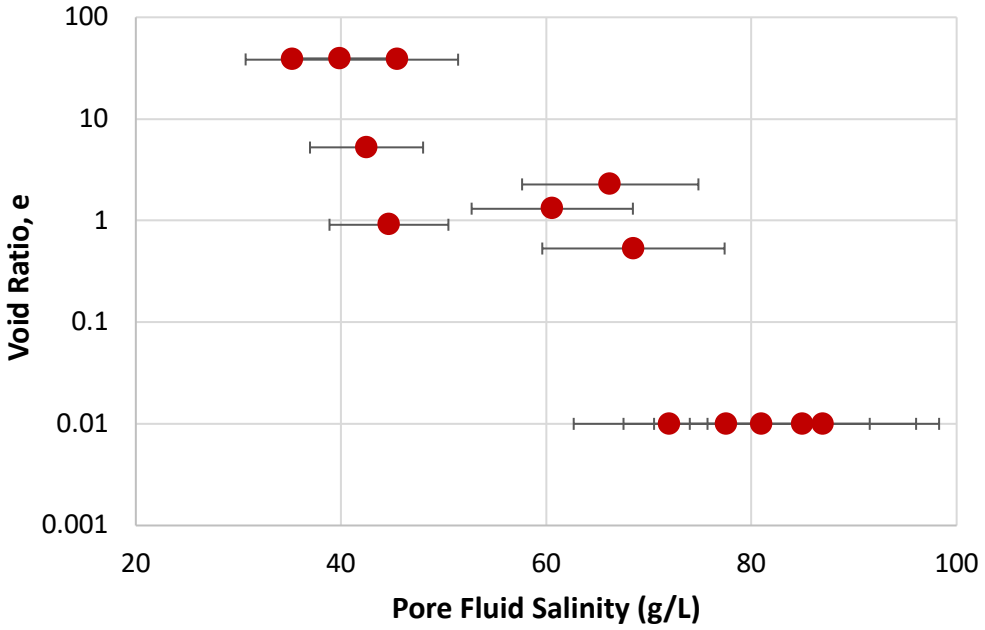

Figure 7-5: Data from salinity tests on resedimentation slices and CRS test specimen (not slurries) plotted versus effective stress.

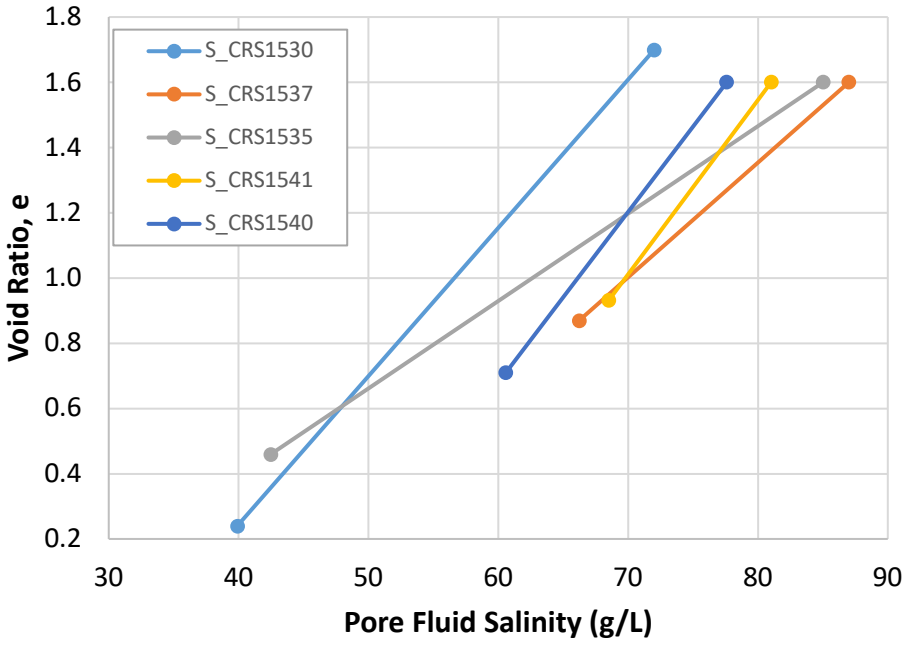

Figure 7-6: Comparison of data pairs pre and post compression. The higher void ratio data point of each pair is the slice from the resedimentation tube and the lower void ratio data point is after CRS compression.

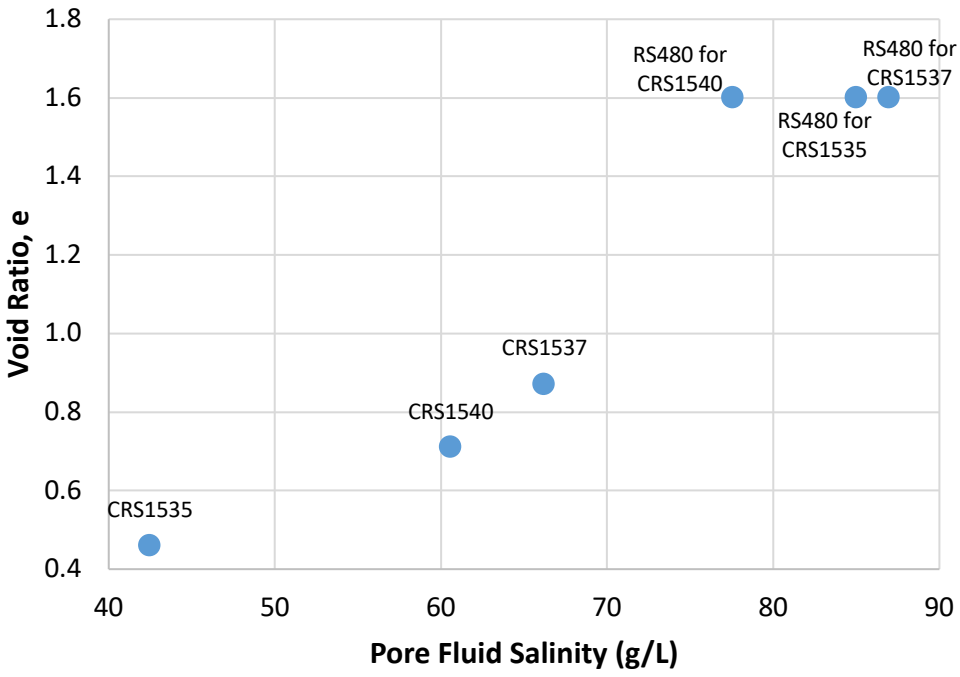

Figure 7-7: Data from salinity tests that are made of material from RS480.

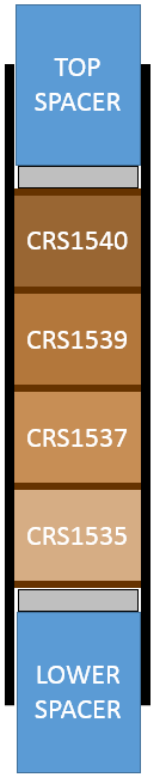

Figure 7-8: Resedimentation tube RS480 with location of salinity test specimen labeled.

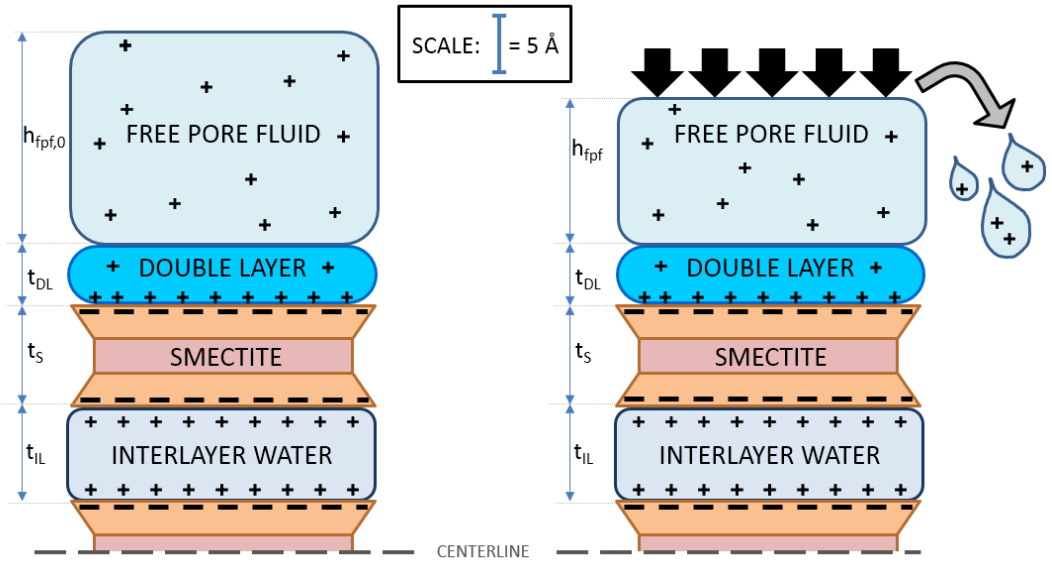

Figure 7-9: Schematic of what happens at clay particle level during a compression test. Free pore fluid is expelled and everything else remains the same.

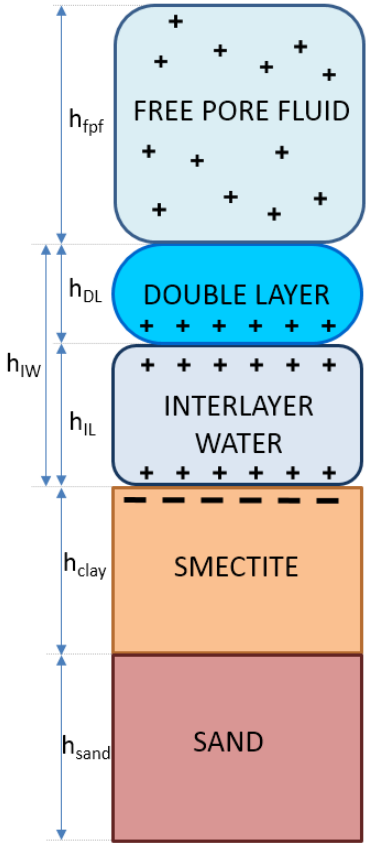

Figure 7-10: Schematic of element with sand solids included (not to scale). This schematic denotes all geometry as heights indicating it is the total amount of that parameter in the element.

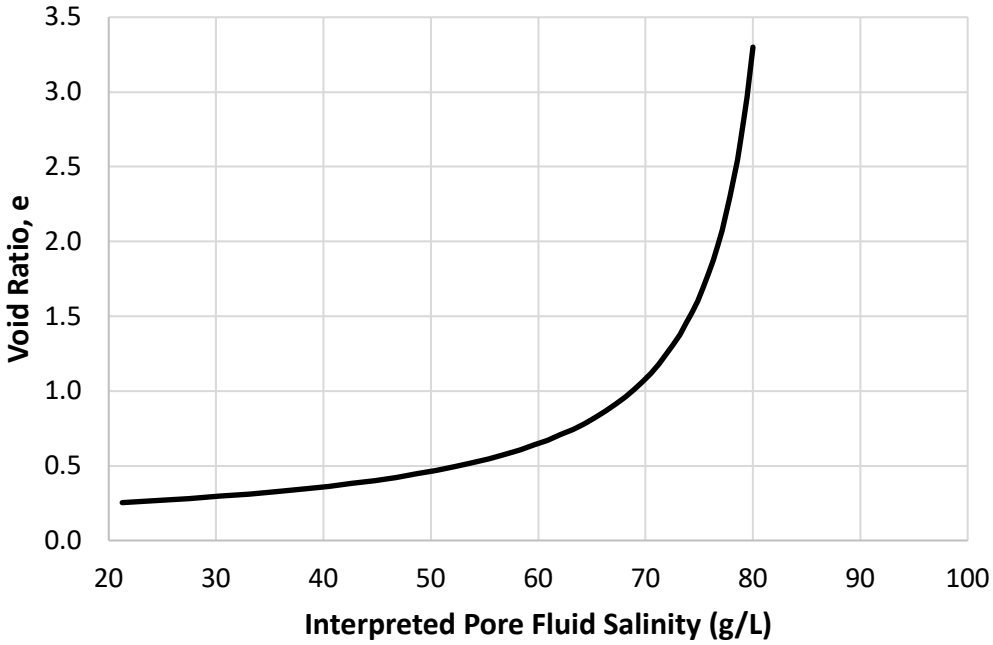

Figure 7-11: Interpreted Pore Fluid Salinity model output using RGoM-EI specific inputs. The inputs are listed in Table 7-3.

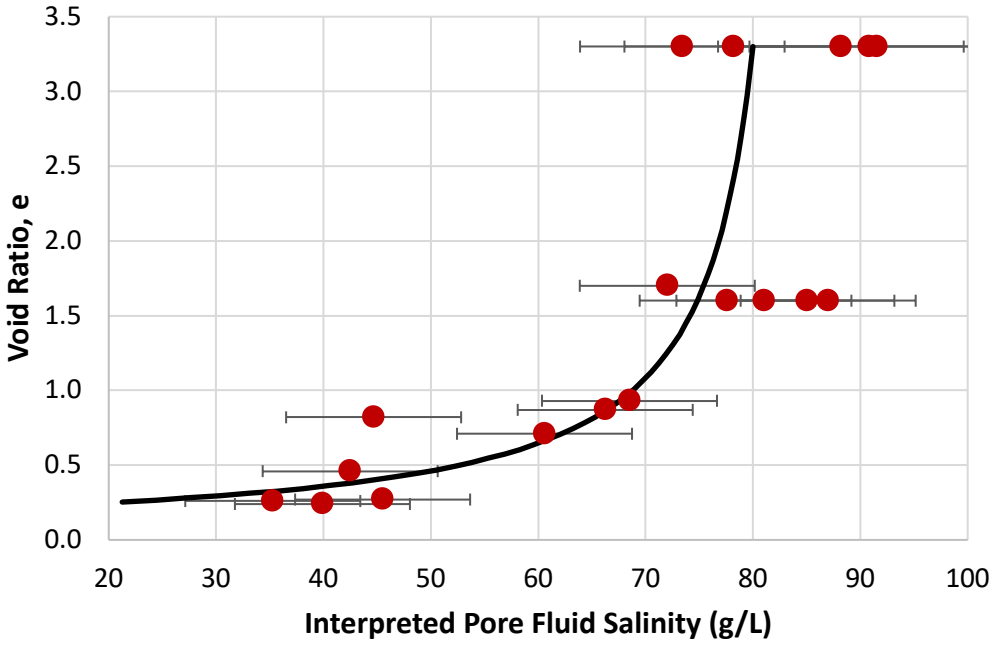

Figure 7-12: Interpreted Pore Fluid Salinity model output for RGoM-EI compared to collected salinity data.

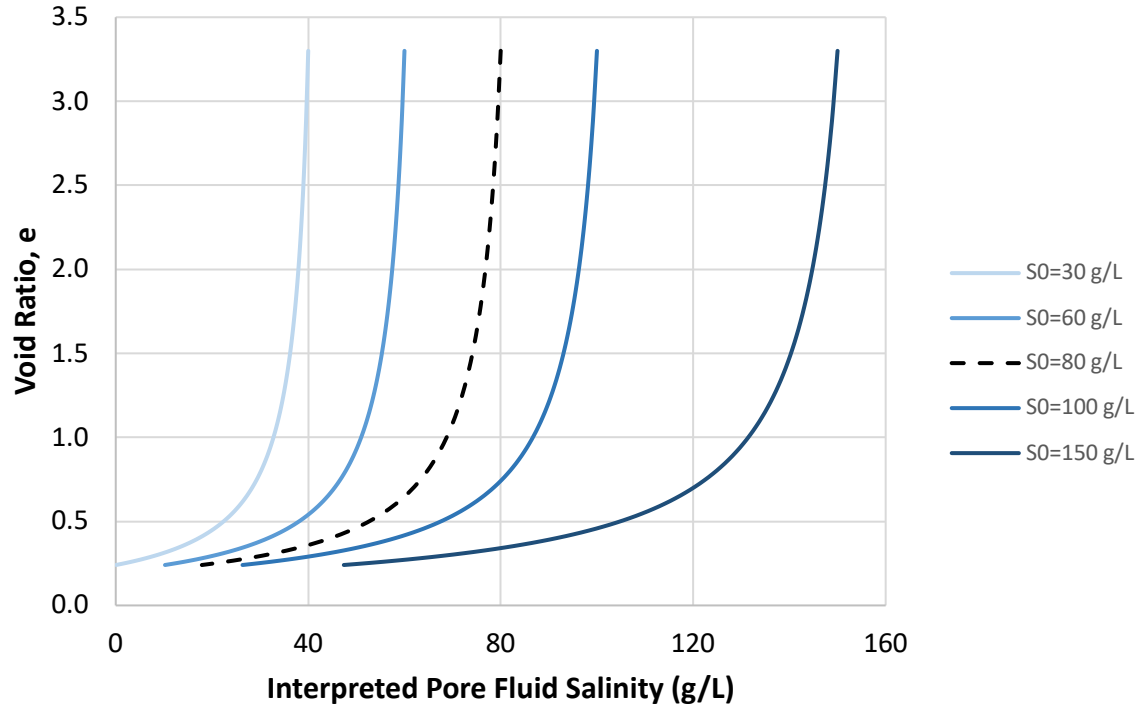

Figure 7-13: Model reaction to changing the initial salinity and therefore the double layer thickness (since double layer thickness is a function of salinity).

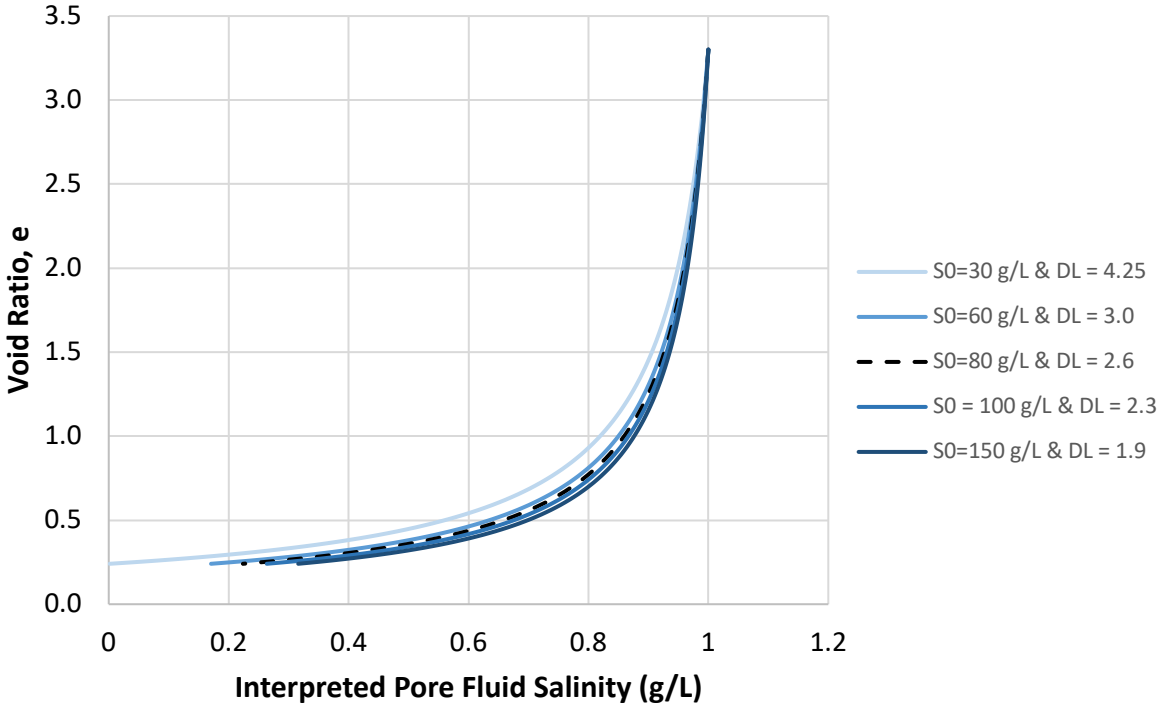

Figure 7-14: Figure 7-13 curves normalized by the initial salinity to see the effect of changing the double layer thickness on the model output.

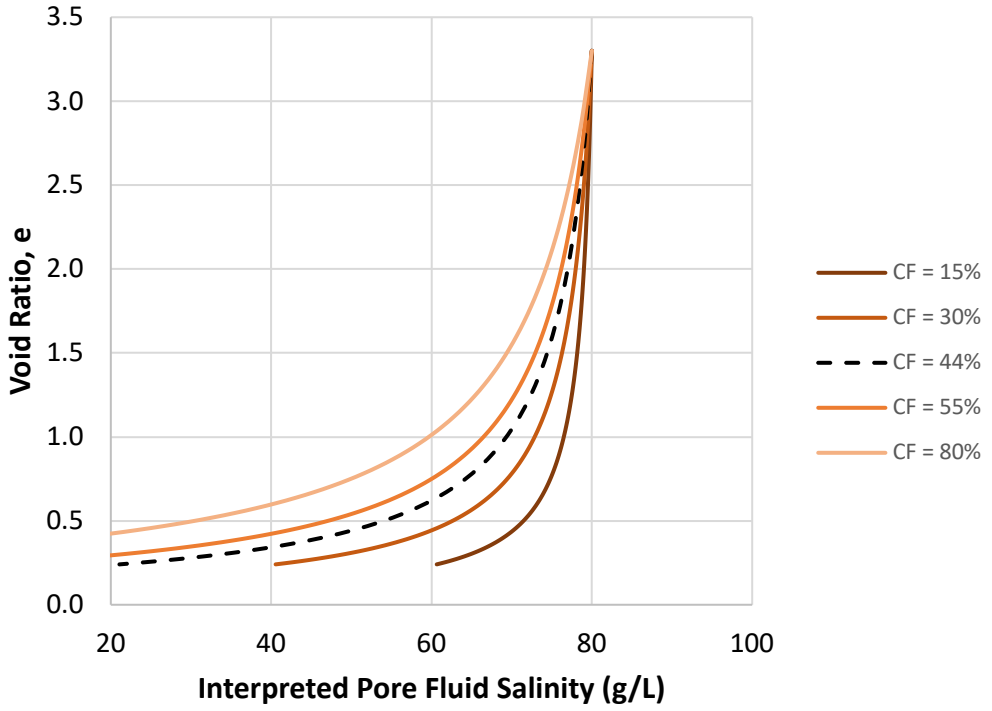

Figure 7-15: Model reaction to changing the clay fraction input.

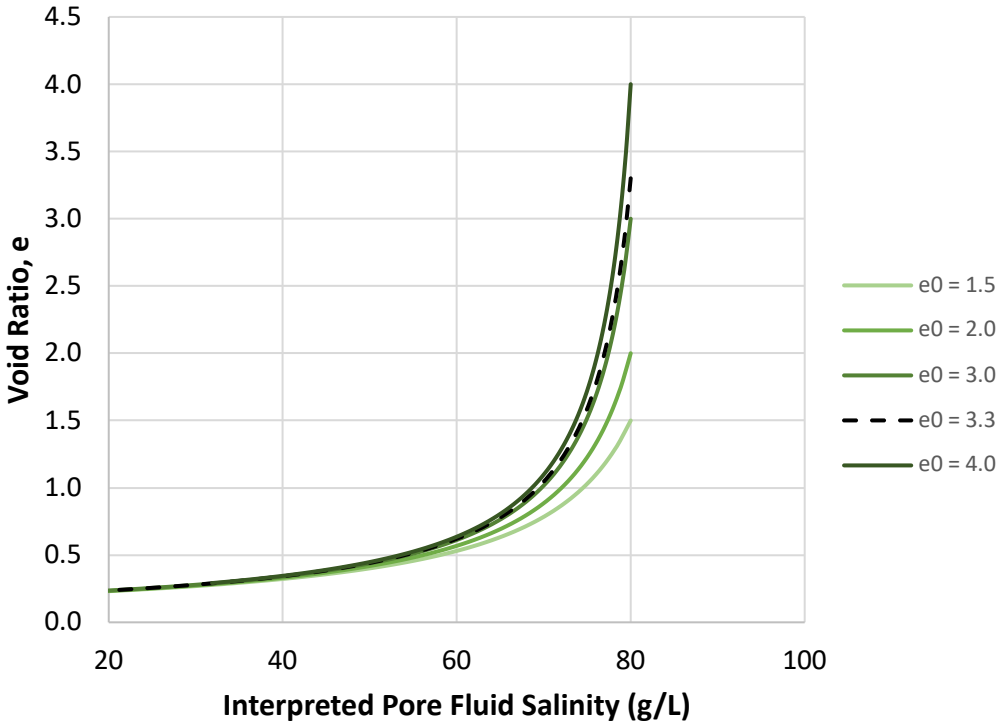

Figure 7-16: Model reaction to changing the initial void ratio of the element.

8 Summary, Conclusions, and Recommendations

8.1 Summary of Work

This research can be divided into two parts; first, the effect of temperature on the compression properties of Resedimented Gulf of Mexico – Eugene Island material, and second, the evolution of specimen salinity due to compression. The motivation for this research was to better understand the compression behavior of RGoM-EI at a particular starting pore fluid salinity. The results of both studies were compared to current research in the literature to understand implications of this work.

The research involved a significant experimental program to collect laboratory data for analysis. All experimental research was conducted on specimen resedimented to 0.1 MPa at a starting salinity of 80 g/L sea water in resedimentation consolidometers. Resedimented material is used to reduce variability and control the stress history across tests. The experiments were performed using state of the art laboratory equipment in the Tufts TAG Lab.

8.2 Effect of Temperature on Compression Behavior

A standard Trautwein© CRS cell was altered to allow controlled laboratory heating for the duration of a compression test (Figure 4-2). A series of five elevated temperature tests and five room temperature tests were run and the data of the two sets of experiments compared to each other (Table 6-1). The room temperature tests were run at 20°C, four of the elevated temperature tests were run at 60°C, and one elevated temperature test was at 40°C. Based on the literature it was expected that the compression curves (vertical effectives stress versus porosity) of the elevated temperature tests would be shifted down below the room temperature tests (Figure 2-9 and Figure 2-10). However, the compression curves from this research show no

systematic difference between the elevated temperature and room temperature tests. In fact, the variation between the five elevated temperature curves is greater than the variation between the regression lines for elevated temperature tests and room temperature tests (Figure 6-7 and Figure 6-8).

In addition to the compression curves, the volumetric compressibility (m_v), compression ratio (CR), and permeability (k) were all computed and the values compared between room temperature and elevated temperature tests. Again, no systematic difference is observed between the elevated temperature test data set and the room temperature data set. The variation in the regression lines for the permeability between the two different temperatures is again less than the difference between two elevated temperature tests or two room temperature tests.

For all of the data sets, regression lines were fit to the compression behavior in the normally consolidated range. There is good repeatability for all the regression lines with all R^2 values above 0.9, however, the room temperature tests consistently have a higher R^2 value than the elevated temperature tests. The implications of the R^2 value is the room temperature tests have more repeatability and less variance than the elevated temperature tests.

The results of this research are compared to the UT GeoFluids published compression curve for RGoM-EI and the average curve produced from research by Nordquist (2016). The data aligns well with the UT GeoFluids curve and converges at high stress levels but does not match the curve by Nordquist (Figure 6-9). This result leads to the hypothesis that perhaps there is variability between the storage buckets of dry clay powder.

Overall, the results of this research do not show the clear shift in compression curves as reported in the literature. This may be because the stress range investigated for this research, 0.1 to 40 MPa, is much greater than any of the stress ranges in the literature.

Additionally, all of this research used material batched to a sea salt salinity of 80 g/L resulting in a material with a collapsed double layer which could affect the compression curves.

8.3 Evolution of Salinity during Compression Tests

The second component of this research also uses a suite of CRS compression tests. The second topic is an analysis of what happens to mudrocks at the microscopic level due to increased stress application. It focuses on how the salinity of the specimen changes.

Existing literature suggests that the expelled pore fluid salinity decreases during compression. The two studies in the literature relied on testing apparatus designed to collect the very small volume of pore fluid that is expelled during compression. The collected pore fluid could then be used for direct salinity measurements. The TAG Lab does not have this type of testing equipment, so instead the salinity is computed based on a measured supernatant conductivity value. Eighteen independent salinity data points are included in the data set used to conclude that there is a clear decrease in the salinity of compressed specimen with increased stress. Each data point also has an associated error band that was evaluated to quantify the error associated with the measurement method.

In addition to quantifying the salinity behavior, a model was developed to predict the Interpreted Pore Fluid Salinity of a specimen at a particular stress level based on seven input parameters related to clay particle geometry and initial clay conditions. The Interpreted Pore Fluid Salinity is defined as the mass of mobile ions in a specimen divided by the total amount of pore fluid water and relies on a key assumption that the free pore fluid salinity is a constant value. The developed model is verified by predicting the Interpreted Pore Fluid Salinity of RGoM-EI material using the seven RGoM-EI specific input parameters and comparing the predicted values to the measured data set. In the case of RGoM-EI, the model works quite well with almost every data point lying on the

predicted curve. No other data sets exist right now that can be compared to the prediction model, but the input parameters can easily be varied to see how the model will shift and react.

8.4 Future Work

Based on the results of this research the following are suggested topics that will expand upon what was learned from these studies:

- There is a large opportunity to prove the developed Interpreted Pore Fluid Salinity model works for other materials with different initial conditions than RGoM-EI. The author suggests starting with RGoM-EI batched to a different salinity (much less than 80 g/L) and measuring the salinity at different stress levels. Then repeat the process with a different clay material that will change other input parameters like the clay fraction and type of clay.
- During the UT GeoFluids Consortium Meeting 9.0, sponsors questioned why the pore fluid expelled during CRS tests was not collected for salinity analysis. A continuation of this research could be the development of a device that can do this for the TAG Lab. This would provide data to close the mass balance loop that is currently problematic.
- The author struggled with the precision that is required in measuring the initial specimen dimensions and mass to calculate and understand the initial conditions of a CRS specimen, particularly the initial percent saturation value. A thorough analysis of which parameters affect the percent saturation value most and what the error associated with these values is should be done. Following this analysis the testing protocol should be evaluated for any areas of adjustment.
- Resedimenting specimen at a pore fluid salinity of 80 g/L results in clay specimen with a collapsed double layer. The temperature research could be repeated using RGoM-EI resedimented at a much lower salinity to expand the double layer to evaluate if there is still little effect on the compression behavior due to temperature.

- The last topic of the four hypothesized reasons for the shift in the porosity versus depth curve between laboratory curves and field measurements is secondary compression. This should be the next major topic tackled in the TAG Lab.

9 References

Abdulhadi, N. O. (2009, September). An Experimental Investigation into the Stress-Dependent Mechanical Behavior of Cohesive Soil with Application to Wellbore Instability (PhD). Massachusetts Institute of Technology, Cambridge, MA.

Adams, A. L. (2014, June). Permeability Anisotropy and Resistivity Anisotropy of Mechanically Compressed Mudrocks (PhD). Massachusetts Institute of Technology, Cambridge, MA.

ASTM Standard D4186. (2014). Standard Method for One-Dimensional Consolidation Properties of Saturated Cohesive Soils Using Controlled Strain Loading. West Conshohocken, PA: ASTM International.

ASTM Standard E691-18. (2018). Standard Practice for Conducting an Interlaboratory Study to Determine the Precision of a Test Method. West Conshohocken, PA: ASTM International.

Betts, W., & Flemings, P. B. (2014a). Compression and Permeability Behavior of Gulf of Mexico Mudrocks, Resedimented vs. In-Situ. Presented at the UT GeoFluids 5.0, University of Texas, Austin.

Betts, W., & Flemings, P. B. (2014b). Compression and Permeability Behavior of Gulf of Mexico Mudrocks, Resedimented vs. In-Situ. Powerpoint presented at the UT GeoFluids 5.0, University of Texas, Austin.

Betts, W. S. (2014, May). Compressibility and Permeability of Gulf of Mexico Mudrocks, Resedimented and In-Situ (Thesis). University of Texas, Austin, Austin, Texas.

Boggs, S. (2006). Principles of Sedimentology and Stratigraphy (4th ed.). New Jersey: Pearson Education, Inc.

Campanella, R. G., & Mitchell, J. K. (1968). Influence of Temperature Variations on Soil Behavior. Journal of the Soil Mechanics and Foundations Division, 94(3), 709–734.

Casey, B. (2014, June). The Consolidation and Strength Behavior of Mechanically Compressed Fine-Grained Sediments (PhD). Massachusetts Institute of Technology, Cambridge, MA.

Engelhardt, W. V., & Gaida, K. H. (1963). Concentration changes of pore solutions during the compaction of clay sediment. Journal of Sedimentary Petrology, 33(4), 919–930.

Fahy, B. P. (2014, June). The Influence of Salinity on the Mechanical Behavior of High Plasticity Soils (Masters). Massachusetts Institute of Technology, Cambridge, MA.

Fitts, T. G., & Brown, K. M. (1999). Stress-induced smectite dehydration: ramifications for patterns of freshening and fluid expulsion in the N. Barbados accretionary wedge. Earth and Planetary Science Letters, 172, 179–197.

Germaine, J. T., & Germaine, A. V. (2009). Geotechnical Laboratory Measurements for Engineers. Hoboken, New Jersey: John Wiley & Sons, Inc.

Hamilton, E. (1976). Variations of Density and Porosity with Depth in Deep-Sea Sediments. Journal of Sedimentary Petrology, 46(2), 280–300.

Hanley, A. J. (2017, August). The Characterization of the Yield Surface for Fine-Grained Sediments (Masters). Tufts University, Medford, MA.

Horan, A. (2012). The Mechanical Behavior of Mudrock as a Function of Pore Fluid Salinity. Presented at the UT GeoFluids Annual Consortium Meeting, University of Texas, Austin.

Hottman, C. E., & Johnson, R. K. (1966). Estimation of Formation Pressures from Log-Derived Shale Properties. Journal of Petroleum Engineering, 17(6), 717–722.

Ladd, C. C., Weaver, J. S., Germaine, J. T., & Sauls, D. P. (1985). Strength-Deformation Properties of Arctic Silt. Arctic ’85: Proceedings of the Conference, 820–829.

Long, H., Flemings, P. B., Dugan, B., Germaine, J. T., & Ferrell, D. (2005). Data report: penetrometer measurements of in situ temperature and pressure, IODP Expedition 308. Proceedings of the Integrated Ocean Drilling Program, 308.

Losh, S., Walter, L., Meulbroek, P., Martini, A., Cathles, L., & Whelan, J. (2002). Reservoir Fluids and Their Migration into the South Eugene Island Block 330 Reservoirs, Offshore Louisiana. AAPG Bulletin, 86(8), 1463–1488.

Mitchell, J. K. (1976). Fundamentals of Soil Behavior. University of California, Berkeley: John Wiley & Sons, Inc.

Nooraiepour, M., Mondol, N. H., & Hellevang, H. (2016). Experimental mechanical compaction of reconstituted shale and mudstone aggregates: Investigation of petrophysical and acoustic properties of SW Barents Sea cap rock sequences. Marine and Petroleum Geology, 80, 265–292.

Nordquist, T. J. (2015, June). Permeability Anisotropy of Resedimented Mudrocks. Massachusetts Institute of Technology, Cambridge, MA.

Plum, R. L., & Esrig, M. I. (1969). Some Temperature Effects on Soil Compressibility and Pore Water Pressure (Special Report No. 103) (pp. 231–242). Washington D.C.: Highway Research Board.

Urmos, J., Wilkens, R. H., Bassinot, F., Lyle, M., & Masters, J. C. (1993). Laboratory and Well-Log Velocity and Density Measurements from the Ontong Java Plateau: New in-situ corrections to laboratory data for pelagic carbonates. Proceedings of the Ocean Drilling Program: Scientific Results, 130, 607–622.

van Oort, E. (2003). On the physical and chemical stability of shales. Journal of Petroleum Science and Engineering, 38, 213–235.

Wissa, A. E. Z., Christian, J. T., Davis, E. H., & Heiberg, S. (n.d.). Consolidation at Constant Rate of Strain. Journal of the Soil Mechanics and Foundations Division, 97(SM10), 1393–1413.

Young, G. A. (1986, September). The Strength Deformation Properties of Smith Bay Arctic Silts (Masters). Massachusetts Institute of Technology, Cambridge, MA.